



---

Publicly Accessible Penn Dissertations

---


Fall 12-22-2010

# Mammary Epithelial Metastatic Phenotype Forced Through the Extracellular Matrix

Olga Shebanova

University of Pennsylvania, [olgash@seas.upenn.edu](mailto:olgash@seas.upenn.edu)

Follow this and additional works at: <http://repository.upenn.edu/edissertations>

 Part of the [Biochemical and Biomolecular Engineering Commons](#), [Biomechanics and Biotransport Commons](#), and the [Other Cell and Developmental Biology Commons](#)

---

## Recommended Citation

Shebanova, Olga, "Mammary Epithelial Metastatic Phenotype Forced Through the Extracellular Matrix" (2010). *Publicly Accessible Penn Dissertations*. 1566.

<http://repository.upenn.edu/edissertations/1566>

This paper is posted at ScholarlyCommons. <http://repository.upenn.edu/edissertations/1566>

For more information, please contact [libraryrepository@pobox.upenn.edu](mailto:libraryrepository@pobox.upenn.edu).

---

# Mammary Epithelial Metastatic Phenotype Forced Through the Extracellular Matrix

## **Abstract**

Biochemical and mechanical cues of the extracellular matrix have been shown to play important roles in cell-matrix and cell-cell interactions. We have experimentally tested the combined influence of these cues on cell motility, cell-cell interaction and assembly and traction force profile in an in vitro breast cancer model. The behavior of non-tumorigenic mammary epithelial cells was observed on surfaces with varying ligand concentration and polyacrylamide gel rigidity. Our data shows that cell velocity is biphasic in both matrix rigidity and adhesiveness, which are inversely related. Traction force microscopy revealed that maximum migration velocity is reached at intermediate force of single cells.

Cell-cell adhesion becomes strongly favored on softer gels with elasticity  $\leq 1250$  Pascals. This result implies an existence of a compliance threshold that promotes cell-cell over cell-matrix adhesion. On softer gels of 400 Pa, stiffness similar to pre-malignant breast tissue in vivo, cells undergo multi-cellular assembly, division and re-arrangement into 3D spherical aggregates on 2D surface. The aggregates resemble the spherical acini found in vivo and are also formed with EpH4-J3B1 mouse mammary epithelial cells at same compliance.

We establish mechanical cross talk between cell-cell and cell-matrix adhesions. Our findings of mechanotransduction show cell pairs exhibit 'tug of war' competitive dynamics between cell-cell and cell-matrix traction forces. Deletion of E-cadherin binding site to  $\beta$ -catenin results in loss of cell-cell tension magnitude and loss of the cross talk.

We are first to show force dynamics of cell division and cytokinesis in adherent mammalian cells. In normal division intercellular force goes through a maximum. Inhibition of myosin II mediated contractility with blebbistatin completely inhibits cell cytokinesis on gel surfaces. However inhibition of Rho-associated kinase ROCK does not inhibit cytokinesis, only reduces the magnitude of the forces. Therefore myosin II mediated contractility is necessary for cytokinesis on physiologically relevant substrates.

## **Degree Type**

Dissertation

## **Degree Name**

Doctor of Philosophy (PhD)

## **Graduate Group**

Chemical and Biomolecular Engineering

## **First Advisor**

Daniel A. Hammer

## **Keywords**

Extracellular matrix, epithelial, traction and intercellular forces

---

**Subject Categories**

Biochemical and Biomolecular Engineering | Biomechanics and Biotransport | Other Cell and Developmental Biology

# Mammary Epithelial Metastatic Phenotype Forced through the Extracellular Matrix.

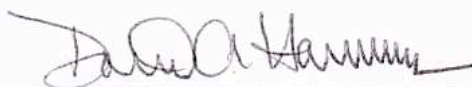
Olga Shebanova

A DISSERTATION  
in

Chemical and Biomolecular Engineering

Presented to the Faculties of the University of Pennsylvania in Partial  
Fulfillment of the Requirements for the Degree of Doctor of Philosophy

2010



Daniel A. Hammer, Professor of Chemical and Biomolecular Engineering  
Supervisor of Dissertation



Raymond J. Gorte, Professor of Chemical and Biomolecular Engineering  
Graduate Group Chairperson

Dissertation Committee:

John C. Crocker, Associate Professor of Chemical and Biomolecular Engineering

Scott L. Dimond, Professor of Chemical and Biomolecular Engineering

Matthew J. Lazzara, Assistant Professor of Chemical and Biomolecular Engineering

*For my grandparents whose value of education and hard work  
will always inspire and drive me*

# Acknowledgments

This thesis work was made possible with the support of mentors, colleagues, family and friends. I owe my deepest gratitude to my advisor, Dan Hammer, for his guidance and passion for science, which fueled my own creative drive for scientific knowledge and advancement.

I would like to thank my thesis committee, John Crocker, Scott Diamond, and Matt Lazzara, as well as Chris Chen. Their inquisitive interest and objective comments helped me to see the bigger picture while focusing on the details of my research projects. The collaborators, Micah Dembo and Valerie Weaver, were instrumental in the feasibility and execution of the research. I am indebted to the members of the Hammer lab, especially Matt Paszek, Risat Jannat, Jered Haun and Randi Saunders, for teaching me the experimental methods and engaging in helpful discussions. In addition I thank Eric Johnston for technical assistance and all my CBE comrades.

Most importantly I would like to thank my family, it was their encouragement and sacrifice that gave me the drive and the opportunity to pursue further education. My mother's immeasurable love and support kept me going in the toughest of times.

Lastly, big thank you to my school and college friends, who provided the much needed re-energizing breaks.

# ABSTRACT

## MAMMARY EPITHELIAL METASTATIC PHENOTYPE FORCED THROUGH THE EXTRACELLULAR MATRIX

Olga Shebanova

Daniel A. Hammer

Biochemical and mechanical cues of the extracellular matrix have been shown to play important roles in cell-matrix and cell-cell interactions. We have experimentally tested the combined influence of these cues on cell motility, cell-cell interaction and assembly and traction force profile in an in vitro breast cancer model. The behavior of MCF10A non-tumorigenic mammary epithelial cells was observed on surfaces with varying fibronectin ligand concentration and polyacrylamide gel rigidity. Our data shows that cell velocity is biphasic in both matrix rigidity and adhesiveness, which are inversely related. Traction force microscopy revealed that maximum migration velocity is reached at intermediate force of single cells.

Cell-cell adhesion becomes strongly favored on softer gels with elasticity  $\leq 1250$  Pascals. This result implies an existence of a compliance threshold that promotes cell-cell over cell-matrix adhesion. On softer gels of 400 Pa, stiffness similar to pre-malignant breast tissue in vivo, cells undergo multi-cellular assembly, division and re-arrangement into 3D spherical aggregates on 2D surface. The aggregates resemble the spherical acini structures found in vivo and are also formed with Eph4-J3B1 mouse mammary epithelial cells at same compliance.

We also establish mechanical cross talk between cell-cell and cell-matrix adhesions. Our findings of mechanotransduction show cell pairs exhibit 'tug of war' competitive dynamics between cell-cell and cell-matrix traction forces. Deletion of E-cadherin binding site to  $\beta$ -catenin results in loss of cell-cell tension magnitude and loss of the cross talk.

Finally, we are first to show force dynamics of cell division and cytokinesis in adherent mammalian cells. We find in normal division intercellular force goes through a maximum. Inhibition of myosin II mediated contractility with blebbistatin completely inhibits cell cytokinesis on gel surfaces. However inhibition of Rho-associated kinase ROCK does not inhibit cytokinesis, only reduces the magnitude of the forces. Therefore myosin II mediated contractility is necessary for cytokinesis on physiologically relevant substrates. The results show affects of the biochemical and mechanical stimuli of the ECM on the strength and force of cell-cell and cell-matrix adhesions.



# Contents

<b>1</b>	<b>Introduction</b>	<b>1</b>
1.1	Cancer pathology and Extracellular Matrix in breast cancer metastases . . .	1
1.2	Cell-matrix and cell-cell mechanotransduction components and pathways .	8
	Cell-matrix adhesion . . . . .	8
	Cell-cell adhesion . . . . .	12
	Cell division . . . . .	17
1.3	ECM mimetic in Traction Force Microscopy . . . . .	20
1.4	TFM definitions and theory for two cells . . . . .	29
	Newton's Laws . . . . .	31
	Statistical Considerations . . . . .	34
1.5	Hypothesis and Thesis overview . . . . .	38
1.6	Bibliography . . . . .	40
<b>2</b>	<b>Materials and Protocols</b>	<b>59</b>
2.1	Cell Culture . . . . .	59
2.2	Immunofluorescence and Imaging . . . . .	60
2.3	Gel Preparation . . . . .	61
	Coverslip Activation Protocol . . . . .	61
	Bulk Functionalization Gel Protocol . . . . .	63

Surface Functionalization Gel Protocol .....	68
Surface Characterization Protocol .....	75
2.4 Bibliography .....	76
<b>3 Cell motility and assembly <i>in vitro</i> as a model for Breast Cancer metastasis</b>	<b>79</b>
3.1 Biochemical and mechanical ECM cues dictate cell migration velocity ...	82
3.2 ECM mediated cell-cell adhesion slows migration .....	85
3.3 ECM compliance promotes formation of 3D multicellular structures on 2D surface .....	90
3.4 Mechanical and Biochemical ECM model .....	99
3.5 Bibliography .....	101
<b>4 Force profile in breast cancer invasiveness and adhesiveness</b>	<b>107</b>
4.1 Motility is a function of cell-matrix traction force mediated through cell- cell adhesion .....	110
4.2 Role of $\beta$ -catenin in cell force profile .....	114
4.3 Bibliography .....	116
<b>5 Force dynamics of cell-cell interactions</b>	<b>119</b>
5.1 Cell-cell interaction quantified through substrate deformation .....	122
5.2 Adherent cells exert anti-parallel forces .....	127
5.3 Statistical interpretation of cell-cell adhesion strength and retraction .....	131
5.4 Mechanical dynamics of cross-talk between cell-matrix and cell-cell adhe- sions .....	132
5.5 Bibliography .....	136

<b>6</b>	<b>Cell division and cytokinesis through Extracellular Matrix</b>	<b>142</b>
6.1	Temporal force profile of cell division and cytokinesis . . . . .	147
6.2	Traction force analysis at each stage of the cell division cycle . . . . .	153
6.3	Myosin II motor and Rho-associated kinase roles in cytokinesis . . . . .	156
6.4	Bibliography . . . . .	163
<b>7</b>	<b>Conclusions and Future Directions</b>	<b>168</b>
7.1	Force cross-talk . . . . .	168
7.2	Cell division mechanics . . . . .	171
7.3	ECM role in chemotaxis of invasive breast cancer . . . . .	172
7.4	Bibliography . . . . .	174

# List of Figures

1.1	Integrin signaling pathways. . . . .	11
1.2	E-cadherin cell-cell junction schematic. . . . .	15
1.3	Polymerization reaction of polyacrylamide gels. . . . .	23
1.4	Characterization of the new polyacrylamide gel functionalization method. . . . .	25
1.5	Two cell TFM. . . . .	26
2.1	Collagen surface distribution. . . . .	67
3.1	Cell migration velocity as a function of the ECM. . . . .	84
3.2	Cell spread area as a function of the ECM. . . . .	86
3.3	Cell velocity profile of single and adherent cells. . . . .	88
3.4	Cell-cell contact inhibits maximum velocity. . . . .	89
3.5	ECM mediated cell interactions visualized. . . . .	91
3.6	Cell assembly and aggregate initiation. . . . .	93
3.7	MCF10A 3D spherical aggregates on 2D substrates. . . . .	95
3.8	Absence of aggregates on stiffer substrates. . . . .	97
3.9	Mouse mammary epithelial cell aggregates. . . . .	98
3.10	Schematic summary of effects of biochemical and mechanical cues of the ECM on cell-cell and cell-matrix interactions leading to cell motility and cell-cell assembly. . .	100
4.1	Traction forces and stresses dictate motility. . . . .	111

4.2	Cell-cell tension and average force relationships. . . . .	113
4.3	MCF10A cells fluorescent staining. . . . .	115
4.4	E-cadherin mutant force profiles. . . . .	115
5.1	EpH4 two cell interaction visualized. . . . .	124
5.2	Temporal force vectors of cell-cell interactions. . . . .	125
5.3	Temporal cyclic interaction dynamics. . . . .	126
5.4	Two cell anti-parallel alignment and average force. . . . .	128
5.5	Cell pair angles and torques. . . . .	129
5.6	MCF10A force and cell-cell tension relationship. . . . .	130
5.7	Statistical analysis of cell-cell force interactions. . . . .	133
5.8	Mechanical cell-matrix and cell-cell crosstalk. . . . .	135
6.1	Temporal force profile of EpH4 mouse mammary epithelial cell division. . . . .	148
6.2	Quantitative analysis of dividing cell mechanics. . . . .	150
6.3	Force profile of cell entering division. . . . .	151
6.4	Force profile of cell spreading. . . . .	152
6.5	EpH4 force and cell-cell tension relationship. . . . .	154
6.6	Force profile at each cell cycle stage. . . . .	155
6.7	TFM results of blebbistatin treated cells. . . . .	158
6.8	TFM results of Y-27632 treated cells. . . . .	160
6.9	Summary of inhibited division and forces at each stage of cell cycle. . . . .	162

# Chapter 1

## Introduction

### **1.1 Cancer pathology and Extracellular Matrix in breast cancer metastases**

Metastasis of tumor cells to distant organs is the primary cause of cancer-related mortality. Breast cancer metastasis accounts for over 90% of lethality in cancer patients [1]. Breast cancer survival rate for women with distant metastasis in the United States is 25% (American Cancer Society Facts and Figures). Progression of benign tumors to invasive carcinomas is a life threatening yet poorly understood phenomenon in the development of the disease. Events of tissue destabilization, increased proliferation, loss of cell-cell adhesiveness, and increased cell-matrix interaction ultimately result in loss of tissue integrity, cell invasion and metastasis, which are the motivation of my thesis work.

The normal mammary tissue consists of globular epithelial cells surrounded by extracellular environment called the stroma. The highly polarized epithelial cells form hollow lumen containing spheres, called acini, and ducts surrounded by less abundant myoepithelial cells and basement membrane [2, 3].

In the human breast the interstitial stroma is abundant, more than 80% of breast vol-

ume, and dynamically changing environment [2]. The stroma consists of fat tissue, blood vessels, interstitial/interlobular dense and intralobular loose connective tissues. The human epithelial cells are located in collagenous compartments separate from the fat tissue, whereas in mouse mammary glands the cells are directly embedded in fatty tissue. The ratio of fibrous interstitial stroma to fat tissue in the human breast is highly unique to the individual [2]. The breast tissue is constantly subjected to changes in hormone levels in addition to the microenvironment changes [4].

It is becoming more apparent that the dynamic mammary gland environment is instrumental in maintaining organ integrity and homeostasis or in promoting and initiating breast cancer development [4, 5]. The extracellular environment is not a passive support for epithelial cells but an active contributor to tumor progression [4]. Diverse factors of aging, inflamed and changing extracellular environment have been found as leading developers of cancer progression and metastasis.

Abnormal breast epithelium in benign tumors shows high proliferation with stromal expansion and fibrosis. Progression of the disease that results in metastasis shows increased stroma deposition of collagens, fibronectin, laminin, proteoglycans, and glycosaminoglycans, compared to a extracellular matrix of a wound healing gone awry [2, 6, 7]. These changes in extracellular environment have been found in tumor tissue and favor invasion through mechanical changes due to increased fibrosis and matrix crosslinking [8, 9]. Collagen deposition is accompanied by loss of collagen curvature and increased fibril linearity and crosslinking, with increase amounts of amine oxidase crosslinking enzyme, LOX [8]. Normal human mammary gland is measured around 160 to 400 Pa, where as breast tumors can be 2 to 4 kPa or even stiffer [8-12].

Mammographic studies on women with dense breast tissue, containing increased collagen and fibronectin deposition in the stroma, found increased risk of breast cancer [13]. Fibronectin (FN) ligand is found abundant in the mammary gland basement membrane dur-

ing development and tumorigenesis [3], but normal adult mammary tissue is largely devoid of fibronectin [14]. The mechanical properties in addition to the biochemical changes alter *in vivo* matrix adhesion and change cellular signaling and subsequent cellular behavior. Differences in cellular response to matrix density and rigidity *in vivo* and *in vitro* attest to the importance of biophysical and biochemical cues of the extracellular matrix (ECM). *In vitro* studies have observed in detail how increasing matrix stiffness, through increasing collagen density or stiffness of polyacrylamide gels coated with basement membrane, disrupts the ordered lumen containing acini and induces cell invasiveness [9].

Biochemically it has been additionally found that deposition of fibronectin in the basement membrane reverses growth arrest of the homeostatic acini tissues and promotes more fibronectin production [3]. Increased fibronectin levels are observed in stroma of various types of mammary tumors [14]. Furthermore FN deposition is up-regulated by the extracellular rigidity [3]. Additionally extracellular tenascin, hyaluronan, and thrombosponin are considered to favor invasion [2]. During progression to invasive breast cancer the tumor cells come in direct contact with the remodeled fibronectin and collagen rich and mechanically stiffer interstitial stroma [4]. Therefore the focus of our research lies in studying these two ligands in combination with mechanical changes to study cell invasiveness through cell-matrix regulated motility and cell-cell adhesivity.

The genetic mutations or other carcinogenic events leading to malignant breast cancer are not discounted in this research. But it is more and more evident that cancer development and progression is not solely dependant on genetic predisposition of the individual cells within the tissue. The tendency to metastasize is preordained by a spectrum of genetic mutations, but it is the extracellular microenvironment of the organ that induces the tumors to metastasize and arrest in specific organs [15]. An inflammation related mechanism is also implicated in ECM changes. The immune response can be caused by number of factors like bacterial and viral infections, carcinogenic substances, obesity, aging, senescence [16].



The inflammatory response contributes to the malignant phenotype through restructuring of the extracellular environment. Changes that promote the invasive malignant transition and are therefore of interest to us.

Furthermore studies on intercellular components of normal and tumorigenic breast tissue revealed loss of polar localization and up-regulation of cell-matrix and cell-cell molecular proteins such as integrins, cadherins, vinculin, talin,  $\alpha$ -actinin and focal adhesion kinase. In normal mammary gland integrins are found on basolateral surface of acini epithelial cells, but in invasive carcinomas the staining was random throughout the cell aggregates [17]. *In vitro* 3D studies of invasive breast cancer cell aggregates treated with anti- $\beta$ 1 integrin antibodies reverted the malignant phenotype to an ordered spherical structure [18, 19]. A direct connection has thus been made between extracellular matrix crosslinking density, that yields the tissue stiffening, and enhanced integrin signalling [8].

Mechanical equilibrium must exist not only with the environment but also between the cells in a tissue. Cell-cell junctions hold together and shape distinct tissues and organs, specifically adherens junctions are the site of connection of transmembrane proteins to the cytoskeletal actin filaments that provide architectural strength and form and maintain tissue homeostasis. Adherent cells modulate forces onto each other to maintain the tissue integrity. Influenced by cues from the ECM these cell-cell tensions and adhesion mechanics change and become unstable, which aids in cell invasion and metastasis [20].

Breast tissue integrity is also dependant on cell-cell adhesion. Epithelial cells rely on cell-cell adhesion to maintain tissue integrity and function [21-23]. Development of benign lesions into invasive metastatic cancer is characterized by a tumour cell's ability to overcome the cell-cell adhesion and invade surrounding tissue [24]. Early classical demonstrations showed tumor cells adhering to each other less avidly than non-tumor cells [25-26].

An important player in epithelial cell adhesion is E-cadherin. The cadherin staining of normal glands is localized to apical cell-cell junctions. This patterning and E-cadherin

adhesion function are lost in invasive tumors [17, 24]. E-cadherin is thought to act as suppressor of epithelial tumor cell invasiveness and metastasis [27]. Loss of E-cadherin or any of the intracellular E-cadherin-catenin complex cause loss of cell adhesion and tumour progression. Studies also show over-expression of E-cadherin leads to growth arrest while inhibition of cadherin function induces tumorigenicity [24]. Thus experimental manipulation established an inverse relationship between E-cadherin expression and function and tumor progression [28]. Overall evidence demonstrates that perturbed E-cadherin expression and function promotes cancer progression to invasion and metastasis [28]. Loss of expression and gain-of-function mutations of  $\beta$ -catenin are also common in human cancers and result in loss of cell-cell adhesion and increased gene transcription [29]. Loss of  $\alpha$ -catenin in some cancer types has served as a stronger prognostic factor for invasion, growth and metastasis [30]. Furthermore 5 year survival rate of cancer patients with  $\alpha$ -catenin loss was drastically decreased compared to those with just E-cadherin loss [30].

The final part of this thesis work that is an important precursor of tumor formation, which is cell division. There is a long standing link between cell division and cancer. The human body itself continually replenishes with  $\sim 10^8$ - $10^9$  cell division events occurring at every moment in time [31]. Therefore successful cell division is critical to human health. Discovery and understanding of cell division have existed since nineteenth century. It originated with the work of German biologist Theodor Boveri in 1888, who introduced the idea of the connection between abnormal mitosis and malignant tumours. It is the final stages of abscission and failure of complete cytokinesis that has been proposed to promote tumorigenesis through tetraploidy and chromosomal instability [32]. Although once presented as a simple picture of constriction of the equatorially positioned cleavage plane containing contractile ring of parallel actin filaments and myosin, cytokinesis has been identified as a more complex process in recent studies. Not only is the mechanism different in different cell types, but also the necessity of attachment to the extracellular environment in mam-

malian cells has become a novel area of discovery. Today the process still remains widely studied with questions left to be explored. Research on cell division is important to lead to understanding and better treatments of disease such as cancer and especially breast cancer in our work.

Numerous studies indicate it is similar molecular players of integrin and cadherin mediated adhesion that alter cell proliferation behavior. Inhibition of cell spreading on two dimensional substrate induces epithelial cells to arrest in the growth phase, G1, of the cell cycle [33]. Integrin mediated matrix adhesion, in addition to growth factors, is important to cell division and in its absence the mitogenic signaling is weak and transient [34]. Increased matrix adhesivity due to increased ligand densities and stiffness and decreased cell-cell cohesivity, both increase cell mitogenic activity. Thus we look at how the necessary adhesion to the extracellular environment controls cell proliferation.

The extracellular environment not only promotes breast cell invasiveness and metastasis, but also the arrest and establishment of metastatic aggregates in distant organs. Breast cancer, in addition to prostate and lung, preferentially metastasize to the bone [35]. In fact 70% of all patients dying of breast cancer have evidence of metastasis to the bone [36]. The bone marrow microenvironment is rich with microvessels and growth factors [35, 37]. The bone is mechanically a very rigid environment, ranging in elastic modulus of 50 to 100kPa [11]. This physiological phenomenon of cell motility at higher breast tissue stiffness, but arrest in stiffest bone tissues hints at a non-linear more unique relationship between cell motility and the extracellular environment. Furthermore bone cells, osteoblasts and osteoclasts secrete paracrine factors that induce chemotaxis and cell adhesion, support cell survival and growth and stimulate angiogenesis [35]. Involvement of chemokines in breast cancer metastasis is an established interesting idea with many unanswered questions to understand as well [38, 39].

The importance of extracellular environment in metastatic tumor progression begs the

question if cancer can be reversed by engineering the tumour microenvironment. Although extracellular adhesion proteins, like integrins, have become molecular targets for developing cancer compounds entering clinical trials on anti-migratory drugs [40], there are no currently published compounds for extracellular matrix modifications. Perspectives have been written to raise the possibility of developing a tissue engineering approach to cancer therapy with materials to induce cancer reversion to normal tissue [41]. Levental and al. also found that inhibition of lysyl oxidase (LOX) enzyme *in vivo* decreases collagen crosslinking and fibrosis and inhibits breast tumour progression [12] and LOX repression inhibits cell invasion *in vitro* [42]. Therefore LOX could be a potential breast cancer therapy target to inhibit tissue stiffening in early detected tumours and thus prevent invasive metastasis.

How the extracellular environment stimulates intracellular pathways, facilitates abnormal cell division, increases cell migration and decreases cell-cell interaction is an important mechanical and biochemical phenomenon in cell invasion, a critical step in cancer progression. Our focus on studying and understanding the important step of tissue destabilization in breast cancer metastasis will advance the knowledge and understanding of the beginning stages of mammary cell invasion. Understanding dynamics and force generation of cell-matrix and cell-cell interactions will aid in understanding the metastasis phenomenon of cancers and additionally will shed light on a diversity of areas such as embryogenesis, organ and tissue development and regeneration. The gained knowledge of the mechanism of cancer metastasis can lead to better diagnosis of breast cancer progression as well as other metastatic cancers, new treatments and therapies.

## 1.2 Cell-matrix and cell-cell mechanotransduction components and pathways

To better understand the role of cell adhesion to the extracellular environment and to its neighbors in metastatic behavior, it is important to look at both intra- and inter- cellular players and pathways involved. The mechanical stretching and unfolding changes to the molecules themselves have been found to mediate the ECM initiated intracellular cascade. Therefore I'll review and summarize key molecular components and pathways leading to the invasive motile mechanosensing and transducing behavior.

### Cell-matrix adhesion

Focal adhesions (FA) provide the platform of connection between the ECM and the cytoskeleton and response to external force. The molecules involved in FAs are called mechanosensors because they detect external mechanical signals and convert them to biochemical signals inside the cell. These biochemical intercellular signals are furthermore interpreted by mechano-transducing molecules at the FA to exert force back onto the extracellular environment. Focal adhesions are mechano sensor and transducer sites that modulate cell behavior and phenotype, *in vitro* and *in vivo* [43].

The key cell connector and signal transducer to the biochemical and mechanical extracellular matrix is the integrin protein. Although multiple other receptors and membrane proteins play a role in interpreting and transmitting signals to the cellular surroundings, integrin family of proteins is key in cell-matrix adhesion. Integrins are interesting and unusual transmembrane receptors because of their bidirectional signalling ability: outside-in and inside-out. Interesting work on inside-out integrin activation via chemokine and the role of ECM is studied in neutrophils, dendritic and other blood cells in Hammer lab [44]. In this work we focus on outside-in affects of ECM on epithelial behavior.

The ECM integrin binding leads to a vast signaling cascade and structural changes within the cell, assembly of cytoplasmic multimolecular complexes, cytoskeletal engagement, pathways that ultimately lead to gene expression and measurable cell behavioral mechanical responses. It is a grand stage of numerous players, of which a few will be mentioned with relation and better understanding of the dynamic ECM-integrin-cytoskeleton linkage in cellular mechanotransduction.

The initial ECM bound integrin-cytoskeleton linkage involves talin recruitment with a 2 pN slip bond initial force applied by the cytoskeleton onto the extracellular ligand [45]. Talin null cells have minimal and delayed focal adhesion formation [46]. Talin binding is readily followed by vinculin recruitment to the nascent adhesion site. Vinculin head binds talin and its tail domain binds to F-actin and paxillin [47]. Vinculin readily available binding sites are supplemented with those exposed only upon mechanical stretching of its helical bundles [48-51]. Vinculin has been found necessary for focal adhesion maturation and required for its stability [52] and is therefore an important mechanotransducing protein in cell-matrix adhesion.

Recent published data from Schwartz lab elegantly measured tension across this mechanotransducing molecule with Fluorescence Resonance Energy Transfer (FRET) [53]. Directly measuring the force across vinculin molecule, ~2.5 pN in stable FAs, shows highest tension during adhesion assembly and lowest during disassembly. The data shows that vinculin recruitment and force transmission are required for FA stabilization under force, but these two are independent processes [53].

Both talin and vinculin establish a 'slippage clutch' between the static matrix adhesions and the treadmilling actin [54]. The continuous myosin pulling of actin transmits the pulling forces onto the ECM, via strong connection between integrin and F-actin through talin and vinculin. Weaker linkage to the integrins leads to detachment of actin and sliding of the cell body over the adhesion. This is a precise local regulation mechanism of cell

motility on integrin-actin level [55]. The clutch mechanism is a local modulation of the strength of the integrin-actin connection in response to the changes in attachment strength to the ECM, either through talin and vinculin or  $\alpha$ -actinin [56]. This proposed mechanism of tunable integrin-actin interaction in response to extracellular cues implicates talin, vinculin and  $\alpha$ -actinin as important mechanotransduction players.

Signalling proteins are also necessary for the mechanical integrin-actin modulation. Paxillin protein is detected in nascent adhesions. Its structure allows for numerous simultaneous interactions and its function is of a molecular platform regulating integrin-actin linkage through modulating the FA composition [43, 57, 58]. Focal Adhesion Kinase (FAK) plays an essential role in promoting focal adhesion turn over, which is necessary to promote cell motility [43, 59]. FAK-null cells cannot detect differences in ECM rigidity unlike normal cells that migrate preferentially on rigid substrates [60]. Furthermore FAK is found over-expressed in invasive breast cancer [61].

Stronger cell-matrix adhesion is dependant on growth and maturation of FAs, which is dependant on inside-out mechanisms of  $\alpha$ -actinin actin crosslinking and myosin II contractile activity [55, 62]. Outside-in externally applied force is found to achieve the same result [63]. Thus outside force affects FA growth through inducing actin cross-linking, which is dependant on  $\alpha$ -actinin and myosin II, although not specifically on the contractile activity of myosin II. The cross-linking and bundling of actin filaments may promote clustering of integrins and induce further accumulation of signaling partners that lead to even further growth of the adhesion plaque [55].

The physical link between integrins and actin is also important in actin polymerization and global control of the cytoskeletal dynamics. In addition to FA components, it is actin that drives cell protrusion and retraction in migration and regulation of cell shape. Local actin polymerization is through a central molecular Arp2/3 complex [64] and is coupled to global regulation of actin dynamics by the family of Rho GTPases. Most important of

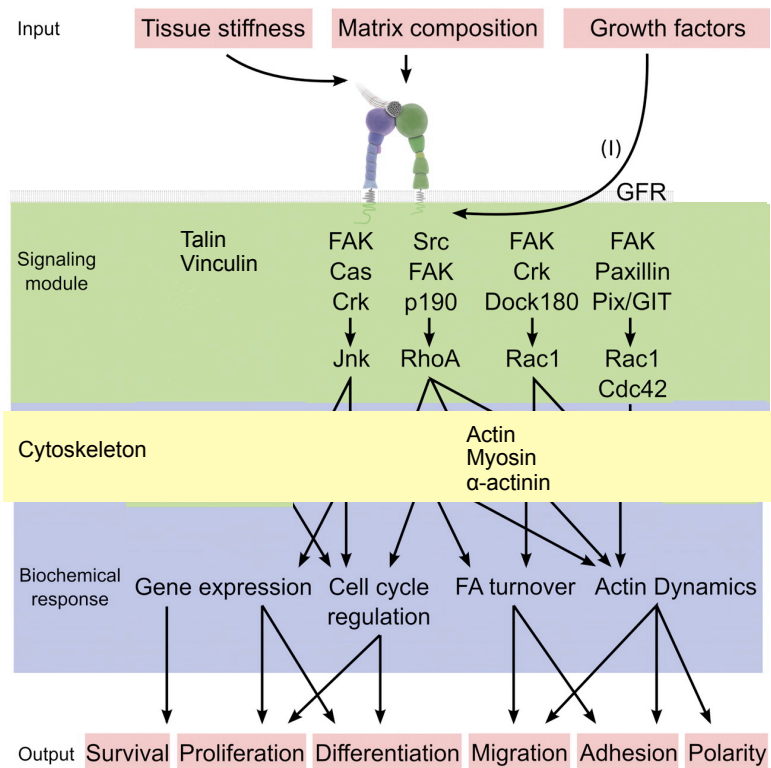


Figure 1.1: Integrin signalling pathways.

Few examples of the integrin mediated mechanical and biochemical input, signaling pathways, responses and the phenotypic output. Highlighted in yellow is intracellular force generating machinery of consequence to our research. Graphic is modified from Legate et al. [55].

these are Rac, Cdc42 and RhoA. Integrin ligation and clustering target Rac to the leading edge where it promotes lamellipodial protrusion and regulates actin polymerization. RhoA promotes cell contractility. One of its effectors is Rho Kinase (ROCK) which affects contractility by increasing phosphorylation of the regulatory light chain of myosin II. Initial phases of cell adhesion and lamellipodial protrusion require Rac activity and RhoA suppression, which can be accomplished by Rac1, and then stabilization of the contacts necessary for motility depends on Rho [43, 55, 65]. These two players are also involved in cell-cell adhesion and become especially interesting in cell division, specifically cytokinesis, of adherent cells.

Integrins are thus unique proteins that connect all these diverse intercellular pathways



to extracellular environment, a modified Fig. 1.1 published by Legate et al. illustrates the connection [55]. They regulate ligand-binding affinity, integrate mechanical and chemical signals of the ECM through direct association with the cytoskeleton and transmit resulting contractile forces onto the ECM. Of course each protein in the vast cell-matrix interaction has an important role, only very few ones are listed and studied in this work. But the briefly described intracellular molecular players implicate and stress the importance of outside environment mechanical force and biochemical ligand cues. These molecules are implicated in mediating signal transduction in response to mechanical stimuli at the mechano-sensor site of focal adhesion. However from all the specific protein-protein binding interactions and players identified in FAs, there still exists a lack of understanding how a cell regulates these combinatorial interactions in a spatial and temporal manner to regulate cell behavior, specifically spreading, motility and force response.

Furthermore it is important to consider that most of these molecular studies have been conducted on tissue culture plastic or glass surfaces, which are not physiologically relevant rigid materials and are not representative of natural cellular environments. Currently it is unknown precisely how changes in matrix composition alter the composition of these signaling complexes. To gain a more thorough and correct understanding of outside-in signaling and activity it is necessary to dissect, supplement and revise the current knowledge on more physiological mimicking substrates.

The work of this thesis focuses exactly on that: the affect of physiologically relevant conditions in breast cancer development on complex cellular response measured and quantified through the cell motile and mechanical behavioral response.

## **Cell-cell adhesion**

Equivalent to cell-matrix focal adhesions with integrins as connectors, cell-cell interactions maintain Adherens Junctions (AJ) with cadherin proteins as the key signal transducer from

outside-in. Cadherins are plasma membrane-spanning proteins that mediate cell-cell adhesion by binding to identical cadherins on the surface of neighboring cells. Interestingly enough, cadherins are found to have inside-out and outside-in signalling capabilities as well [66]. Outside-in signaling is elicited by cadherin ectodomain binding which triggers local accumulation of phosphorylated proteins, recruitment and redistribution of actin filaments and membrane remodeling. The inside-out signaling is seen in altered extracellular cadherin binding which is changed by microfilament and microtubule depolymerization affecting intracellular cadherin domain [66].

The cytoplasmic domain is linked to the actin cytoskeleton and therefore modulates mechanical cell-cell adhesion, serving in tissue recognition and sorting, boundary formation, maintenance, coordinating cell movement and inducing polarity, influencing both integrin-matrix adhesions and growth factor signaling pathways [67]. Cadherin-mediated cell-cell adhesion is fortified by catenin molecules that bind to the cytoplasmic tail of cadherins and link it to the actin cytoskeleton. Just like integrins, cadherins have been found to cluster at sites of cell-cell adherens junctions, allowing for the development of mechanical stress within the epithelium [68, 69].

Cadherins are type 1 membrane glycoproteins that function as dynamic membrane spanning macro-molecular complexes [22]. The extracellular domain of cadherins consists of calcium binding repeats which are important for homophilic recognition and adhesion, although heterophilic interactions between classical cadherins have also been reported [28, 67]. Cytoplasmic domain of cadherins is highly conserved between different subtypes and binds directly to several cytoplasmic proteins including  $\beta$ -catenin and p120 [67, 147]. These binding proteins are important in connection with the cytoskeleton. p120 directly binds and inhibits RhoA and indirectly activates Rac1 and cdc42 [70, 71].  $\beta$ -catenin binding to E-cadherin is necessary for cell-cell adhesion [72].

$\beta$ -catenin binds directly to  $\alpha$ -catenin which is connected to actin cytoskeleton, although

the mechanism is not yet clearly defined. Work by Nelson lab has shown that it is in fact excess unbound  $\alpha$ -catenin dimers that engage the actin filaments, suppress actin assembly and strengthen cell-cell adhesion [30]. In fact  $\alpha$ -catenin binding to  $\beta$ -catenin and actin was found to be mutually exclusive, due to an allosteric switch in the monomer conformation of  $\alpha$ -catenin to bind preferentially E-cadherin/ $\beta$ -catenin complex versus the homodimer binding and bundling actin filaments [73]. Since  $\beta$ -catenin/ $\alpha$ -catenin binding affinity is relatively weak at  $\sim 1 \mu\text{M}$  and cytoplasmic  $\alpha$ -catenin homodimer concentration is  $\sim 10\text{X}$  that of the monomer. The role of the  $\alpha$ -catenin is then thought to be in dimer reorganization of actin dynamics at cell-cell contact to decrease membrane activity, stabilize cadherin-mediated cell-cell adhesion and further decrease cell migration [30, 73, 74].

Furthermore if E-cadherin bound  $\beta$ -catenin serves a supportive role in cell-cell adhesion and tissue connectivity and integrity, the unbound intracellular  $\beta$ -catenin serves an antagonistic role. Intracellular stabilization and accumulation of unbound  $\beta$ -catenin results in nuclear translocation and transcription factor induction of the protein, which will be discussed with cell division.  $\beta$ -catenin stabilization and nuclear translocation tips the equilibrium from normal to uncontrolled proliferation, differentiation and tissue disruption in colorectal cancer.  $\beta$ -catenin and Wnt protein signaling pathway has also been found to trigger tumorigenesis in breast cancer in addition to skin, bone marrow and colorectal cancers [75]. Immunohistochemical staining of  $\beta$ -catenin and E-cadherin in different types of cervical carcinomas found strong cytoplasmic and nuclear stains, versus membrane bound in normal tissue [76]. Tumor cells with nuclear accumulation of  $\beta$ -catenin have also been found to undergo loss of E-cadherin expression and epithelial-mesenchymal transition, a phenomenon describing transformation events to invasive epithelial cancers [75]. The E-cadherin  $\beta$ -catenin relationship in cancer cell invasion has been further modeled and simulated as well [77].

RhoA and Rac1 have been found to regulate E-cadherin function and reorganization

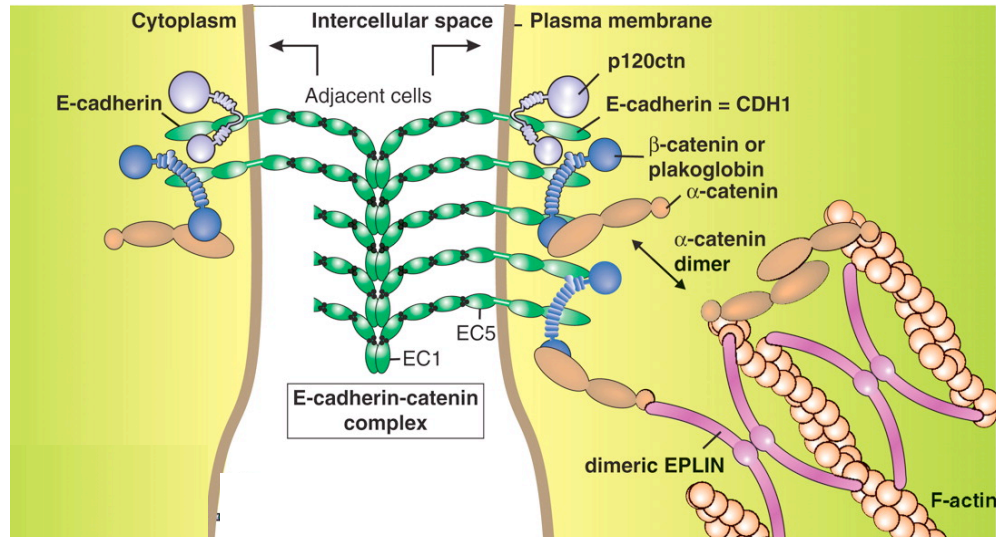


Figure 1.2: E-cadherin cell-cell junction schematic.

Schematic overview of the E-cadherin-catenin complex involved in cell-cell adhesion. Key proteins of interest in our research are E-cadherin and  $\beta$ -catenin and their connection to the actin cytoskeleton. Adopted and modified from Berx et al. [147]

of cadherin-catenin complex and the underlying actin cytoskeleton [24, 78]. Rac1 spatiotemporally reorganizes the plasma membrane at newest cell-cell adhesion sites and decreases at older, stabilized sites [79]. Rac1 is activated upon and co-localizes to E-cadherin adhesion and regulates local actin dynamics through promoting its nucleators, such as Arp2/3. The Rac1 mediated lamellipodial initiation of contact is suppressed and followed by actomyosin contraction in later stages of cell-cell adhesion [78].  $\alpha$ -catenin homodimer concentration grows as clusters of cadherin-catenin complexes grow and local inhibition and decrease in Arp2/3-mediated actin polymerization is observed [78]. RhoA activity is detected after the *de novo* cell-cell adhesions are formed - however its role and actomyosin contraction are not as clear. One theory is that at cell-cell contact RhoA actually aids in contact expansion and does not maintain contractile activity [78].

Mechanotransducers like myosin II and myosin VI are also found in cell-cell adhesions. Recruited and stimulated by E-cadherin, myosin II is responsible for regional distribution and clustering of the cadherins [80]. Myosin VI is recruited to mature cohesive cell-cell

contacts and is necessary for maintaining the strong cadherin adhesion and interaction with vinculin [81]. Fig. 1.1 can thus be adopted and slightly changed to represent the E-cadherin cascade from cell-cell adhesion input to output change in cellular phenotype. Fig. 1.2, adopted from Berx et al. [147], is a pictorial representation of the described intracellular proteins involved in E-cadherin mediated cell-cell adhesions.

Cadherins can be further influenced by integrin-mediated signaling. Assembly of new cell-cell adhesion complexes on the periphery of old ones has been found to be aided by presence of integrins [78, 82, 83]. This cross-talk between FAs and AJs is further implicated through shared molecular players like Rac1, RhoA, and vinculin. Since the cadherin-catenin complex does not bind actin directly, Nelson lab hypothesizes that actin cytoskeleton is anchored by integrin based focal adhesions co-localized with the cell-cell cadherin based adherens junctions [78], leading to a direct dependence of AJs on FAs.

A recent study from the Nelson lab of epithelial cell behavior on micropatterned E-cadherin and Collagen functionalized surfaces demonstrated the cross-talk between E-cadherin and integrin adhesion complexes for a single cell. The results showed migration and traction force dependence on integrin pathway but directionality and lamellipodia activity is dependant on E-cadherin related signalling [84], leading to dependence of newly forming FAs on AJs. Although cadherin-based binding did not dictate migration rate on the micropatterned surfaces, Leckband group found that E-cadherin expression reduced cell motility in both adhesion dependant and independent manner. Expressing E-cadherin in null breast tumor epithelial cells decreased migration with expression level and with immobilized E-cadherin surface density [85].

Therefore motility is affected by a delicate interplay of both adhesion complexes, which convinces that a mechanical interplay must exist. In migration the connection is shown through the actin cytoskeleton and the mechanosensor molecules involved in both cell-matrix and cell-cell adhesions. Similar to focal adhesions where force is transmitted to the

extracellular environment, in adherens junctions, mechanical force signals must be transmitted between neighboring cells as well [33]. Traction forces in fact have been detected and measured through cadherin mediated adhesions [86, 87]. Although the magnitude of force is lower than that detected in integrin adhesion mediated traction forces, they are significant and similarly increase with increasing substrate rigidity. Furthermore myosin II disruption through blebbistatin shows decrease in cadherin mediated cell-cell adhesion and force generation, again similar to findings in FA studies [80, 87]. Cell-cell adhesion complexes therefore mechanosense stiffness of the neighbor and mechanotransduce contractile myosin II dependant forces.

The cross-talk between FAs and AJs is additionally thought to be in dynamic competition with each other, leading to a regulated balance between cell-cell and cell-ECM adhesion. Sharing same intercellular components, such as Rac1, RhoA, and vinculin, could also contribute to the competition between FAs and AJs. The Differential Adhesion Hypothesis (DAH) addresses this competitive cross-talk through tissue surface tension of intercellular adhesive differences and elegant experimental results [88, 89]. Ryan et al. found that increasing cell-cell adhesion through increased cadherin expression or decreased substrate ligand expression leads to a decrease in cell-substratum adhesion and more tissue like cohesivity [90]. The hypothesis thus supports the competition between cell-cell and cell-matrix adhesions.

## **Cell division**

Cell-matrix adhesion is imperative and necessary in adherent mammalian cells. Furthermore both, integrin and cadherin mediated adhesions and their shared intracellular molecular players have all been found important in cell proliferation.

$\beta$ 1 integrin has been found to associate with epidermal growth factor (EGF) receptor in epithelial cells and be necessary for the cell cycle to proceed to mitotic (G2/M) phase [91].

Integrin dependent activation of the EGF receptor activates extracellular signal-regulated kinase (Erk) and protein kinase B (Akt) dependent growth phase (G1) progression [92]. Rho, actin polymerization, actin-myosin contractility and myosin light chain-dependant contractility are all necessary for cyclin D1 expression and cell cycle progression [33]. FAK has been shown to stimulate cyclin D1 promoter and that cyclin D1 mRNA is a major target for FAK [93-95]. Rac1 also increases c-Jun N-terminal kinases (JNK) and Erk activity which increase proliferation [34].

Both biochemical ECM cues, such ligands as fibronectin and collagen, and mechanical strain have been shown to cause S phase (interphase) entry [33]. Substrate rigidity increases cell proliferation rate [96]. Kumar et al [97] demonstrated that cyclic mechanical strain increases cell proliferation of myoblasts.

Proliferation is also linked to cell-cell adheren junctions. Increase in cytosolic  $\beta$ -catenin acts as a transcription promoter and promotes proliferation [24, 34]. Although under basal conditions cadherins serve as sinks for  $\beta$ -catenin binding and free cytosolic  $\beta$ -catenin levels are kept low by rapid degradation [28]. This normal homeostatic state can be inhibited by Wnt signalling, which is upregulated in tumors [75]. Thus it appears cadherin's capacity to bind and buffer  $\beta$ -catenin is critical during active cell signaling to keep proliferation in check, especially in tumors. Furthermore studies suggest E-cadherin has a capacity to negatively regulate mitogenic signaling through growth factor receptors [28]. But VE-cadherin has been found to stimulate S phase entry in cells with intact actin cytoskeleton and actin-myosin contractility [98].  $\alpha$ -catenin conditional deletions in mouse epithelia cells cause them to be hyperproliferative, multinucleated and more motile [99].

The research on intramolecular pathways of cell division is vast and astounding, which motivated us to look closer at the events of cell division through the extracellular matrix. The mechanical role of the ECM or cell-cell adhesion is very unclear in cell division, especially in mammalian adherent cells. Therefore it is imperative to better understand the

ECM and intercellularly mediated mitotic behavior. In this inherently mechanical process, the dynamic cytoskeletal polymers and motors cooperate and work together to generate the forces necessary for mitosis and cytokinesis in cell division [100]. Intact actin cytoskeleton and retrograde signalling are required for onset of mitosis, but cell-cycle machinery can control the state of actin organization, therefore cell division is a complicated inside-out and outside-in signalling process [101]. Through the actomyosin cytoskeleton engagement, force is generated at the equator during the cytokinesis of a dividing cell to separate it into the two new daughter cells. Myosin-dependent equatorial contraction model has been estimated to contain thousands of myosin molecules and generate maximal contractile force of 1 to 100 nN in the contractile ring [100]. Other computational models of the contractile ring mechanism have been published [102, 103] and raise an interesting question of whether cytokinetic contraction is local to the equator of the division furrow or is global in the cell.

Overall it is clear the mechanical process of dividing the cell body into two daughter cells is a complex system with genetic code, mechanical as well as biochemical sensors, feedback loops and force transducing machinery. The feedback mechanosensory loop has been observed in the early stages of cytokinesis. Mechanical perturbation with micropipette aspiration technique applied to the cortical pole of an early stage dividing cell shows the division process delayed. Myosin II localizes to the stressed and deformed pole and cytokinesis halts until the cell is able to readjust itself. When the cell recovers by rearranging myosin II and cytoskeletal components in the equator ring region, cytokinesis proceeds. However this is not the case in late stage cytokinesis. In late stages, the myosin does not localize to the site of mechanical disturbance. The contractile ring remains intact and cytokinesis continues and cell divides even under mechanical stress [104]. Nonetheless this is even more evidence of an important role force and mechanical stimuli play in cell division, specifically cytokinesis.



Myosin II inhibition experiments of adherent mammalian cell lines showed that substrate adhesion rescues cytokinesis in 90% myosin II inhibited cells. Blebbistatin inhibition only blocked cytokinesis when >95% of myosin was blocked and the observed cellular behavior implicated the inability of the daughter cells to spread in opposing polar direction which caused the failure of scission [105]. All this implicates substrate adhesion as necessary driver in addition to myosin contraction in the equatorial furrow region in the mechanical cytokinetic process.

### **1.3 ECM mimetic in Traction Force Microscopy**

Cell traction forces are crucial and necessary in a range of biological processes such as wound healing, inflammation, angiogenesis and metastasis, which is the specific focus of our work [106]. Mechanical cues of the extracellular environment influence intracellular pathways as discussed in previous section and thus dictate and influence cellular phenotype and behavior. To study the changes in the cell behavior we use quantitative methods of cell spread area, motility, cell-cell interaction and traction force measurements.

Epithelial cellular traction forces originate in the actin polymerization, actomyosin contraction and intracellular protein regulation of the cytoskeleton. The force is transmitted to the Extracellular Matrix (ECM) through the stress fibers via adhesive sites termed Focal Adhesions (FA). These micrometer-sized regions are highly organized and are crucial for cell development, movement and proliferation. Furthermore these adhesions are sensitive to the ECM compliance and adhesivity. FAs serve as not only transmitters of traction but sensors as well. The cell senses biochemical and mechanical adhesivity of the substrate through the integrin mediated FAs. Then the cellular cytoskeleton acts as the contractile force generator and transmits force through these adhesions. The crosslinked actin filament bundles, myosin crossbridges and proteins of the cytoskeleton generate the tension to

contract the cell body [107].

Several experimental setups quantified the mechanosensitivity of FA's through the underlying cell-substrate traction force measurement [107, 108]. There are three methods for cell traction force measurement: cell-embedded protein gel contraction, thin silicone membrane wrinkling and force sensor arrays. The protein gel, usually collagen but may be fibrin, laminin, or basement membrane, method measures change in the free floating gels dimensions to calculate the force exerted [43, 109-112]. The free floating gel contraction method is used for a wide range of cells and biochemical manipulations [112-115]. However published work with this method does not measure traction forces of individual cells, although significant advancements have been made towards 3D traction force calculations [116].

In recent work from Ravichandran group calculations of traction forces in three dimensions were done for 3T3 fibroblasts plated on 2D fibronectin coated polyacrylamide gels [116]. Further applying the calculation theory to individual cells embedded into a 3D gel environment would yield more realistic *in vivo* representative results.

Second method is the thin silicone membrane introduced by Harris et al. in 1981. It was the first to show that individual cells exert force and to be used to determine traction forces during cellular cytokinesis [117]. However the quantitative computational method of this technique does not accurately predict the wrinkles caused by the complex, non-isotropic cellular traction force field.

The third method is the force sensor array. It uses deflection-force relationship in a fabricated elastic substrate. The calibrated null state and elastic theory are used to solve the inverse problem of the traction force required to generate the substrate deformations. Micropatterned elastomers and polyacrylamide gel substrates are the most common substrates used in this type of traction force analysis [107]. The deformation of cell adherent substrate has been measured with patterned elastomers [63, 118, 119], deflection of elastomer pillars

[120-122], and in our lab - specifically functionalized fluorescent bead embedded polyacrylamide gels [9, 44, 123, 124].

A point must be discussed here to address a biological phenomenon called strain stiffening observed only in native biological gels and not in perfectly elastic gels. A synthetic material cannot simulate this native phenomenon of stiffening of the biological material as it gets strained, which prevents large deformation and preserves tissue integrity [125-126]. The biophysical property that is directly related to strain-stiffening behaviour of biopolymer gels is the negative normal stress in response to shear stress [126]. The importance of this phenomenon on a single cell level is that cells have been found to spread even on soft gels, communicate over long distances and influence local and global extracellular environment on such gels, like fibrin gels [127]. Therefore the strain-stiffening property of biologic materials is important in cell motility, cell-cell communication and durotaxis. However due to the non-elastic properties of the fibrin protein gel, a quantitative theory to interpret cell force behavior has not been developed yet. Therefore we use the elastic gel system as the best available quantifiable option.

The gels are fabricated with bis-acrylamide that acts as the cross linker of the acrylamide monomer, Fig. 1.3. The specific ratios of crosslinker to monomeric subunit polymerize into gels with specific elasticity, measured and referenced by Young's Elastic Modulus (Chapter 2). Polyacrylamide gel itself is not adhesive to cells. The surface of the gels is then functionalized with a use of a reactive linker molecule via bulk co-polymerization or surface modification (Chapter 2). Neither method affects the cross linking elastic nor surface mechanical properties of the gel, as characterized in Fig.1.4

The cross linkers used in our protocols are commercially available or lab synthesized acrylic acid *N*-hydroxysuccinimide esters. *N*-6-((acryloyl)amino)hexanoic acid (N6) is a 6 carbon chain linker and is synthesized in accordance with published protocols and considerations [129-132]. Two carbon acrylic acid *N*-hydroxysuccinimide ester (N2) is purchased

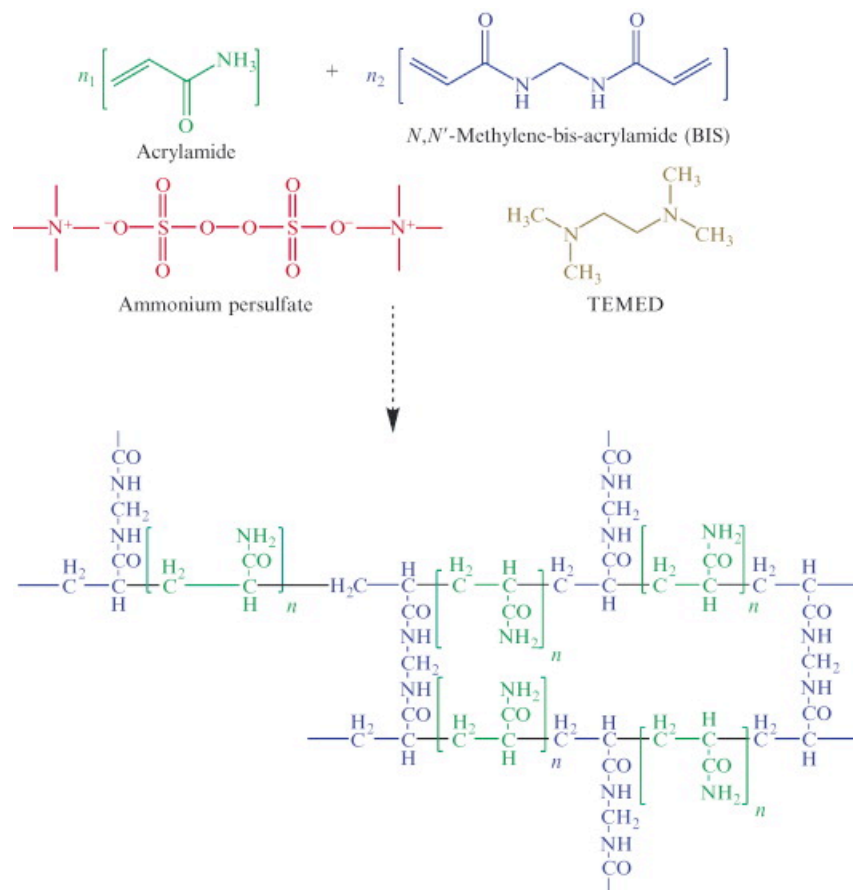


Figure 1.3: Polymerization reaction of polyacrylamide gels.

*N,N'*-Methylene-bis-acrylamide (bis) cross-links acrylamide subunits with the catalytic free radical initiation by ammonium persulfate (APS) and TEMED. Final gel mechanical properties can be controlled by total concentrations of acrylamide and bis, see Chapter 2 for details [128].

from Sigma-Aldrich. In both cross linkers it is the acrylic acid group that covalently bonds the linker to the gel, a reaction that can happen at slightly acidic conditions. The NHS moiety, only in basic conditions, is displaced by the primary amine present on proteins and peptides resulting in a covalent bond between the gel and the ligand [128]. Therefore the gel can be functionalized with any protein and peptide that contains an available amine.

The new functionalization protocol was not only characterized for mechanical properties with Atomic Force Microscopy (AFM) and compared to unconjugated gels, but also the two different linkers, N6 and N2 with and without bis-acrylamide were quantified, Fig. 1.4. The FN ligand surface distribution is more uniform compared to old protocol, Fig. 1.4D. Further quantification of surface FN coverage was done with HRP ELISA method. N2 bound FN surface concentration was found to be increasing with or without bis-acrylamide and compared to N6 as well, Fig. 1.4 D-F.

In this research both conjugation methods were used successfully, although for future experiments the new method is highly recommended. Fibronectin and collagen type I ligands as well as respective binding site peptides, RGD and GFOGER, were used to functionalize the surface for optimal cell adhesion. GFOGER is a newly found interesting peptide in that it has a helical structure but it does not aggregate or forms fibrils in neutral conditions, like its protein inspiration collagen [133-136].

For Traction Force Microscopy (TFM) studies the gels also contain embedded fluorescent beads for displacement tracking of cell deformed substrate. TFM is an essential tool for measuring stresses that cells exert on a hydrogel substrate and thus mechanotransduction on the surface [60, 123, 137, 138]. In our work with use TFM code developed by Dembo and Wang (1999) [132, 137, 139-141].

Cell motility and interaction brightfield images serve to outline cell area of the stress contact region and the null image is obtained with trypsin cell removal (Fig.1.5). The method uses correlation-based optical flow algorithm where a grid is set for the unstressed

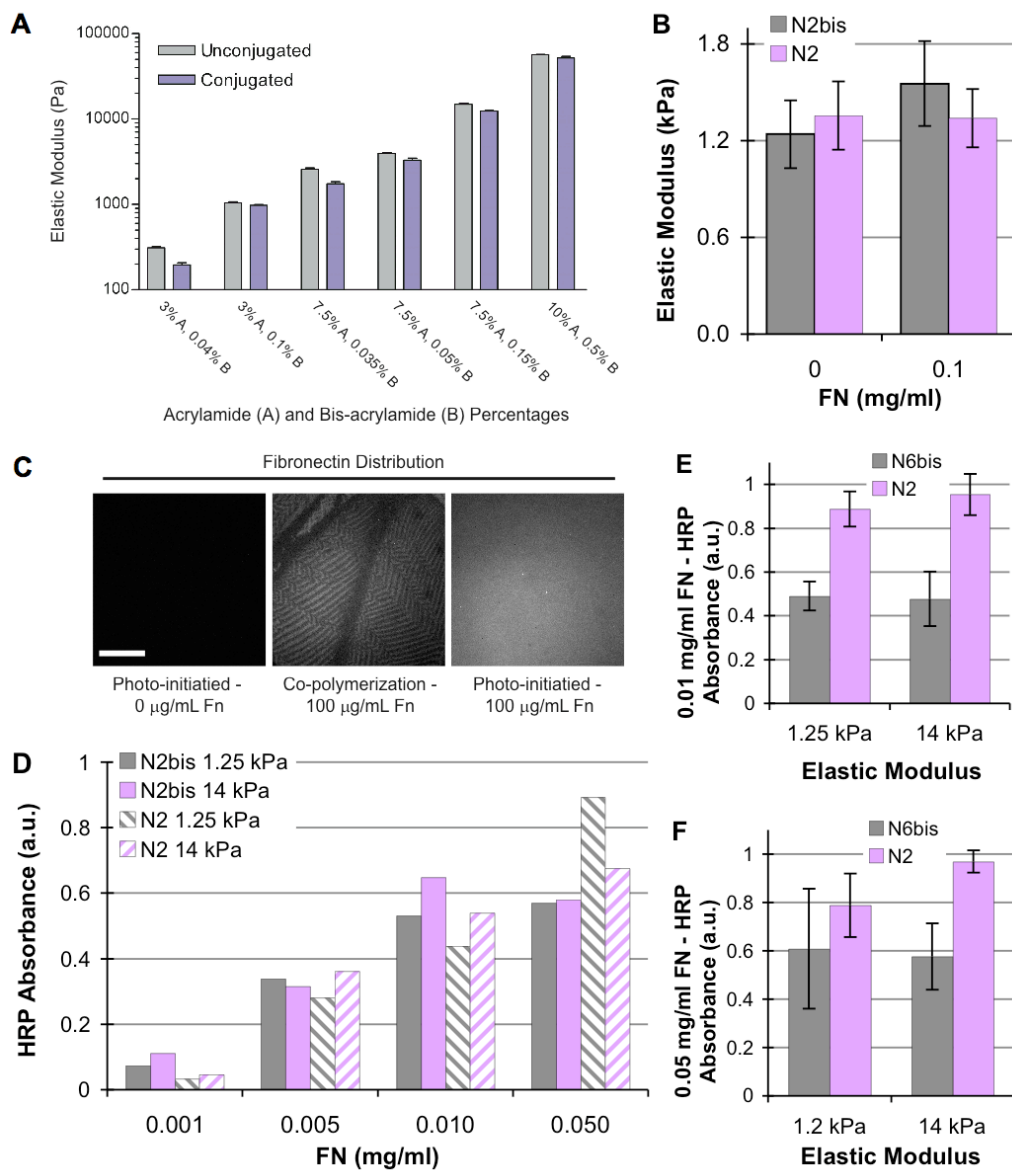


Figure 1.4: Characterization of the new polyacrylamide gel functionalization method. (A) AFM measurements taken over a range of stiffnesses by collaborators in V.M. Weaver lab show no statistical difference between N6+bis-acrylamide (bis) FN conjugated and unconjugated gels. (B) Synthesized 1250 Pa gels (3% acrylamide and 0.2% bis) measure at 1250 Pa elastic modulus average, with AFM, after conjugation with N2 and N2+bis linker, with 0 or 0.1 mg/ml FN functionalization. (C) Fibronectin surface distribution of bulk co-polymerization and new surface functionalization methods, is visualized with Alexa 488 anti-FN fluorescent antibody. Scale bar = 100  $\mu$ m (D-F) Fibronectin surface coverage is quantified with HRP ELISA on soft and stiff gels, 1.25 and 14 kPa respectively. (D) Surface concentration of FN increases with increasing bulk concentration, with and without bis addition on soft and stiff gels. (E and F) FN coverage is plotted for N2 versus N6+bis method as quantified by HRP absorbance at 0.01 and 0.05 mg/ml FN respectively.

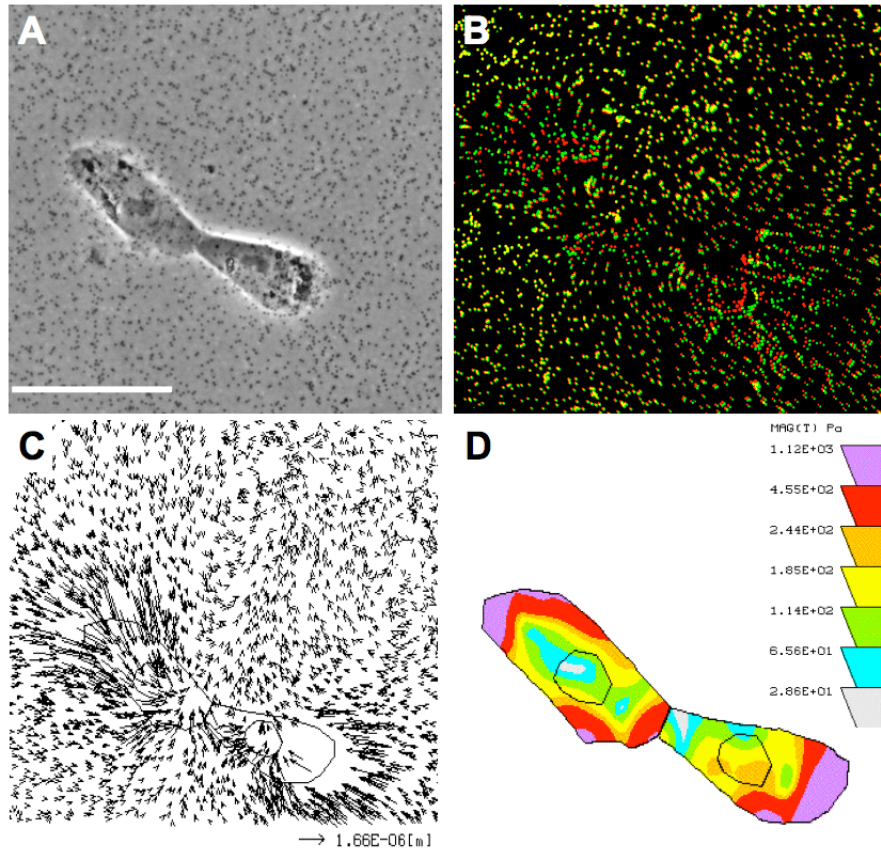


Figure 1.5: Two cell TFM.

EpH4 mouse mammary epithelial cells (A) are depicted for Traction Force Microscopy. Scale bar =  $50 \mu\text{m}$  (B) Fluorescent beads are imaged stressed (red) and relaxed cell-free after trypsin removal (green). Beads further from the cells remain unstressed before and after cell removal, as seen with red and green overlay giving yellow color. (C) Corresponding displacement vectors are calculated with TFM code. (D) Traction force map solution in pseudo color represents the stresses the cells exert onto the substrate (cell size not to scale).

null image to determine the lattice nodes. Then the best correlation is determined between the unstressed nodes and the stressed pixels, with further quadratic interpolation of the optimum to get the best match. The in-plane strain norm is computed not to exceed the maximum strain norm. The distance between the unstressed node and matching stressed pixel then generates the overall displacement field. The displacement field is then corrected to eliminate noise and error due to mismatch.

Next the traction forces are estimated from the displacement field with elastic deformation equations in two dimensions, with an inverse method calculation through [137, 139]. To perform such calculations there are three conditions: a solution must exist, the solution must be unique and the solution depends continuously on the data. This solution method is combined with a forward model that relies on the fact that polyacrylamide gels are linearly elastic and employ elasticity theory. Although recent published data states at higher applied pressures the elasticity of polyacrylamide gels becomes non-linear [142], the range of stress applied by our cells is well below these values.

Dembo method adopts a constraint of a smooth traction field with a Bayesian probability chi-square statistic of the obtained traction map. Furthermore there are constraints that guide the solution, like Newton's laws of total force of the system being equal to zero, since the cell mass is very small nor is the cell accelerating. In two cell model these constraints are important and the theory is discussed in more detail in next section.

Polyacrylamide gel method has its limitations. The traction force solution method utilizing Fourier transform traction cytometry or boundary element methods [139], both reach a limit in small adhesion sizes. Simulation and optimization work is underway to combine a traction reconstruction with point forces method with the two aforementioned ones [143]. However even this method is not optimal because it depends on discrete user-specified adhesion sites, which is faulted if the location of these small adhesions is unknown, such is the case on polyacrylamide gels.



Further limitations of this method are its dependence on concentrated number of fluorescent beads and failure to include bead displacements in z direction. Three dimensional stress is not an uncommon phenomenon for cells that exert larger stresses especially on softer, more porous polyacrylamide substrates. Advancement in force calculations in the third dimension has been recently published [116, 144].

Other methods of traction force calculations such as micropillars have been utilized successfully. In fact the micropillars have been used to study forces exerted by sheets of cells [121]. Findings concluded that the cells on the periphery exerted highest forces onto the substrate and those on the inside of the sheet, much lower [121]. It would also be interesting to find the intercellular forces in the sheet - if these forces are higher on the inside of the sheet versus the periphery. Nonetheless the connection between forces and mechanics of behavior of single cell and multi-cellular tissue is still very much unclear.

There are a few concerns with the micropillar technologies as well, in comparison to the polyacrylamide set up used in this research. Taken into consideration were the facts that ligands are not covalently bonded, but stamped to the PDMS punctate surface and thus uniform concentration and surface ligand density is not easily controlled. There is no deformation or propagation of signal, because the surface is not continuous. Furthermore micro-pillar set up is still in the process of optimization, as studies have found that elastic pillars anchored to elastic underlying substrate (which also deforms) can overestimate the applied forces [145].

TFM has been successfully used to date for numerous insights into cell behavior and phenotype, like force generation during motility, specific molecular knock out or mutant cell lines and intercellular forces, as it is used in this work as well!

## 1.4 TFM definitions and theory for two cells

For two interacting cells,  $c1$  and  $c2$  and let  $r1$  and  $r2$  denote the associated cell-substrate contact regions. The forces exerted on the substrate as a result of cell activity will be described by a 2D traction field,  $\mathbf{T}(\mathbf{x}) \equiv (T_x(\mathbf{x}), T_y(\mathbf{x}))$ . Such forces are mediated by direct cell-substrate contacts and in consequence the associated traction field must vanish outside the contact regions. The traction field at some location  $\mathbf{x}$  is thus said to be “exerted” or “produced” by  $c1$  if  $\mathbf{x} \in r1$  and by  $c2$  if  $\mathbf{x} \in r2$ .

In general, the field of torque density created by a traction field is given by a vector with three components;

$$\mathbf{x} \wedge \mathbf{T} = \begin{bmatrix} \omega_x(\mathbf{x}) \\ \omega_y(\mathbf{x}) \\ \omega_z(\mathbf{x}) \end{bmatrix} = \begin{bmatrix} x_y T_z - x_z T_y \\ x_z T_x - x_x T_z \\ x_x T_y - x_y T_x \end{bmatrix}. \quad (1.1)$$

In the present context however, the position and traction vectors both lie in the plane of the substrate surface which means that  $T_z = x_z = 0$ . As a result,  $\omega_x = \omega_y = 0$  at all points and the torque always corresponds to a simple clockwise or counterclockwise twisting around the  $z$ -axis.

Finite element meshes that exactly cover  $r1$  and  $r2$  allow for any continuous field over these regions to be approximated by a large multi-dimensional vector with discrete components, much as the pixel values of a raster image can approximate a continuous field of light intensity. For example if the mesh covering  $r1$  has  $n_{n1}$  nodes and if the so called “nodal” traction acting at the  $i$ -th node is a vector  $\mathbf{s}_i = (s_{ix}, s_{iy})$ , then the traction field generated by  $c1$  is uniquely specified by giving a vector having  $2n_{n1}$  scalar components;

$$\mathbf{t}_{c1} = (s_{1x}, s_{1y}, s_{2x}, s_{2y} \cdots s_{n_{n1}x}, s_{n_{n1}y})_{c1}. \quad (1.2)$$

When represented in this fashion, the integral of the traction over  $r_1$  is given by a finite sum;

$$\int_{r_1} \mathbf{T} dx dy = \begin{bmatrix} \sum_{i \in r_1} s_{ix} a_i \\ \sum_{i \in r_1} s_{iy} a_i \end{bmatrix} = \begin{bmatrix} \langle T_x \rangle_{c1} \\ \langle T_y \rangle_{c1} \end{bmatrix} \equiv \langle \mathbf{T} \rangle_{c1}. \quad (1.3)$$

where  $a_i$  is the area of the “pixel” associated with the  $i$ -th mesh node. Simplified notation of the numerical integral of an arbitrary function  $f(\mathbf{x})$  over  $r_1$  is denoted by the symbol  $\langle f \rangle_{c1}$ , extended to the case of Cartesian traction vectors over  $r_1$ .

The special cases  $\langle 1 \rangle_{c1}$  or  $\langle 1 \rangle_{c2}$  correspond to the integrals of the function  $f = const = 1$ , over the contact regions. These brackets are thus identical to the areas of  $r_1$  and  $r_2$  respectively. The average value of a scalar function,  $f(\mathbf{x})$ , over one or the other contact region is defined by a ratio of area integrals (e.g.  $\langle f \rangle_{c1} / \langle 1 \rangle_{c1}$ ). We will denote the area integral with pearly brackets “{}”, such that  $\{\mathbf{T}\}_{c1}$  will be completely equivalent to writing out the ratio  $\langle \mathbf{T} \rangle_{c1} / \langle 1 \rangle_{c1}$ .

To further illustrate the bracket notation for integrals and averages, consider the root-mean-square average of the traction over  $c_1$ :

$$\sqrt{\{\mathbf{T} \cdot \mathbf{T}\}_{c1}} = \sqrt{\{T_x^2\}_{c1} + \{T_y^2\}_{c1}}. \quad (1.4)$$

A related but quite distinct quantity is the area average of the traction magnitude;

$$\{\|\mathbf{T}\|\}_{c1} = \left\{ \sqrt{T_x^2 + T_y^2} \right\}_{c1}. \quad (1.5)$$

As yet another example, consider the integral of the torque generated by  $c_1$ ;

$$\langle \mathbf{x} \wedge \mathbf{T} \rangle_{c1} = \mathbf{k} \langle \omega_z \rangle_{c1} \equiv \mathbf{k} \sum_{i \in r_1} (x_{ix} s_{iy} - x_{iy} s_{ix}) a_i. \quad (1.6)$$

Further we defined angle between traction vector fields of two cells as

$$\cos\vartheta = \frac{\langle \mathbf{T} \rangle_{c1} \cdot \langle \mathbf{T} \rangle_{c2}}{|\langle \mathbf{T} \rangle_{c1}| |\langle \mathbf{T} \rangle_{c2}|}. \quad (1.7)$$

## Newtons Laws

To allow the possibility of cell-cell mechanical linkage, then the total force acting on c1, can be broken into a sum of two terms;

$$\mathbf{F}_1 = \mathbf{F}_{s1} + \mathbf{F}_{21}, \quad (1.8)$$

where  $\mathbf{F}_{s1}$  is the force on c1 from contact with the substrate and  $\mathbf{F}_{21}$  is the force from contact with c2. Using logical symmetry, the total force acting on c2 is given in similar fashion. Corrections involved in neglecting factors such as gravitational forces, pressure forces, buoyancy and viscous forces from culture medium are all very small for the conditions of the present study.

Applying the 1st law of motion, (action and reaction), to c1 and c2 considered as closed mechanical systems, the force on c1 from c2 must be exactly the opposite of the force on c2 from c1;

$$\mathbf{F}_{21} = -\mathbf{F}_{12}. \quad (1.9)$$

We also conclude that the force acting on a given cell from the substrate must be the negative of the force on the substrate from the given cell. But as discussed in the last section, the force on the substrate from a cell is the integral of  $\mathbf{T}(\mathbf{x})$  over the appropriate contact region. Hence, making use of our bracket notation;

$$\begin{aligned} \mathbf{F}_{s1} &= -\langle \mathbf{T} \rangle_{c1}, \quad \text{and,} \\ \mathbf{F}_{s2} &= -\langle \mathbf{T} \rangle_{c2}. \end{aligned} \quad (1.10)$$

Suppose now that  $c1$  and  $c2$  have masses  $m_1$  and  $m_2$  and that their centers-of-mass are accelerating at rates  $\mathbf{a}_1$  and  $\mathbf{a}_2$ . Combining Eqs. 1.9 and 1.10 with Eq. 1.8 yields the following expressions for the 2nd law of motion for  $c1$  and  $c2$ ;

$$\begin{aligned} m_1 \mathbf{a}_1 = \mathbf{F}_1 &= -\langle \mathbf{T} \rangle_{c1} + \mathbf{F}_{21}, \quad \text{and,} \\ m_2 \mathbf{a}_2 = \mathbf{F}_2 &= -\langle \mathbf{T} \rangle_{c2} - \mathbf{F}_{21}. \end{aligned} \tag{1.11}$$

The mass of a typical cell (e.g. fibroblast) is  $\sim 10^{-11}$  kg and the acceleration exhibited by its center of mass is typically less than  $\sim 10^{-8}$  m/sec<sup>2</sup>. From this it follows that the  $m\mathbf{a}$  terms on the left of the last two equations are very small (less than one millionth of a pico-Newton). In comparison, the force produced by a typical myosin motor, or by a single polymerizing actin filament, is on the order of 10 pico-Newtons. We may therefore safely conclude that for studies related to cell motion, the expression  $\mathbf{F} = m\mathbf{a}$  reduces to the special form  $\mathbf{F} = 0$ .

This simplification means that the various driving forces acting on the cell-cell and cell-substrate interfaces must exactly counterbalance each other;

$$0 = -\langle \mathbf{T} \rangle_{c1} + \mathbf{F}_{21}, \quad \text{and,} \tag{1.12}$$

$$0 = -\langle \mathbf{T} \rangle_{c2} - \mathbf{F}_{21}. \tag{1.13}$$

Adding Eq. 1.12 and Eq. 1.13 causes cancellation of the cell-cell forces and yields the expected result for global force balance of the cell pair as a whole;

$$0 = [\langle \mathbf{T} \rangle_{c1} + \langle \mathbf{T} \rangle_{c2}]. \tag{1.14}$$

On the other hand subtracting the equations and rearranging allows us to directly calculate

the cell-cell force;

$$\mathbf{F}_{21} = \frac{1}{2} [\langle \mathbf{T} \rangle_{c1} - \langle \mathbf{T} \rangle_{c2}]. \quad (1.15)$$

Magnitude of the interaction force than can be derived by taking the dot product of Eqs 1.12 and 1.13;

$$|\mathbf{F}_{21}| = \mathbf{F}_{21} \cdot \mathbf{F}_{21} = -\langle \mathbf{T} \rangle_{c1} \cdot \langle \mathbf{T} \rangle_{c2}. \quad (1.16)$$

The force  $\mathbf{F}_{21}$  corresponds to the rate of momentum transfer from c2 to c1 (opposite to the transfer from c1 on c2). Such inter-cellular momentum fluxes are tiny and occur in the intricate cleft of the cell-cell interface. It is therefore difficult or impossible to observe them by any known direct mechanical method. On the other hand we now see that Eqs. 1.15 and 1.16 provide unambiguous ways to express these “invisible” cell-cell forces in terms of traction integrals that can be directly measured. The present study is the first to show that measurement of cell-cell forces is feasible, significant and temporally dynamic.

In addition to inter-cell forces we also study and apply the theories to inter-cell torques. Thus we derived equations that relate the torque exerted on c1 by c2,  $\mathbf{\Omega}_{21}$ , with measurable integrals of torques exerted across the cell-substrate contact;

$$\begin{aligned} 0 &= -\langle \mathbf{x} \wedge \mathbf{T} \rangle_{c1} + \mathbf{\Omega}_{21}, \quad \text{and,} \\ 0 &= -\langle \mathbf{x} \wedge \mathbf{T} \rangle_{c2} - \mathbf{\Omega}_{21}. \end{aligned} \quad (1.17)$$

As previously, we further conclude that the inter-cell torque is given by a difference of two integrals;

$$\begin{aligned} \mathbf{\Omega}_{21} &= \frac{1}{2} [\langle \mathbf{x} \wedge \mathbf{T} \rangle_{c1} - \langle \mathbf{x} \wedge \mathbf{T} \rangle_{c2}] \\ &= \frac{1}{2} \mathbf{k} [\langle \omega_z \rangle_{c1} - \langle \omega_z \rangle_{c2}], \end{aligned} \quad (1.18)$$

and that the magnitude is a dot product;

$$|\mathbf{\Omega}_{21}| = \mathbf{\Omega}_{21} \cdot \mathbf{\Omega}_{21} = -\langle \omega_z \rangle_{c1} \cdot \langle \omega_z \rangle_{c2} . \quad (1.19)$$

Torques are not commonly encountered in cell biology and indeed a very strange idea to think of two interacting cells as though they were a couple of gears in a wristwatch ratcheting and shearing against each other. The strangeness of these ideas is all the more reason why we discuss them and make some estimate about the magnitude and character of the cell-cell torque.

## Statistical Considerations

Quantities like cellular traction integrals have two values; ideal *exact* values that exist only in theory and real *measured* values that are derived in an experiment. One may acknowledge this distinction by using a Tilda to denote the measured value corresponding to some exact quantity. Thus the experimentally measured traction field reported by the LIBTRC code may be denoted by  $\tilde{\mathbf{T}}(\mathbf{x})$  . Likewise, the vector representation of the experimental traction with respect to a mesh over r1 is vector with many scalar components;

$$\tilde{\mathbf{t}}_{c1} = \left( \tilde{s}_{1x}, \tilde{s}_{1y}, \tilde{s}_{2x}, \tilde{s}_{2y} \cdots \tilde{s}_{n_1x}, \tilde{s}_{n_1y} \right)_{c1} . \quad (1.20)$$

As a general proposition, experimental and exact variables are related according to equations of the form;

$$\tilde{\mathbf{T}}(\mathbf{x}) = \mathbf{T}(\mathbf{x}) + \boldsymbol{\varepsilon}(\mathbf{x}) \quad (1.21)$$

where  $\boldsymbol{\varepsilon}$ , the “experimental error”, is a scalar or a vector with random numbers as components. These numbers are drawn from a distribution with mean=0 and with stdev=  $\sigma_{\boldsymbol{\varepsilon}}$ .

Any integral of an experimental traction field is related to a corresponding exact integral

as one would expect. For example,

$$\begin{aligned}\langle \tilde{\mathbf{T}} \rangle_{c1} &= \langle \mathbf{T} \rangle_{c1} + \langle \boldsymbol{\varepsilon} \rangle_{c1} \\ &= \begin{bmatrix} \langle T_x \rangle_{c1} \\ \langle T_y \rangle_{c1} \end{bmatrix} + \begin{bmatrix} \langle \varepsilon_x \rangle_{c1} \\ \langle \varepsilon_y \rangle_{c1} \end{bmatrix}.\end{aligned}\tag{1.22}$$

In view of Eqs. 1.12 and 1.13 it follows that;

$$\begin{bmatrix} \langle \tilde{T}_x \rangle_{c1} \\ \langle \tilde{T}_y \rangle_{c1} \end{bmatrix} = \begin{bmatrix} F_{x,21} \\ F_{y,21} \end{bmatrix} - \begin{bmatrix} \langle \varepsilon_x \rangle_{c1} \\ \langle \varepsilon_y \rangle_{c1} \end{bmatrix}, \quad \text{and,}\tag{1.23}$$

$$\begin{bmatrix} \langle \tilde{T}_x \rangle_{c2} \\ \langle \tilde{T}_y \rangle_{c2} \end{bmatrix} = \begin{bmatrix} -F_{x,21} \\ -F_{y,21} \end{bmatrix} - \begin{bmatrix} \langle \varepsilon_x \rangle_{c2} \\ \langle \varepsilon_y \rangle_{c2} \end{bmatrix}.\tag{1.24}$$

Combining these expressions to eliminate  $F_{x,21}$  and  $F_{y,21}$ , we derive the following general relation between the experimental traction integrals of two interacting cells;

$$\langle \tilde{T}_\beta \rangle_{c1} = -\langle \tilde{T}_\beta \rangle_{c2} - (\langle \varepsilon_\beta \rangle_{c2} + \langle \varepsilon_\beta \rangle_{c1}) \text{ where } \beta = x, y.\tag{1.25}$$

This relation should be valid for all interacting cell pairs regardless of the physiological circumstances, background traction magnitudes, experimental error and for either the x or the y components of traction.

From Eq. 1.25 it is clear that an integral of the experimental traction produced by a cell is always the sum of an exact part and an error term. The exact part is a weighted sum of many large nodal tractions that need to satisfy constraints of force balance. These exact terms are thus systematically organized into blocks or subgroups of opposing forces that tend to cancel each other except for a small residual. On the other hand the error part of an integral is composed of individual terms that may be small on a point by point percentage



basis but that are random and are not subject to systematic global constraints. Thus the nodal errors do not cancel very efficiently and the percentage error of a traction integral tends to be much larger than the percentage error of its component terms.

Applying Eqs. 1.14 and 1.15 results in an approximation of the cell-cell force derived by using measured integrals instead of exact integrals. Rearranging Eq. 1.25 and substituting the result into Eqs. 1.14 and 1.15 and rearranging Eqs. 1.23 and 1.24 yields

$$\langle \tilde{\mathbf{T}} \rangle_{c1} + \langle \tilde{\mathbf{T}} \rangle_{c2} = -(\langle \boldsymbol{\varepsilon} \rangle_{c1} + \langle \boldsymbol{\varepsilon} \rangle_{c2}), \quad \text{and}, \quad (1.26)$$

$$\langle \tilde{\mathbf{T}} \rangle_{c1} - \langle \tilde{\mathbf{T}} \rangle_{c2} = 2\mathbf{F}_{21} + (\langle \boldsymbol{\varepsilon} \rangle_{c2} - \langle \boldsymbol{\varepsilon} \rangle_{c1}). \quad (1.27)$$

One may conclude from this that the left of Eq 1.26 defines a certain noise level and that the left of Eq.1.27 corresponds to the sum of a noise term with identical properties, superimposed on a signal that we wish to detect (the value of  $\mathbf{F}_{21}$ ). In order for us to detect the signal accurately, the absolute value of the signal-plus-noise, i.e.  $|\langle \tilde{\mathbf{T}} \rangle_{c1} - \langle \tilde{\mathbf{T}} \rangle_{c2}|$ , should typically be much bigger than the absolute value of the noise alone, i.e.  $|\langle \tilde{\mathbf{T}} \rangle_{c1} + \langle \tilde{\mathbf{T}} \rangle_{c2}|$ .

From the usual bootstrap analysis of traction maps we know that the error vectors associated with the individual nodal tractions are uniform in space and randomly orientated. On the other hand if we consider sets of images of different cells or of the same cell at different times, then the magnitude of the error from image to image tends to vary in a way that correlates with the magnitude of the largest nodal traction. This happens because the parts of an image where the tractions are intense tend to overshadow the parts where the traction are small, just as an intense light source will tend to overshadow a weak source. We may conclude from this that in a given image of interacting cells, the magnitude of terms like,  $(\langle \boldsymbol{\varepsilon} \rangle_{c1} + \langle \boldsymbol{\varepsilon} \rangle_{c2})$  and  $(\langle \boldsymbol{\varepsilon} \rangle_{c2} - \langle \boldsymbol{\varepsilon} \rangle_{c1})$ , will scale in proportion to measures of the background traction magnitude (e.g.  $\langle |\tilde{\mathbf{T}}| \rangle_{c1} + \langle |\tilde{\mathbf{T}}| \rangle_{c2}$ ). Since there are usually consider-

able variations in background traction, the signal-to-noise ratio in different images will also fluctuate. Fortunately these fluctuations can be compensated by appropriate scaling of the signal.

The scaling of the traction signals should be particularly useful to demonstrate the temporal dynamics of cell-cell interaction forces. Thus we will define the scaled non-dimensional traction “residuals” as:

$$C_- = \frac{|\langle \tilde{\mathbf{T}} \rangle_{c1} - \langle \tilde{\mathbf{T}} \rangle_{c2}|}{\langle |\tilde{\mathbf{T}}| \rangle_{c1} + \langle |\tilde{\mathbf{T}}| \rangle_{c2}}, \quad \text{and}, \quad (1.28)$$

$$C_+ = \frac{|\langle \tilde{\mathbf{T}} \rangle_{c1} + \langle \tilde{\mathbf{T}} \rangle_{c2}|}{\langle |\tilde{\mathbf{T}}| \rangle_{c1} + \langle |\tilde{\mathbf{T}}| \rangle_{c2}}. \quad (1.29)$$

The normalization of these residuals is intended to insure that the signal/noise level is constant.  $C_-$  and  $C_+$  should both undergo similar random fluctuations with the same mean and variance when the cells are not in physical contact. The value of  $C_-$  should be at higher level for cells in contact, as the interaction forces become significant. The values of  $C_+$  should remain flat regardless of contact, since the normalization removes effects due to changes in background contractile activity. The key prediction tested with this analysis is that  $C_+ \lesssim C_-$  when cells are in contact and  $C_+ \approx C_-$  when cells are separated.

Equations 1.26 and 1.27 can also be used to devise formal tests for accepting or rejecting the “null interaction hypothesis”:  $\mathbf{F}_{21} = 0$ . Student t-test is performed to test the null hypothesis of  $\mathbf{F}_{21} = 0$ , by comparing Eqs. 1.26 and 1.27 implying that  $\langle \tilde{\mathbf{T}} \rangle_{c1} + \langle \tilde{\mathbf{T}} \rangle_{c2}$  and  $\langle \tilde{\mathbf{T}} \rangle_{c1} - \langle \tilde{\mathbf{T}} \rangle_{c2}$  (or equivalently  $C_+$  and  $C_-$ ), and statistical significance is presented in experimental results.

## 1.5 Hypothesis and Thesis overview

In our experimental approach to study breast cancer invasiveness and metastasis as a function of extracellular matrix, we engineer an ECM mimetic surface where both the biochemical and mechanical properties can be varied simultaneously. This *in vitro* platform allows us to study phenotype changes in normal non-transformed cells as function of only extracellular environment cues. It is a very controlled system that can decouple and at the same time combine the affect of the two cues to give novel results. Furthermore the quantified behavior can be linked to the intracellular components to study the key proteins in a physiologically meaningful ways. The experimental set up is described in detail in Chapter 2.

Our initial question started at the unique lumen containing structure of the mammary glands called the acini. Specifically, applying the ideas of adhesive dynamics and the differential adhesion hypothesis, we set up to show that if the cell-matrix adhesion can be engineered to decrease below an energetically favored minimum, the cell-cell adhesion will drive the mammary epithelial cells to form the interesting acinar structures. Moreover we wanted to confirm if there exists a universal compliance switch, around 1000 Pa, below which the cell-cell adhesion would drive the formation of almost native looking structures, in our case 3D spheres, just like the networks observed in endothelial cells [124, 146].

Although it has been shown before that motility goes through a maximum as a function of matrix stiffness in smooth muscle cells, we further ask if the similar result exists in mammary epithelial cells and as a function of biochemical matrix cues. Furthermore we wanted to see if in stride with the differential adhesion hypothesis, cell-cell adhesion will play a role in cell motility as well. All this work is reported in Chapter 3.

The motility and cell-cell inhibition results of Chapter 3 raised questions of cross-talk between the two adhesion platforms. In Chapter 4 I explore the question of cell-cell and cell-matrix adhesion through traction force results. The biphasic motility results and cell-

cell contact duration inhibition of motile behavior shaped my hypothesis: it takes intermediate force to elicit maximum motility and cell-cell adhesion will increase this force requirement. To my surprise the predicted outcome was observed in experimental data. Further interesting cell area, force, and cell-cell tension and velocity relationships emerged. In this Chapter 4, I further tested  $\beta$ -catenin, the intracellular component of that links cell-cell adhesions to the cytoskeleton and its affect on traction force profile of the cell.

My observed and reported connection between the cell-cell and cell-matrix interactions and the computational ability of traction force microscopy guided me to take a more detailed look at cell-cell interaction force dynamics and temporal resolution of the behavior through the underlying ECM substrate. Force vectors, angles and even torque are discussed for two interacting cells in Chapter 5.

In the last question of ECM driven cancer progression I focused on cell division and cytokinesis. In adherent mammalian cells adhesion to the underlying ECM is imperative in cell survival, but the mechanics of the division cycle have not been studied or fully understood through the cellular environment. In Chapter 6 of this thesis I report novel findings of cell division and cytokinesis force dynamics through the underlying gel. Furthermore, the role of myosin II mediated contractile ring constriction as the cytokinetic driver of daughter cell abscission is put to the test via blebbistatin and Y-27632 inhibition traction force experiments. All these novel and interesting results shed light on the mechanics of cell division through the ECM, a process that has not been previously studied.

In Chapter 7, I close the thesis with future directions and ideas of further important cell invasiveness and metastasis questions and hypothesis to test.

## 1.6 Bibliography

1. Bendre M., D. Gaddy, R. W. Nicholas, and L. J. Suva. Breast cancer metastasis to bone: it is not all about PTHRP. *Clinical Orthopology Related Research*, (415):S39–45, Oct 2003.
2. Ronnov-Jessen L., O. W. Petersen, and M. J. Bissell. Cellular changes involved in conversion of normal to malignant breast: importance of the stromal reaction. *Physiological Reviews*, 76(1):69–125, Jan 1996.
3. Williams C. M., A. J. Engler, R. D. Slone, L. L. Galante, and J. E. Schwarzbauer. Fibronectin expression modulates mammary epithelial cell proliferation during acinar differentiation. *Cancer Research*, 68(9):3185–92, May 2008.
4. Ronnov-Jessen L. and M. J. Bissell. Breast cancer by proxy: can the microenvironment be both the cause and consequence? *Trends in Molecular Medicine*, 15(1):5–13, Jan 2009.
5. Kass L., J. T. Erler, M. Dembo, and V. M. Weaver. Mammary epithelial cell: influence of extracellular matrix composition and organization during development and tumorigenesis. *The International Journal of Cell Biology and Biochemistry*, 39(11):1987–94, 2007.
6. Ioachim E., A. Charchanti, E. Briasoulis, V. Karavasilis, H. Tsanou, D. L. Arvanitis, N. J. Agnantis, and N. Pavlidis. Immunohistochemical expression of extracellular matrix components tenascin, fibronectin, collagen type iv and laminin in breast cancer: their prognostic value and role in tumour invasion and progression. *European Journal of Cancer*, 38(18): 2362–70, Dec 2002.
7. Soikkeli J., P. Podlasz, M. Yin, P. Nummela, T. Jahkola, S. Virolainen, L. Krogerus, P. Heikkila, K. von Smitten, O. Saksela, and E. Holtta. Metastatic outgrowth en-

- compasses col-I, fn1, and postn up-regulation and assembly to fibrillar networks regulating cell adhesion, migration, and growth. *The American Journal of Pathology*, 177(1): 387–403, Jul 2010.
8. Levental K. R. and H. Yu, L. Kass, J. N. Lakins, M. Egeblad, J. T. Erler, S. F. Fong, K. Csiszar, A. Giaccia, W. Weninger, M. Yamauchi, D. L. Gasser, and V. M. Weaver. Matrix crosslinking forces tumor progression by enhancing integrin signaling. *Cell*, 139(5):891–906, 2009.
  9. Paszek M. J. and N. Zahir, K. R. Johnson, J. N. Lakins, G. I. Rozenberg, A. Gefen, C. A. Reinhart-King, S. S. Margulies, M. Dembo, D. Boettiger, D. A. Hammer, and V. M. Weaver. Tensional homeostasis and the malignant phenotype. *Cancer Cell*, 8(3):241–254, 2005.
  10. Butcher D. T., T. Alliston, and V. M. Weaver. A tense situation: forcing tumour progression. *Nature Reviews of Cancer*, 9(2):108–22, 2009.
  11. Levental I., P. C. Georges, and P. A. Janmey. Soft biological materials and their impact on cell function. *Soft Matter*, 3(3):299–306, 2007.
  12. Levental I., K. R. Levental, E. A. Klein, R. K. Assoian, R. T. Miller, R. G. Wells, and P. A. Janmey. A simple indentation device for measuring micrometer scale tissue stiffness. *Journal of Physics: Condensed Matter*, 22, 2010.
  13. Boyd N. F., G. A. Lockwood, J. W. Byng, D. L. Tritchler, and M. J. Yaffe. Mammographic densities and breast cancer risk. *Cancer Epidemiology Biomarkers Prev*, 7(12): 1133–44, Dec 1998.
  14. Koukoulis G. K., A. A. Howedy, M. Korhonen, I. Virtanen, and V. E. Gould. Distribution of tenascin, cellular fibronectins and integrins in the normal, hyperplas-

- tic and neoplastic breast. *Journal of Submicroscopic Cytology and Pathology*, 25 (2):285–95, Apr 1993.
15. Wittekind C. and M. Neid. Cancer invasion and metastasis. *Oncology*, 69:14–6, 2005.
  16. Grivennikov S. I., F. R. Greten, and M. Karin. Immunity, inflammation, and cancer. *Cell*, 140(6):883–99, Mar 2010.
  17. Glukhova M., V. Koteliansky, X. Sastre, and J. P. Thiery. Adhesion systems in normal breast and in invasive breast carcinoma. *The American Journal of Pathology*, 146(3): 706–16, Mar 1995.
  18. Bissell M. J., D. C. Radisky, A. Rizki, V. M. Weaver, and O. W. Petersen. The organizing principle: microenvironmental influences in the normal and malignant breast. *Differentiation*, 70(9-10):537–46, Dec 2002.
  19. Weaver V. M., O. W. Petersen, F. Wang, C. A. Larabell, P. Briand, C. Damsky, and M. J. Bissell. Reversion of the malignant phenotype of human breast cells in three-dimensional culture and in vivo by integrin blocking antibodies. *Journal of Cell Biology*, 137(1):231–45, Apr 1997.
  20. Yonemura S., Wada Y, Watanabe T, Nagafuchi A, Shibata M. alpha-Catenin as a tension transducer that induces adherens junction development. *Nature Cell Biology*, 12(6):533-42, Jun 2010.
  21. Dejana E., G. Bazzoni, and M. G. Lampugnani. The role of endothelial cell-to-cell junctions in vascular morphogenesis. *Thrombosis and Haemostasis*, 82(2):755–61, Aug 1999.

22. Goodwin M. and A. S. Yap. Classical cadherin adhesion molecules: coordinating cell adhesion, signaling and the cytoskeleton. *Journal of Molecular Histology*, 35(8-9):839–44, Nov 2004.
23. Gumbiner B. M. Cell adhesion: the molecular basis of tissue architecture and morphogenesis. *Cell*, 84(3):345–57, Feb 1996.
24. Christofori G. and H. Semb. The role of the cell-adhesion molecule e-cadherin as a tumour-suppressor gene. *Trends in Biochemical Sciences*, 24(2):73–6, 1999.
25. Brugmans M., J. J. Cassiman, and H. van den Berghe. Selective adhesion and impaired adhesive properties of transformed cells. *Journal of Cell Science*, 33:121–32, Oct 1978.
26. Coman D. R. Mechanism of the invasiveness of cancer. *Science*, 105:347–8, Apr 1947.
27. Birchmeier W., K. M. Weidner, J. Hulsken, and J. Behrens. Molecular mechanisms leading to cell junction (cadherin) deficiency in invasive carcinomas. *Seminars in Cancer Biology*, 4(4):231–9, Aug 1993.
28. Jeanes A., C. J. Gottardi, and A. S. Yap. Cadherins and cancer: how does cadherin dysfunction promote tumor progression? *Oncogene*, 27(55):6920–9, Nov 2008.
29. Hajra K. M. and E. R. Fearon. Cadherin and catenin alterations in human cancer. *Genes Chromosomes Cancer*, 34(3):255–68, Jul 2002.
30. Benjamin J. M. and W. J. Nelson. Bench to bedside and back again: molecular mechanisms of alpha-catenin function and roles in tumorigenesis. *Seminars in Cancer Biology*, 18(1):53–64, Feb 2008.



31. Effler J. C., P. A. Iglesias, and D. N. Robinson. A mechanosensory system controls cell shape changes during mitosis. *Cell Cycle*, 6(1):30–35, 2006.
32. Sagona A. P. and H. Stenmark. Cytokinesis and cancer. *FEBS Letters*, 584(12): 2652–61, 2010.
33. Walker J. L., A. K. Fournier, and R. K. Assoian. Regulation of growth factor signaling and cell cycle progression by cell adhesion and adhesion-dependent changes in cellular tension. *Cytokine and Growth Factor Reviews*, 16 (4-5):395–405, 2005.
34. Danen E. H. and K. M. Yamada. Fibronectin, integrins, and growth control. *Journal of Cellular Physiology*, 189(1):1–13, 2001.
35. Nannuru K. C. and R. K. Singh. Tumor-stromal interactions in bone metastasis. *Current Osteoporosis Reports*, 8(2):105–13, Jun 2010.
36. Coleman R. E. Clinical features of metastatic bone disease and risk of skeletal morbidity. *Clinical Cancer Research*, 12(20 Pt 2): 6243–49, Oct 2006.
37. Suva L. J., R. J. Griffin, and I. Makhoul. Mechanisms of bone metastases of breast cancer. *Endocrine-Related Cancer*, 16(3):703–13, Sep 2009.
38. Muller A., B. Homey, H. Soto, N. Ge, D. Catron, M. E. Buchanan, T. McClanahan, E. Murphy, W. Yuan, S. N. Wagner, J. L. Barrera, A. Mohar, E. Verastegui, and A. Zlotnik. Involvement of chemokine receptors in breast cancer metastasis. *Nature*, 410(6824):50–6, Mar 2001.
39. Shields J. D. , M. E. Fleury, C. Yong, A. A. Tomei, G. J. Randolph, and M. A. Swartz. Autologous chemotaxis as a mechanism of tumor cell homing to lymphatics via interstitial flow and autocrine CCR7 signaling. *Cancer Cell*, 11(6):526–38, Jun 2007.

40. Decaestecker C., O. Debeir, P. Van Ham, and R. Kiss. Can anti-migratory drugs be screened in vitro? A review of 2D and 3D assays for the quantitative analysis of cell migration. *Medicinal research reviews*, 27(2):149–76, Mar 2007.
41. Ingber D. E. Can cancer be reversed by engineering the tumor microenvironment? *Seminars in Cancer Biology*, 18(5):356–64, Oct 2008.
42. Santhanam A. N., A. R. Baker, G. Hegamyer, D. A. Kirschmann, and N. H. Colburn. Pcd4 repression of lysyl oxidase inhibits hypoxia-induced breast cancer cell invasion. *Oncogene*, 29(27):3921–32, Jul 2010.
43. Wozniak M. A., K. Modzelewska, L. Kwong, and P. J. Keely. Focal adhesion regulation of cell behavior. *Biochimica et Biophysica Acta*, 1692(2-3): 103–19, Jul 2004.
44. Jannat R. A., M. Dembo, and D. A. Hammer. Neutrophil adhesion and chemotaxis depend on substrate mechanics. *Journal of Physics: Condensed Matter*, 22(19):194117, May 2010.
45. Jiang G., G. Giannone, D. R. Critchley, E. Fukumoto, and M. P. Sheetz. Two-picoNewton slip bond between fibronectin and the cytoskeleton depends on talin. *Nature*, 424(6946):334–7, Jul 2003.
46. Priddle H., L. Hemmings, S. Monkley, A. Woods, B. Patel, D. Sutton, G. A. Dunn, D. Zicha, and D. R. Critchley. Disruption of the talin gene compromises focal adhesion assembly in undifferentiated but not differentiated embryonic stem cells. *Journal of Cell Biology*, 142(4):1121–33, Aug 1998.
47. Ziegler W. H., A. R. Gingras, D. R. Critchley, and J. Emsley. Integrin connections to the cytoskeleton through talin and vinculin. *Biochemical Society Transactions*, 36(Pt 2):235–9, Apr 2008.

48. Critchley D. R. and A. R. Gingras. Talin at a glance. *Journal of Cell Science*, 121(Pt 9):1345–7, May 2008.
49. Fillingham I., A. R. Gingras, E. Papagrigoriou, B. Patel, J. Emsley, D. R. Critchley, G. C. K. Roberts, and I. L. Barsukov. A vinculin binding domain from the talin rod unfolds to form a complex with the vinculin head. *Structure*, 13(1):65–74, Jan 2005.
50. Lee S. E., R. D. Kamm, and M. R. K. Mofrad. Force-induced activation of talin and its possible role in focal adhesion mechanotransduction. *Journal of Biomechanics*, 40(9):2096–106, 2007.
51. Papagrigoriou E., A. R. Gingras, I. L. Barsukov, N. Bate, I. J. Fillingham, B. Patel, R. Frank, W. H. Ziegler, G. C. K. Roberts, D. R. Critchley, and J. Emsley. Activation of a vinculin-binding site in the talin rod involves rearrangement of a five-helix bundle. *The EMBO Journal*, 23(15):2942–51, Aug 2004.
52. Saunders R. M., M. R. Holt, L. Jennings, D. H. Sutton, I. L. Barsukov, A. Bobkov, R. C. Liddington, E. A. Adamson, G. A. Dunn, and D. R. Critchley. Role of vinculin in regulating focal adhesion turnover. *European Journal of Cell Biology*, 85(6):487–500, Jun 2006.
53. Grashoff C., B. D. Hoffman, M. D. Brenner, R. Zhou, M. Parsons, M. T. Yang, M. A. McLean, S. G. Sligar, C. S. Chen, T. Ha, and M. A. Schwartz. Measuring mechanical tension across vinculin reveals regulation of focal adhesion dynamics. *Nature*, 466(7303):263–6, Jul 2010.
54. Hu K., L. Ji, K. T. Applegate, G. Danuser, and C. M. Waterman-Storer. Differential transmission of actin motion within focal adhesions. *Science*, 315(5808):111–5, Jan 2007.

55. Legate K. R., S. A. Wickstrom, and R. Fassler. Genetic and cell biological analysis of integrin outside-in signaling. *Genes and Development*, 23(4):397–418, Feb 2009.
56. Brown C. M., B. Hebert, D. L. Kolin, J. Zareno, L. Whitmore, A. R. Horwitz, and P. W. Wiseman. Probing the integrin-actin linkage using high-resolution protein velocity mapping. *Journal of Cell Science*, 119(Pt 24):5204–14, Dec 2006.
57. Digman M. A., C. M. Brown, A. R. Horwitz, W. W. Mantulin, and E. Gratton. Paxillin dynamics measured during adhesion assembly and disassembly by correlation spectroscopy. *Biophysical Journal*, 94(7):2819–31, Apr 2008.
58. Laukaitis C. M., D. J. Webb, K. Donais, and A. F. Horwitz. Differential dynamics of alpha 5 integrin, paxillin, and alpha-actinin during formation and disassembly of adhesions in migrating cells. *Journal of Cell Biology*, 153(7):1427–40, Jun 2001.
59. Mitra S. K., D. A. Hanson, and D. D. Schlaepfer. Focal adhesion kinase: in command and control of cell motility. *Nature Reviews of Molecular Cell Biology*, 6(1):56–68, Jan 2005.
60. Wang H. B., M. Dembo, S. K. Hanks, and Y. Wang. Focal adhesion kinase is involved in mechanosensing during fibroblast migration. *PNAS*, 98(20):11295–300, Sep 2001.
61. Behmoaram E., K. Bijian, S. Jie, Y. Xu, A. Darnel, T. A. Bismar, and M. A. Alaoui-Jamali. Focal adhesion kinase-related proline-rich tyrosine kinase 2 and focal adhesion kinase are co-overexpressed in early-stage and invasive erbB-2-positive breast cancer and cooperate for breast cancer cell tumorigenesis and invasiveness. *The American journal of pathology*, 173(5): 1540–50, Nov 2008.
62. Clark K., M. Langeslag, C. G. Figdor, and F. N. van Leeuwen. Myosin II and mechanotransduction: a balancing act. *Trends in Cell Biology*, 17(4):178–86, Apr 2007.

63. Balaban N. Q., U. S. Schwarz, D. Riveline, P. Goichberg, G. Tzur, I. Sabanay, D. Mahalu, S. Safran, A. Bershadsky, L. Addadi, and B. Geiger. Force and focal adhesion assembly: a close relationship studied using elastic micropatterned substrates. *Nature Cell Biology*, 3(5):466–72, 2001.
64. Higgs H. N. and T. D. Pollard. Regulation of actin filament network formation through arp2/3 complex: activation by a diverse array of proteins. *Annual Review of Biochemistry*, 70:649–76, 2001.
65. Sastry S. K. and K. Burridge. Focal adhesions: a nexus for intracellular signaling and cytoskeletal dynamics. *Experimental Cell Research*, 261(1):25–36, Nov 2000.
66. Lambert M., F. Padilla, and R. M. Mege. Immobilized dimers of N-cadherin-Fc chimera mimic cadherin-mediated cell contact formation: contribution of both outside-in and inside-out signals. *Journal of Cell Science*, 113(12):2207–19, Jun 2000.
67. Halbleib J. M. and W. J. Nelson. Cadherins in development: cell adhesion, sorting, and tissue morphogenesis. *Genes and Development*, 20(23):3199–214, Dec 2006.
68. Braga V. Epithelial cell shape: cadherins and small gtpases. *Experimental Cell Research*, 261(1):83–90, Nov 2000.
69. Chen C. S., J. Tan, and J. Tien. Mechanotransduction at cell-matrix and cell-cell contacts. *Annual Review of Biomedical Engineering*, 6:275–302, 2004.
70. Anastasiadis P. Z. and A. B. Reynolds. Regulation of Rho GTPases by p120-catenin. *Current Opinion in Cell Biology*, 13(5): 604–10, Oct 2001.
71. Noren N. K., B. P. Liu, K. Burridge, and B. Kreft. p120 catenin regulates the actin cytoskeleton via Rho family GTPases. *Journal of Cell Biology*, 150(3):567–80, Aug 2000.

72. Nagafuchi A. and M. Takeichi. Transmembrane control of cadherin-mediated cell adhesion: a 94 kda protein functionally associated with a specific region of the cytoplasmic domain of E-cadherin. *Cell Regulation*, 1(1):37–44, Nov 1989.
73. Drees F., S. Pokutta, S. Yamada, W. J. Nelson, and W. I. Weis. Alpha-catenin is a molecular switch that binds E-cadherin-beta-catenin and regulates actin-filament assembly. *Cell*, 123(5):903–15, 2005.
74. Weis W. I. and W. J. Nelson. Re-solving the cadherin-catenin-actin conundrum. *Journal of Biological Chemistry*, 281(47):35593–7, Nov 2006.
75. Fodde R. and T. Brabletz. Wnt/beta-catenin signaling in cancer stemness and malignant behavior. *Current Opinion in Cell Biology*, 19(2): 150–8, Apr 2007.
76. Rodriguez-Sastre M. A., L. Gonzalez-Maya, R. Delgado, M. Lizano, G. Tsubaki, A. Mohar, and A. Garcia-Carranca. Abnormal distribution of E-cadherin and beta-catenin in different histologic types of cancer of the uterine cervix. *Gynecologic Oncology*, 97(2):330–6, May 2005.
77. Ramis-Conde I., D. Drasdo, A. R. A. Anderson, and M. A. J. Chaplain. Modeling the influence of the E-cadherin-beta-catenin pathway in cancer cell invasion: a multiscale approach. *Biophysical Journal*, 95(1):155–65, Jul 2008.
78. Nelson W. J. Regulation of cell-cell adhesion by the cadherin-catenin complex. *Biochemical Society Transactions*, 36:149–55, 2008.
79. Ehrlich J. S., M. D. H. Hansen, and W. J. Nelson. Spatio-temporal regulation of Rac1 localization and lamellipodia dynamics during epithelial cell-cell adhesion. *Developmental Cell*, 3(2):259–70, Aug 2002.

80. Shewan A. M., M. Maddugoda, A. Kraemer, S. J. Stehbens, S. Verma, E. M. Kovacs, and A. S. Yap. Myosin II is a key Rho kinase target necessary for the local concentration of E-cadherin at cell-cell contacts. *Molecular Biology of the Cell*, 16(10):4531–42, 2005.
81. Maddugoda M. P., M. S. Crampton, A. M. Shewan, and A. S. Yap. Myosin VI and vinculin cooperate during the morphogenesis of cadherin cell cell contacts in mammalian epithelial cells. *Journal of Cell Biology*, 178(3):529–40, 2007.
82. Chen X. and B. M. Gumbiner. Crosstalk between different adhesion molecules. *Current Opinion in Cell Biology*, 18(5):572–8, 2006.
83. Tsai J. and L. Kam. Rigidity-dependent cross talk between integrin and cadherin signaling. *Biophysical Journal*, 96(6):L39–41, 2009.
84. Borghi N., M. Lowndes, V. Maruthamuthu, M. L. Gardel, and W. J. Nelson. Regulation of cell motile behavior by crosstalk between cadherin- and integrin-mediated adhesions. *PNAS*, 107 (30):13324–13329, 2010.
85. Silvestre J., P. J. A. Kenis, and D. E. Leckband. Cadherin and integrin regulation of epithelial cell migration. *Langmuir*, 25(17):10092–9, Sep 2009.
86. Ganz A., M. Lambert, A. Saez, P. Silberzan, A. Buguin, R. M. Mege, and B. Ladoux. Traction forces exerted through N-cadherin contacts. *Biologie Cellulaire*, 98(12):721–30, 2006.
87. Ladoux B., E. Anon, M. Lambert, A. Rabodzey, P. Hersen, A. Buguin, P. Silberzan, and R. M. Mege. Strength dependence of cadherin-mediated adhesions. *Biophysical Journal*, 98(4):534–42, 2010.

88. Foty R. A. and M. S. Steinberg. Cadherin-mediated cell-cell adhesion and tissue segregation in relation to malignancy. *International Journal of Developmental Biology*, 48 (5-6):397–409, 2004.
89. Foty R. A. and M. S. Steinberg. The differential adhesion hypothesis: a direct evaluation. *Developmental Biology*, 278(1):255–63, 2005.
90. Ryan P. L., R. A. Foty, J. Kohn, and M. S. Steinberg. Tissue spreading on implantable substrates is a competitive outcome of cell-cell vs. cell-substratum adhesivity. *PNAS*, 98(8):4323–7, 2001.
91. Moro L., M. Venturino, C. Bozzo, L. Silengo, F. Altruda, L. Beguinot, G. Tarone, and P. Defilippi. Integrins induce activation of egf receptor: role in map kinase induction and adhesion-dependent cell survival. *The EMBO Journal*, 17(22):6622–32, Nov 1998.
92. Bill H. M., B. Knudsen, S. L. Moores, S. K. Muthuswamy, V. R. Rao, J. S. Brugge, and C. K. Miranti. Epidermal growth factor receptor-dependent regulation of integrin-mediated signaling and cell cycle entry in epithelial cells. *Molecular Cell Biology*, 24(19):8586–99, Oct 2004.
93. Zhao J. H., H. Reiske, and J. L. Guan. Regulation of the cell cycle by focal adhesion kinase. *The Journal of Cell Biology*, 143(7): 1997–2008, Dec 1998.
94. Zhao J., R. Pestell, and J. L. Guan. Transcriptional activation of cyclin d1 promoter by fak contributes to cell cycle progression. *Molecular Biology of the Cell*, 12(12): 4066–77, Dec 2001.
95. Zhao J., Z. C. Bian, K. Yee, B. P. C. Chen, S. Chien, and J.-L. Guan. Identification of transcription factor klf8 as a downstream target of focal adhesion kinase in its



- regulation of cyclin D1 and cell cycle progression. *Molecular Biology of the Cell*, 11(6): 1503–15, Jun 2003.
96. Klein E. A., L. Yin, D. Kothapalli, P. Castagnino, F. J. Byfield, T. Xu, I. Levental, E. Hawthorne, P. A. Janmey, and R. K. Assoian. Cell-cycle control by physiological matrix elasticity and in vivo tissue stiffening. *Current Biology*, 19(18):1511–8, Sep 2009.
97. Kumar A., R. Murphy, P. Robinson, L. Wei, and A. M. Boriek. Cyclic mechanical strain inhibits skeletal myogenesis through activation of focal adhesion kinase, Rac-1 GTPase, and NF-kappaB transcription factor. *The FASEB Journal*, 18(13):1524–35, Oct 2004.
98. Nelson C. M. and C. S. Chen. VE-cadherin simultaneously stimulates and inhibits cell proliferation by altering cytoskeletal structure and tension. *Journal of Cell Science*, 116(17):3571–81, Sep 2003.
99. Vasioukhin V., C. Bauer, L. Degenstein, B. Wise, and E. Fuchs. Hyperproliferation and defects in epithelial polarity upon conditional ablation of alpha-catenin in skin. *Cell*, 104(4):605–17, Feb 2001.
100. Scholey J. M., I. Brust-Mascher, and A. Mogilner. Cell division. *Nature*, 422(6933): 746–52, 2003.
101. Heng Y. W. and C. G. Koh. Actin cytoskeleton dynamics and the cell division cycle. *International Journal of Biochemistry and Cell Biology*, 2010.
102. Shlomovitz R. and N. S. Gov. Physical model of contractile ring initiation in dividing cells. *Biophysical Journal*, 94(4):1155–68, 2008.

103. Zumdieck A., K. Kruse, H. Bringmann, A. A. Hyman, and F. Julicher. Stress generation and filament turnover during actin ring constriction. *PLoS One*, 2(1):e696, 2007.
104. Effler J. C., Y. S. Kee, J. M. Berk, M. N. Tran, P. A. Iglesias, and D. N. Robinson. Mitosis-specific mechanosensing and contractile-protein redistribution control cell shape. *Current Biology*, 16(19):1962–7, 2006.
105. Kanada M., A. Nagasaki, and T. Q. P. Uyeda. Adhesion-dependent and contractile ring-independent equatorial furrowing during cytokinesis in mammalian cells. *Molecular Biology of the Cell*, 16(8):3865–3872, 2005.
106. Chen C. S. Mechanotransduction - a field pulling together? *Journal of Cell Science*, 121(20):3285–3292, 2008.
107. Wang J. H.-C. and J.-S. Lin. Cell traction force and measurement methods. *Biomechanics and Modeling in Mechanobiology*, 6 (6):361–71, Nov 2007.
108. Nicolas A., A. Besser, and S. A. Safran. Dynamics of cellular focal adhesions on deformable substrates: consequences for cell force microscopy. *Biophysical Journal*, 95(2):527–39, Jul 2008.
109. Bell E., B. Ivarsson, and C. Merrill. Production of a tissue-like structure by contraction of collagen lattices by human fibroblasts of different proliferative potential in vitro. *PNAS*, 76(3):1274–8, Mar 1979.
110. Ehrlich H. P. The role of connective tissue matrix in wound healing. *Progress in Clinical and Biological Research*, 266:243–58, 1988.
111. Guido S. and R. T. Tranquillo. A methodology for the systematic and quantitative study of cell contact guidance in oriented collagen gels. correlation of fibroblast orientation and gel birefringence. *Journal of Cell Science*, 105(2):317–31, Jun 1993.

112. Wozniak M. A., R. Desai, P. A. Solski, C. J. Der, and P. J. Keely. Rock-generated contractility regulates breast epithelial cell differentiation in response to the physical properties of a three-dimensional collagen matrix. *Journal of Cell Biology*, 163(3):583–95, Nov 2003.
113. Jiang H. and F. Grinnell. Cell-matrix entanglement and mechanical anchorage of fibroblasts in three-dimensional collagen matrices. *Molecular Biology of the Cell*, 16(11): 5070–6, Nov 2005.
114. Lee K. M., K. Y. Tsai, N. Wang, and D. E. Ingber. Extracellular matrix and pulmonary hypertension: control of vascular smooth muscle cell contractility. *The American Journal of Physiology*, 274(1): H76–82, Jan 1998.
115. Smith K. D., A. Wells, and D. A. Lauffenburger. Multiple signaling pathways mediate compaction of collagen matrices by egf-stimulated fibroblasts. *Experimental Cell Research*, 312(11): 1970–82, Jul 2006.
116. Maskarinec S. A., C. Franck, D. A. Tirrell, and G. Ravichandran. Quantifying cellular traction forces in three dimensions. *PNAS*, 106(52):22108–13, Dec 2009.
117. Burton K. and D. L. Taylor. Traction forces of cytokinesis measured with optically modified elastic substrata. *Nature*, 385(6615):450–4, 1997.
118. Goffin J. M., P. Pittet, G. Csucs, J. W. Lussi, J. J. Meister, and B. Hinz. Focal adhesion size controls tension-dependent recruitment of alpha-smooth muscle actin to stress fibers. *The Journal of Cell Biology*, 172(2): 259–68, Jan 2006.
119. Merkel R., N. Kirchgessner, C. M. Cesa, and B. Hoffmann. Cell force microscopy on elastic layers of finite thickness. *Biophysical Journal*, 93(9):3314–23, Nov 2007.
120. Galbraith C. G. and M. P. Sheetz. A micromachined device provides a new bend on fibroblast traction forces. *PNAS*, 94(17):9114–8, Aug 1997.

121. Saez A., A. Buguin, P. Silberzan, and B. Ladoux. Is the mechanical activity of epithelial cells controlled by deformations or forces? *Biophysical Journal*, 89(6):L52–4, Dec 2005.
122. Tan J. L., J. Tien, D. M. Pirone, D. S. Gray, K. Bhadriraju, and C. S. Chen. Cells lying on a bed of microneedles: an approach to isolate mechanical force. *PNAS*, 100(4):1484–9, Feb 2003.
123. Reinhart-King C. A., M. Dembo, and D. A. Hammer. Endothelial cell traction forces on RGD-derivatized polyacrylamide substrata. *Langmuir*, 19(5):1573–1579, 2003.
124. Saunders R. L. and D. A. Hammer. Assembly of human umbilical vein endothelial cells on compliant hydrogels. *Cellular and Molecular Bioengineering*, 3 (1):60–67, March 2010.
125. Kang H., Q. Wen, P. A. Janmey, J. X. Tang, E. Conti, and F. C. MacKintosh. Nonlinear elasticity of stiff filament networks: strain stiffening, negative normal stress, and filament alignment in fibrin gels. *Journal of Physical Chemistry B*, 113(12):3799–805, Mar 2009.
126. Storm C., J. J. Pastore, F. C. MacKintosh, T. C. Lubensky, and P. A. Janmey. Non-linear elasticity in biological gels. *Nature*, 435(7039):191–4, May 2005.
127. Winer J. P., S. Oake, and P. A. Janmey. Non-linear elasticity of extracellular matrices enables contractile cells to communicate local position and orientation. *PLoS One*, 4(7):e6382, 2009.
128. Kadow C. E., P. C. Georges, P. A. Janmey, and K. A. Beningo. Polyacrylamide hydrogels for cell mechanics: steps toward optimization and alternative uses. *Methods in Cell Biology*, 83:29–46, 2007.

129. Pless D. D., Y. C. Lee, S. Roseman, and R. L. Schnaar. Specific cell-adhesion to immobilized glycoproteins demonstrated using new reagents for protein and glycoprotein immobilization. *Journal of Biological Chemistry*, 258(4): 2340–2349, 1983.
130. Schnaar R. L., P. H. Weigel, M. S. Kuhlenschmidt, Y. C. Lee, and S. Roseman. Adhesion of chicken hepatocytes to polyacrylamide gels derivatized with Nacetylglucosamine. *Journal of Biological Chemistry*, 253(21):7940–51, Nov 1978.
131. Wang Y. L. and R. J. Pelham. Preparation of a flexible, porous polyacrylamide substrate for mechanical studies of cultured cells. *Molecular Motors and the Cytoskeleton, Pt B*, 298: 489–496, 1998.
132. Wong J. Y., J. B. Leach, and X. Q. Brown. Balance of chemistry, topography, and mechanics at the cell-biomaterial interface: Issues and challenges for assessing the role of substrate mechanics on cell response. *Surface Science*, 570(1):119–133, 2004.
133. Emsley J., C. G. Knight, R. W. Farndale, M. J. Barnes, and R. C. Liddington. Structural basis of collagen recognition by integrin alpha2beta1. *Cell*, 101(1):47–56, 2000.
134. Knight C. G., L. F. Morton, A. R. Peachey, D. S. Tuckwell, R. W. Farndale, and M. J. Barnes. The collagen-binding a-domains of integrins alpha(1)beta(1) and alpha(2)beta(1) recognize the same specific amino acid sequence, gfoget, in native (triple-helical) collagens. *Journal of Biological Chemistry*, 275(1):35–40, 2000.
135. Kramer R. Z., J. Bella, B. Brodsky, and H. M. Berman. The crystal and molecular structure of a collagen-like peptide with a biologically relevant sequence. *Journal of Molecular Biology*, 311(1):131–47, Aug 2001.
136. Reyes C. D. and A. J. Garcia. Engineering integrin-specific surfaces with a triple-helical collagen-mimetic peptide. *Journal of Biomedical Material Research A*, 65(4): 511–23, 2003.

137. Dembo M. and Y. L. Wang. Stresses at the cell-to-substrate interface during locomotion of fibroblasts. *Biophysical Journal*, 76(4):2307–16, 1999.
138. Gaudet C., W. A. Marganski, S. Kim, C. T. Brown, V. Gunderia, M. Dembo, and J. Y. Wong. Influence of type I collagen surface density on fibroblast spreading, motility, and contractility. *Biophysical Journal*, 85(5):3329–35, Nov 2003.
139. Dembo M., T. Oliver, A. Ishihara, and K. Jacobson. Imaging the traction stresses exerted by locomoting cells with the elastic substratum method. *Biophysical Journal*, 70(4):2008–22, 1996.
140. Marganski W. A., M. Dembo, and Y. L. Wang. Measurements of cell-generated deformations on flexible substrata using correlation-based optical flow. *Methods in Enzymology*, 361:197–211, 2003.
141. Yeung T. , P. C. Georges, L. A. Flanagan, B. Marg, M. Ortiz, M. Funaki, N. Zahir, W. Y. Ming, V. Weaver, and P. A. Janmey. Effects of substrate stiffness on cell morphology, cytoskeletal structure, and adhesion. *Cell Motility and the Cytoskeleton*, 60(1): 24–34, 2005.
142. Boudou T., J. Ohayon, C. Picart, R. I. Pettigrew, and P. Tracqui. Nonlinear elastic properties of polyacrylamide gels: implications for quantification of cellular forces. *Biorheology*, 46(3):191–205, 2009.
143. Stricker J., B. Sabass, U. S. Schwarz, and M. L. Gardel. Optimization of traction force microscopy for micron-sized focal adhesions. *Journal of Physics: Condensed Matter*, 22(19):194104, Apr 2010.
144. Hur S. S., Y. Zhao, Y.-S. Li, E. Botvinick, and S. Chien. Live cells exert 3-dimensional traction forces on their substrata. *Cellular and Molecular Bioengineering*, 2(3): 425–36, Sep 2009.

145. Schoen I., W. Hu, E. Klotzsch, and V. Vogel. Probing cellular traction forces by micropillar arrays: contribution of substrate warping to pillar deflection. *Nano Letters*, 10(5):1823–30, May 2010.
146. Califano, J.P., and C.A. Reinhart-King, A balance of substrate mechanics and matrix chemistry regulates endothelial cell network assembly. *Cellular and Molecular Bioengineering*, 1:122-32, 2008.
147. Berx, G., and F. van Roy, Involvement of members of the cadherin superfamily in cancer. *Cold Springs Harbor Perspectives in Biology*, 1:a3129, 2009.

# Chapter 2

## Materials and Protocols

### 2.1 Cell Culture

MCF10A human breast epithelial cells were purchased from American Type Culture Collection (ATCC) and maintained at 37°C and 5% CO<sub>2</sub> in growth media as described [1]. Growth media consisted of DMEM/F12 with 5% Donor Horse Serum (Invitrogen, Carlsbad, CA) supplemented with 20 ng/ml EGF (Peprotech, Rocky Hill, NJ), 0.5 µg/ml hydrocortisone, 100 ng/ml cholera toxin, and 10 µg/ml insulin (Sigma-Aldrich, St. Louis, MO). Tet-off E-cadherin β-catenin GFP-tagged plasmid transfected MCF10A cells were a generous gift from V.M. Weaver lab. These cells were maintained in a non induced state with between 1 µg/ml of doxycycline (Clontech, Mountain View, CA). Plasmid induction required 3 day incubation in the absence of doxycycline.

EpH4-J3B1 [2] mouse breast epithelial cells were a gift from V.M. Weaver lab and were maintained at 37°C and 5% CO<sub>2</sub> in DMEM/F12 supplemented with 2% Fetal Bovine Serum (Invitrogen) and 5 µg/ml insulin (Sigma-Aldrich) growth media. In division experiments these cells were incubated on the functionalized gels for 4 hours to allow adhesion and then serum starved overnight to synchronize the cell cycle. On the day of the experi-



ment cells were serum stimulated for 4 hours to initiate division cycle. 30  $\mu$ M Blebbistatin (Sigma-Aldrich) was used to block myosin II actin-binding site without adverse side effects on other molecular pathways. 40  $\mu$ M Y-27632 was used to inhibit ROCK (Rho-associated protein kinase) (Sigma-Aldrich). Chemical inhibition was initiated with incubation for 1 hour prior to imaging.

Experimental media for all cell lines was supplemented 1/1000 parts Penn/Strep, Fungizone and Gentamicin (Invitrogen). Experiments were conducted on cells between passages 3 and 8. Cells were also synchronized prior to plating on functionalized gels. Cells were allowed to fully spread on the functionalized glass for 4 hours and overnight on gel substrates, prior to experimenting.

## **2.2 Immunofluorescence and Imaging**

Cell nuclei were stained with Hoechst 33342 FluoroPure dye and Qtracker Cell Labeling Kit was used for long term cell tracking (Invitrogen). Cells were imaged in real time with Nikon Inverted Eclipse TE300 microscope (Nikon Instruments Inc, Tokyo, Japan) and a Photometric Cool Snap HQ camera (Roper Scientific, Trenton, NJ) in a temperature controlled chamber at 37°C and 5% CO<sub>2</sub>. Fluorescence was detected with 4900 DAPI and 51004v2 FITC/TRITC filter sets (Chroma Technology Corp, Rockingham, VT). A LabView (National Instruments, Austin, TX) program was used to control the mechanical stage and timed exposure for picture capture.

Cells were plated sparsely at 1000 cells/cm<sup>2</sup> overnight and isolated single or two interacting cells were observed for 2 to 6 hours. Images were taken at 10-30 minute intervals, to minimize long-term light exposure while accurately capturing behavior. Cells on 400 Pascal gels were imaged every hour for 8 hours. The time stamp HH:MM records the time hours:minutes. In motility experiments each gel experimental condition was repeated at

least twice and more than 10 cells or cell pairs were analyzed per experiment. Cell area and two cell interaction duration and distance were quantified manually with NIH ImageJ software (<http://rsbweb.nih.gov/ij/>). Cell velocity was quantified with macros code written in ImageJ software that tracked the fluorescent tagged nucleus. All data was then compiled and analyzed separately for single cells and cell pairs that maintained contact, with code written in Matlab 7.0 software (Mathworks Inc., Natick, MA).

Fluorescent bead displacements at the cell-substrate adhesion surface were calculated with respect to the no-cell containing unstressed trypsinized surface. Displacement vectors were used to calculate substrate strain and the corresponding cell traction stresses with LIBTRC 2.x code developed by Prof. Micah Dembo, Boston University [3-8].

## **2.3 Gel Preparation**

Coverslip activation, *N*-6-((acryloyl)amino)hexanoic acid (N-6) synthesis and ligand functionalized polyacrylamide gels were all prepared and characterized in accordance with published protocols and included below [6-14]. Protein A gels were further incubated with recombinant human E-cadherin/FC chimera (R&D Systems), per the published protocol from Prof. Nelson's group [15].

### **Coverslip Activation Protocol**

1. Place coverslips in single 100 mm dish. Use 150 mm dish if using 50 mm coverslips.
2. Add 20 ml (40-50 ml for 150 mm dish) of 0.2 M HCl, shake to disperse coverslips and leave on orbital shaker overnight.
3. Decant 0.2 M HCl (can reuse at least a couple of times).

4. Rinse coverslips several changes (4 to 5) with deionized water couple of minutes shaking on orbital shaker.
5. Add 20 ml of 0.1 M NaOH and incubate room temperature on orbital shaker for 10 minutes or more.
6. Rinse coverslips several changes (4 to 5) with deionized water couple of minutes shaking on orbital shaker.
7. Add 20 ml of deionized water and add 100  $\mu$ L aminopropyl trimethoxysilane (0.5% v/v final).
8. Incubate with shaking on orbital shaker a minimum of 30 minutes at room temperature.
9. Rinse coverslips with deionized water 4 or 5 times quickly just at the sink, then rinse well on orbital shaker with 4 to 5 changes of water for several minutes (must remove all traces of aminopropyl trimethoxysilane).
10. Thaw glutaraldehyde briefly and in the chemical hood add 0.5% (v/v) glutaraldehyde in 1xPBS (20 ml total volume for 100 mm dish). Incubate on orbital shaker for at least 1 hr.
11. Rinse coverslips with deionized water 4 or 5 times quickly - disposing of the bulk glutaraldehyde into chemical waste container, then rinse well on orbital shaker with 4 to 5 changes of water for several minutes.
12. Dry coverslips on a piece of kimwipe. Store dry in dry 100 mm dish.

## Bulk Functionalization Gel Protocol

### Gel Synthesis

The following recipes are for the indicated gel stiffness. pH all solutions to pH=6 with 5N HCl, about 10  $\mu$ L. Accurate measurement of functionalized gel stiffness was taken and Young's modulus calculated with steel ball method [16] and confirmed with atomic force microscopy.

Stiffness (Pa)	40% acr % final	2% bis % final	40% (mL)	2% (mL)	0.25M HEPES (mL)	ddH <sub>2</sub> O (mL)	TEMED ( $\mu$ L)
140	3	0.04	1.62	0.44	2.6	13.80	10
400	3	0.05	1.62	0.55	2.6	13.69	10
675	3	0.06	1.62	0.66	2.6	13.58	10
1050	3	0.1	1.62	1.1	2.6	13.14	10
1250	3	0.2	1.62	2.2	2.6	12.00	10
2500	5	0.2	2.7	2.2	2.6	10.94	10
2700	7.5	0.035	4.0	0.385	2.6	11.455	10
7900	7.5	0.07	4.0	0.77	2.6	11.07	10
15700	7.5	0.15	4.0	1.65	2.6	10.19	10
22000	7.5	0.25	4.0	2.75	2.6	9.09	10
60000	10	0.5	5.4	5.5	2.6	4.95	10

1. Put 50  $\mu$ L of 500-nm fluorescent beads in a 0.5-ml eppendorf tube and sonicate for 5-10 minutes (be careful that you just turn the time dial and not turn on the heat switch).
2. Weigh 5.6 mg of N6 crosslinker (either synthesized in lab or commercially purchased from Molecular Probes: 6-((acryloyl amino)hexanoic acid succinimidyl ester 4) in 1.5 ml eppendorf tube per ml of solution in an eppendorf tube, add 70  $\mu$ L of 200 proof

- ethanol and with a pipette tip mechanically break up the larger chunks of crosslinker in ethanol. Brief sonication of the crosslinker will help break up and dissolve the chunks too. Scale all amounts in the next steps of final volumes to that of crosslinker.
3. Add 845  $\mu\text{L}$  of gel solution to the dissolved crosslinker in ethanol and vortex for up to 10 minutes until the crosslinker is fully dissolved. Add 40  $\mu\text{L}$  of deionized research grade  $\text{H}_2\text{O}$  (dd $\text{H}_2\text{O}$ ) and 40  $\mu\text{L}$  of beads to the gel solution (if not doing TFM, just add 80  $\mu\text{L}$  dd $\text{H}_2\text{O}$ ). Mix with a pipette and DO NOT VORTEX once beads are added.
  4. Place eppendorfs in a vacuum flask or a bubble vacuum chamber and de-gas for 30 or more minutes.
  5. Coat some top cover slips (18mm circular cover slips) with rain-x. Initially apply with a cotton swab, but use your gloved fingertip to smear the rain-x evenly over the coverglass. Place on kimwipes with rain-x coated surface up. Allow rain-x to dry about 5 minutes and wipe reasonably clean with a kimwipe.
  6. Add 6.0  $\mu\text{L}$  of freshly made 10% APS to a gel solution. Mix up and down with a pipette. One gel at a time, dispense 30  $\mu\text{L}$  on top of the activated glass (see Coverslip Activation Procedure) and immediately after, place a rain-x coated top coverglass on top of the gel solution, sandwiching the gel solution between the activated glass and rain-x coated cover slip. Immediately flip the coverslip over so that the 18-mm coverglass is on the bottom. Place a wet paper towel near the gels so they don't dry out while gelling.
  7. Chill a wash bottle of dd $\text{H}_2\text{O}$  in the refrigerator for use.

### **Conjugation Procedure**

1. Prepare sterile fibronectin (Fn), collagen or peptide solution to bind to the polyacrylamide gels.

2. You will need about 200  $\mu\text{L}$  of solution for each gel. Keep the solutions on ice.
3. After EXACTLY 45 minutes remove the top circular cover slip from the gel (carefully either with a razor blade, 2 pairs of fine tipped tweezers or another device). Try swelling the gel with ice cold ddH<sub>2</sub>O so the gel doesn't dry out or crack. Rinse again with ICE-COLD ddH<sub>2</sub>O and place gel side up. Immediately dispense 200  $\mu\text{L}$  of the prepared Fn, collagen or peptide solution onto the gel and cover to help prevent evaporation. Place gels in the refrigerator and incubate overnight.
4. Prepare a solution of 1/100 parts of ethanolamine in 50 mM HEPES buffer pH=8.0 in the chemical hood and then vortex. You will need 300  $\mu\text{l}$  for each gel that you made. Place the solution on ice to cool completely.
5. After the overnight incubation, rinse the gels one at a time with ICE-COLD PBS and dispense 300  $\mu\text{L}$  of the prepared ethanolamine solution onto each gel. Incubate for 30 minutes covered in the cold-room or refrigerator.
6. After the 30 minute incubation, rinse gels one at a time with ICE-COLD PBS. Store hydrated gels in 1xPBS wrapped in parafilm and aluminum foil up to 4 days in the cold-room or refrigerator.

### **Cell Plating**

1. UV gels for 30 minutes in culture hood to sterilize (make sure the chambers are open). Aspirate off the PBS.
2. Add 2 ml of cell media into each chamber on top of the gel. Incubate for 30 minutes at 37°C prior to plating cells.
3. Passage your cells. For each gel that you are going to plate prepare 3 ml of growth media. For example, for 5 gels, place 15 ml of growth media in a 15-ml tube. Add

1:1000 gentamicin, fungizone and penn/strep to the media.

4. Dispense  $3 \times 10^3$  cells for each ml of media into the media. For example, dispense  $3 \times 10^4$  cells into 10 ml of media. Mix media and cells well pipetting up and down carefully without bubbles.
5. Aspirate the culture media from each chamber and add 3 ml of the growth media with cells. Place chambers in the incubator overnight.

NOTE: It is important to note that extracellular matrix ligands are not single proteins, not only in the fact that they adhere and interact with each other, but form fibrillar complicated structures they form. Collagen is such a complicated protein, being that it is both thermally unstable as a monomer and its triple helix structure is stable as a monomer only in acidic conditions [18, 19]. However NHS ester group is not reactive under acidic conditions. Therefore if a tightly controlled non-fibrillar distribution of surface collagen is required other options need to be explored, such as using low concentrations of well processed and digested collagen solutions, interpolating the ligands into the bulk polyacrylamide mixture prior to gelation, or using an acidic linker, such as 2-Acrylamido-2-methyl-1-propanesulfonic acid sodium salt (Sigma-Aldrich). This linker contains  $\text{SO}_3$  group that interacts with the primary amine on the collagen protein while maintaining the acidic environment. It also has the acrylic acid group that covalently binds polyacrylamide. Low concentration of 3 mg  $\text{SO}_3$  per ml of polyacrylamide solution or lower is sufficient. Higher concentrations of  $\text{SO}_3$  affect and deform the gel. Then collagen ligand can be dissolved in 20 mM Acetic acid solution in 1xPBS (pH 4.33) and evenly adherent on the surface compared to the uneven fibrillar aggregates of collagen observed when using N6 linker with collagen diluted in 1xPBS (pH 7.4), Fig. 2.1. However,  $\text{SO}_3$  does not covalently bind collagen but rather adhere.

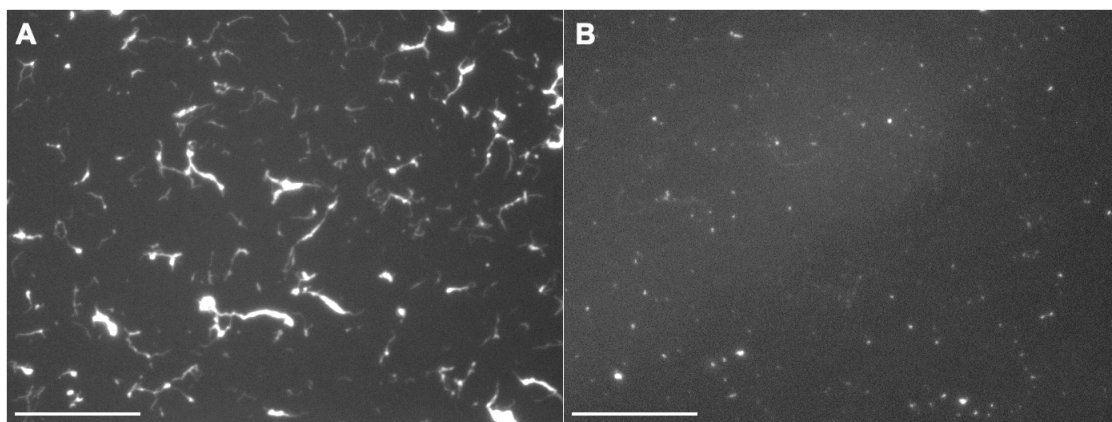


Figure 2.1: Collagen surface distribution.

FITC conjugated collagen (Sigma-Aldrich) on (A) 7900 Pa gel coated with 0.1 mg/ml collagen in 1xPBS prepared with N6 bulk protocol and (B) 2500 Pa gel coated with 0.05 mg/ml collagen in Acetic acid 1xPBS pH 4.33 prepared with 3 mg/ml SO<sub>3</sub> bulk method. Scale bar = 50  $\mu$ m



# Surface Functionalization Gel Protocol

## Reagents

- 40% acrylamide (Bio-Rad)
- 2% bis-acrylamide (Bio-Rad)
- cold 50mM HEPES pH 8.0
- TEMED
- 10xPBS
- 1xPBS
- cold deionized H<sub>2</sub>O (ddH<sub>2</sub>O)
- 10 mg/ml (1%) APS solution in ddH<sub>2</sub>O
- 0.5M HEPES pH 6.0
- 200 proof EtOH
- 30 mg/ml (3%) Irgacure 2959 (Ciba) solution in EtOH
- 30 mg/ml (3%) N6 (*N*-6-((acryloyl)amino)hexanoic acid) solution in EtOH, MW 282.3 g/mol
- 18 mg/ml N2 (*N*-Acryloxysuccinimide) solution in EtOH, MW 169.1 g/mol
- protein/peptide of interest

## Gel Synthesis

1. Prep acrylamide solution according to this recipe below and vortex the solution briefly. Final volume should be 1.6ml add 160  $\mu\text{L}$  of 10xPBS and 1.6  $\mu\text{L}$  TEMED. If storing or reusing the solution – mix it without TEMED and without APS. APS is added LAST to activate gelation. The recipes below are for a gel without beads. Accurate measurement of functionalized gel stiffness was taken and Young’s modulus calculated with steel ball method [17] and confirmed with atomic force microscopy.

Stiffness	40% acr	2% bis	40%	2%	10xPBS	ddH <sub>2</sub> O	TEMED	1% APS
(Pa)	% final	% final	( $\mu\text{L}$ )	( $\mu\text{L}$ )	( $\mu\text{L}$ )	( $\mu\text{L}$ )	( $\mu\text{L}$ )	( $\mu\text{L}$ )
140	3	0.04	120	32	160	1126.4	1.6	160
400	3	0.05	120	40	160	1118.4	1.6	160
675	3	0.06	120	48	160	1110.4	1.6	160
1050	3	0.1	120	80	160	1078.4	1.6	160
1250	3	0.2	120	160	160	998.4	1.6	160
2700	7.5	0.035	300	28	160	950.4	1.6	160
4000	7.5	0.05	300	40	160	938.4	1.6	160
7900	7.5	0.07	300	56	160	922.4	1.6	160
14000	7.5	0.15	300	120	160	858.4	1.6	160
22000	7.5	0.25	300	200	160	778.4	1.6	160
60000	10	0.5	400	400	160	478.4	1.6	160

2. For TFM: Put 50  $\mu\text{L}$  of 500-nm fluorescent beads in a 0.5-ml eppendorf tube and sonicate for 5-10 minutes (be careful that you just turn the time dial and not turn on the heat switch). Be sure to subtract the volume of bead solution added from the volume of ddH<sub>2</sub>O! Add about 40  $\mu\text{L}$  of beads to the gel solution containing all ingredients minus APS. Mix with pipette, DO NOT VORTEX once beads are added.
3. De-gas in a vacuum flask or a bubble vacuum chamber for 30 mins.

4. Coat some top cover slips (18mm circular coverslips) with rain-x. Initially apply with a cotton swab, but use your gloved fingertip to smear the rain-x evenly over the coverglass. Place on kimwipes with rain-x coated surface up. Allow rain-x to dry about 5 minutes and wipe dry and clean with a kimwipe.
5. Put activated glass cover slips (described in Coverslip Activation Procedure) on a plate of water or with wet paper towel to humidify the gelation. The gels should not dry out during the gelation!
6. Add 160  $\mu\text{L}$  of 1% APS (freshly made in ddH<sub>2</sub>O) to the degassed solution. Mix up and down with a pipette gently not to introduce too much air to the solution.
7. One gel at a time, dispense 20  $\mu\text{l}$  on top of the activated glass and immediately after, place a rain-x coated top coverglass on top of the gel solution, sandwiching the gel solution between the activated glass and rain-x coated cover slip. Do this carefully not to trap any bubbles in the sandwiched gel because the gel then won't gel and its elasticity is compromised! For TFM thin gels are desired, for other experiments can increase volume to 30  $\mu\text{l}$  or more - if in doubt, make sure the final height of the gel is not above 50-70  $\mu\text{m}$ , otherwise the cells might feel the stiffness of the underlying glass.
8. Immediately flip the chamber over so that the 18-mm coverslips is on the bottom and the beads will settle to the top surface of the gel. Let the gel for about 30 minutes – until it gels (visibly confirmed through coverslip separation around the edges). Carefully with a razor blade remove the top circular cover slip from the gel – do not rip or damage the gel. Rinse well and store in cold ddH<sub>2</sub>O or 1xPBS for up to 10 days.

## Conjugation Procedure

1. To conjugate the surface with protein or peptide, aspirate off the liquid from the gel surface and prep the conjugation solution per recipe below (recipe is for 30  $\mu\text{L}$  per gel, therefore multiply by number of gels plus extra volume). NOTE: If the peptide or ligand is very small or surface topography is desired, 2% bis solution will help. 0.1% final volume of bis should be sufficient. Make sure if adding volume of 2% bis, to subtract the appropriate volume from ddH<sub>2</sub>O.

N2 or N6 linker	Irgacure 2959	0.5M HEPES	ddH <sub>2</sub> O	N2 or N6	Irgacure 2959
% final	% final	pH 6 ( $\mu\text{L}$ )	( $\mu\text{L}$ )	( $\mu\text{L}$ )	( $\mu\text{L}$ )
1	0.1	3	16	10	1

2. Dissolve 18 mg/ml (3%) of N2 in 200 proof EtOH mechanically or with a vortex or by sonicating the N2 briefly. Don't sonicate too long as it warms up the solution. Smaller volumes dissolve N2 better. Adding ddH<sub>2</sub>O volume and vortex together will also help the linker dissolve. If using N6 – adjust the amount of linker appropriately for difference in MW!
3. Mix N2, HEPES and ddH<sub>2</sub>O and degas for 30 mins. Chill a wash bottle of ddH<sub>2</sub>O.
4. Prepare sterile and fresh protein/peptide solution in 50 mM HEPES buffer pH 8.0 (if the protein is not stable, you can also prepare the solution in 1xPBS) and keep On ICE for the following steps. You will need about 200  $\mu\text{L}$  of solution per 18mm coverslip gel.
5. Coat some top cover slips (18mm circular cover slips) with rain-x. Initially apply with a cotton swab, but use your gloved fingertip to smear the rain-x evenly over the coverglass. Place on kimwipes with rain-x coated surface up. Allow rain-x to dry about 5 minutes and wipe dry and clean with a kimwipe.

6. Prepare fresh Irgacure 2959 (3%) stock solution by dissolving 30 mg/ml in 200 proof EtOH, vortex if needed.
7. After solution is degassed add Irgacure solution to it to make final solution. Mix up and down with a pipette gently not to introduce too much air to the solution.
8. One gel at a time, dispense 30  $\mu$ L to each gel surface and spread it around gently with a pipette tip or a glass pipette, without touching the surface.
9. Place rain-x coated cover slip on top of the gel with N2 solution (rain-x side down) carefully not to squeeze the solution out and not to introduce any bubbles to the surface!
10. Place the gel under UV lamp (350nm and 115V lamp like spectroline EN-180) for 10 to 20 minutes.
11. Continue each gel one at a time. After UV is done – you might see whitish residue around the gel if it contains 2% bis.
12. Carefully with a razor blade or with a stream of wash remove the top circular cover slip from the gel – do not rip or damage the gel. Rinse well 2x 5 min in ice cold ddH<sub>2</sub>O dish on ice - cold temperature and acidity of water will keep NHS from hydrolyzing.
13. One gel at a time, aspirate carefully the ddH<sub>2</sub>O wash from the gel and dispense 200  $\mu$ L of prepared ice cold protein solution onto the gel surface. Incubate gels in a parafilm sealed environment to prevent evaporation of the protein solution for 2+ hours at RT or in the refrigerator overnight.

## **Blocking Procedure**

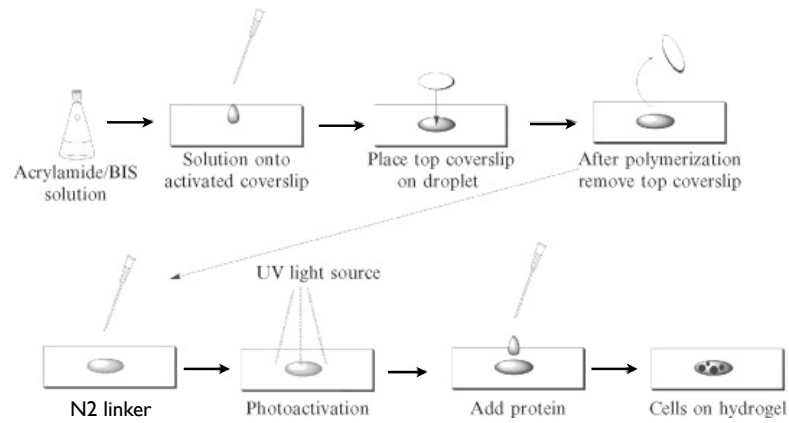
1. Prepare a solution of 1/100 parts of ethanolamine in 50 mM HEPES buffer pH 8.0 in the chemical hood and then vortex. You will need 200  $\mu$ l for each gel that you made. Place the solution on ice to cool completely.
2. After the 2-hr or overnight incubation, rinse the gels one at a time with cold 1xPBS and dispense 200  $\mu$ L of the prepared ethanolamine solution onto each gel.
3. Incubate for 30 minutes covered in the cold-room or refrigerator.
4. After the 30 minute incubation, rinse gels one at a time with ice cold 1xPBS. Gels can be stored in cold 1xPBS wrapped in parafilm and aluminum foil up to 4 days in the cold-room or refrigerator.

## **Cell Plating**

1. UV gels for 30 minutes in culture hood to sterilize (make sure the chambers are open).
2. Aspirate off the PBS. Add 2 ml of cell growth medium into each chamber on top of the gel.
3. Incubate for 30 minutes at 37°C prior to plating cells, unless specific control of surface ligand type or concentration is desired.
4. Passage your cells. Add 1:1000 gentamicin, fungizone and penn/strep to the plating media.
5. Dispense no more than  $3 \times 10^3$  cells for each ml of media. For example, dispense  $3 \times 10^4$  cells into 10 ml of media. Mix media and cells well, pipetting up and down

carefully without bubbles. Aspirate the media from each chamber and add appropriate amount of the cell containing growth media.

6. Place chambers in the incubator overnight or for at least 4 hrs to spread.



Pictorial representation of the protocol procedure. Adopted from Kadow et al. [16]

# Surface Characterization Protocol

## Reagents

- 1xPBS
- 1% heat denatured (30 mins at 56°C) BSA in 1xPBS blocking solution or Pierce Starting Block
- 1xPBS + 0.1% Triton
- O-Phenylenediamine dihydrochloride (Sigma Aldrich)
- Hydrogen Peroxide solution 30% w/w in H<sub>2</sub>O (Sigma Aldrich)
- 50 mM Citric Acid 100 mM Na<sub>2</sub>HPO<sub>4</sub> pH 5 solution
- 2N HCl
- 1° Antibody (ex: BD mouse anti-Fibronectin) on ice
- 2° Antibody (ex: BD goat anti-mouse IgG HRP or FITC conjugated) on ice

## Procedure

1. Prep substrate as usual
2. Block at RT for 30 mins with 1% BSA solution or Pierce Starting Block or another blocking solution
3. Add 250  $\mu$ L per 18 mm coverslip gel (titrate amount depending on size of surface, take into account in wells – solution sticks to sides so might need higher volume) of 1:200 diluted 1° Antibody in 1% BSA solution (or higher dilution depending on antibody – 2  $\mu$ g/ml is on the lower end) and incubate for 30 mins gently shaking at RT on orbital shaker



4. Rinse 3x with 1xPBS + 0.1% Triton
5. Add 250  $\mu$ L of 1:200 diluted 2° Antibody in 1% BSA solution (can use a higher dilution since this is a secondary) and incubate for 30 mins gently shaking at RT.
6. Rinse well 3x with 1xPBS + 0.1% Triton
7. Fluorescent development is done now – just image.
8. For HRP: Prep HRP development solution fresh. Dissolve 2.5 mg/ml O-phenylene-diamine dihydrochloride in Citric  $\text{Na}_2\text{HPO}_4$  solution (this might be titrated down to 1 mg/ml if there is large amount of protein on surface). Add 1  $\mu$ L/mL  $\text{H}_2\text{O}_2$  last and vortex.
9. Put plate with samples on plate shaker and aspirate off all wash liquid.
10. Do these steps FAST: add 200  $\mu$ L of HRP solution to each well and shake the plate and start timer.
11. Depending on how fast the solution color changes within 1 minute to as long as 10 minutes, add 100  $\mu$ L 2N HCl to stop the reaction. Do not let the reaction to go to completion! Stop it as soon as color change is apparent. Develop the color.

## **2.4 Bibliography**

1. Debnath, J., S.K. Muthuswamy, and J.S. Brugge, Morphogenesis and oncogenesis of MCF-10A mammary epithelial acini grown in three-dimensional basement membrane cultures. *Methods*, 2003. 30(3): p. 256-268.
2. Montesano, R. et al, Isolation of EpH4 mammary epithelial cell subpopulations which differ in their morphogenetic properties. *In Vitro Cellular Developmental Biology*, 1998. 34: p. 468-477.

3. Dembo, M., et al., Imaging the traction stresses exerted by locomoting cells with the elastic substratum method. *Biophysical Journal*, 1996. 70: p. 2008-22.
4. Dembo, M. and Y.L. Wang, Stresses at the cell-to-substrate interface during locomotion of fibroblasts. *Biophysical Journal*, 1999. 76(4): p. 486-94.
5. Marganski, W.A., M. Dembo, and Y.L. Wang. Measurements of cell-generated deformations on flexible substrata using correlation-based optical flow. *Methods in Enzymology*, 2003. 361: p. 197-211.
6. Pless, D.D., et al., Specific Cell-Adhesion to Immobilized Glycoproteins Demonstrated Using New Reagents for Protein and Glycoprotein Immobilization. *Journal of Biological Chemistry*, 1983. 258(4): p. 2340-2349.
7. Wang, Y.L. and R.J. Pelham, Preparation of a flexible, porous polyacrylamide substrate for mechanical studies of cultured cells. *Molecular Motors and the Cytoskeleton, Pt B*, 1998. 298: p. 489-496.
8. Wong, J.Y., J.B. Leach, and X.Q. Brown, Balance of chemistry, topography, and mechanics at the cell-biomaterial interface: Issues and challenges for assessing the role of substrate mechanics on cell response. *Surface Science*, 2004. 570(1-2): p. 119-133.
9. Damljanovic, V., B.C. Lagerholm and K. Jacobson. Bulk and micropatterned conjugation of extracellular matrix proteins to characterized polyacrylamide substrates for cell mechanotransduction assays. *Biotechniques*, 2005. 39(6): p. 847-51.
10. Levental, I. et al., A simple indentation device for measuring micrometer-scale tissue stiffness. *J. Physics: Condensed Matter*, 2010. 22: p. 194120-194129.
11. Paszek, M.J., et al., Tensional homeostasis and the malignant phenotype. *Cancer Cell*, 2005. 8(3): p. 241-254.

12. Peyton, S.R. and A.J. Putnam, Extracellular matrix rigidity governs smooth muscle cell motility in a biphasic fashion. *Journal of Cellular Physiology*, 2005. 204(1): p. 198-209.
13. Reinhart-King, C.A., M. Dembo, and D.A. Hammer, Cell-cell mechanical communication through compliant substrates. *Biophysical Journal*, 2008. 95(12): p. 6044-51.
14. Yeung, T., et al., Effects of substrate stiffness on cell morphology, cytoskeletal structure, and adhesion. *Cell Motility and the Cytoskeleton*, 2005. 60(1): p. 24-34.
15. Drees, F., et al., Cell adhesion assays: Fabrication of an E-cadherin substratum and isolation of lateral and basal membrane patches. *Methods in Molecular Biology*, 2005. 294: p. 303-23.
16. Kadow, C.E. et al. Polyacrylamide hydrogels for cell mechanics: steps toward optimization and alternative uses. *Methods in Cell Biology*, 2007. 83: p. 29-46.
17. Park, S., K.D. Costa and G.A. Ateshian, Microscale frictional response of bovine articular cartilage from atomic force microscopy. *Journal of Biomechanics*, 2004. 37(11): p. 1679-1687.
18. Leikina, E., et al., Type I collagen is thermally unstable at body temperature. *Proceedings of the National Academy of Sciences*, 2002. 99(3): p. 1314-1318.
19. Perumal, S., O. Antipova, and J.P. Orgel. Collagen fibril architecture, domain organization, and triple-helical conformation govern its proteolysis. *Proceedings of the National Academy of Sciences*, 2008. 105(8): p. 2824-2829.

## Chapter 3

# Cell motility and assembly *in vitro* as a model for Breast Cancer metastasis

Progression of benign tumors to invasive carcinomas is a life threatening yet poorly understood phenomenon in the development of breast cancer. Events of tissue destabilization, loss of cell-cell adhesiveness and increased cell-matrix interaction ultimately result in cell invasion and metastasis. Understanding cell migration and cell-cell interaction are keys to understanding cell invasion, a critical step in cancer progression. Both genetic events and extracellular matrix (ECM) changes play important roles in this invasive cell phenotype [1-3]; however the role that the ECM plays is still unclear. The quantitative relationship between adhesiveness and compliance of the ECM leading to disruption of multicellular structures and cell invasion are the primary focus of this research.

Research on mammary epithelial cells has shown progression of breast cancer is associated with tissue stiffening *in vivo* and in three dimensional culture [1, 4, 5]. Experiments in 3D basement membrane gels found the breast epithelial cells to form ordered multicellular aggregates called acini – a concentric spherical shell of cells with a hollow lumen [5-7]. At higher substrate stiffness such as coincidentally observed in cancerous tissue, the acini

tend to be disordered and display an invasive cancerous phenotype [5]. Furthermore progression and invasiveness of breast cancer in vivo is also associated with increasing ligand density, such as fibronectin (FN) and collagen [8, 9]. The ECM expression levels of FN are significantly elevated in sites of breast cancer metastases [10], as in the common site for carcinoma metastasis, the fibronectin rich lymph node [11].

The question then arises whether this tissue disassembly and cell invasiveness is regulated by differential cell-cell interaction modulated by cell-cell communication or altered cell motility due to cell adhesion and substrate stimuli. Previously Steinberg and Foty showed that cell assembly into multicellular structures could be controlled by differential cell-cell interaction. However, these investigations were carried out solely through manipulating the level and specificity of cadherin expression [12, 13]. But it is now apparent that it is not only intrinsic cell properties but also extracellular substrate stiffness and adhesiveness that play significant roles in cell-cell interaction and multicellular structure formation as well [1, 5-7, 14, 15, 41].

Further motivation to better understand the cell-cell cohesion and tissue disassembly stems from 2D in vitro experiments that have shown ECM properties to affect individual cell behavior. Mechanical properties of substrates, such as can be engineered in polyacrylamide gels, have shown to affect cell speed, persistence and direction of migration [16-19]. Recently we showed that endothelial cells display reduced motility on compliant gels due to communication through the substrate [20]. The mechanical properties of the ECM thus affect signaling pathways within the cell through mechanically responsive sensors [21, 22], such as decrease of FAK phosphorylation on compliant substrates [5] and regulation of actomyosin contractility [21, 23]. Changes in biochemical extracellular environment, such as increasing surface ligand density also affects individual cell spreading and force generation [24, 25]. Cellular response to biochemical and mechanical ECM properties has been found convoluted in the type of biochemical cue as well, as measured by difference in response to

stiffness on collagen versus fibronectin coated gels [42]. Further computational predictions of the impact of the mechanical and biochemical cues on migration in 3D have been developed [26-28]. However the effect of both biochemical and mechanical ECM properties on migratory and interactive cell behavior have yet to be experimentally tested or quantified.

Furthermore, cell motility has been connected on intracellular level to cell-cell interaction through key common intracellular players in integrin and cadherin molecular pathways [5, 29-32]. However, this cross-talk between the two molecular mechanisms has yet to be translated to cellular phenotype and behavior. It is still unclear how the interplay of both adhesion and compliance collectively affect cell phenotype and behavior, such as motility and cell-cell interaction. Here we further investigate effects of substrate adhesiveness and compliance on cell motility, spreading, cell-cell interaction and assembly. We examine how cell-cell adhesivity further modulates cell motility and invasiveness in breast epithelial cells as a model of oncogenesis.

To effectively isolate and understand the ECM influence on the invasive phenotype, our experimental system connects the behavior of an individual cell to that of multi-cellular structure. This connection between the single cell, two cells and tissue-like aggregates is the key in learning about the fundamental factors controlling tumorigenic and metastatic development. Thus our research focuses on individual and interacting cell behavior in a strictly controlled environment. This controlled in vitro extracellular environment is designed such that adhesion and elasticity can be varied simultaneously and independently. The mechanical properties are reproduced with polyacrylamide gels [33, 34]. In this work, we vary the stiffness of the gels from an elastic modulus of 400 Pascals (Pa), which is close to pre-malignant tissue, to 1250 Pa, which is the elastic modulus of stroma adjacent to the tumor, to 2500 and 7900 Pa, which represents the range of stiffness of tumors [5, 21, 46]. A wide range in FN ligand coating density is tested as well. To decouple the genetic predisposition for tumorigenesis from cell behavior we studied normal non-tumorigenic

human breast epithelial cells [6]. Furthermore the cells are not stimulated by any growth or soluble factors that may change, enhance or diminish the intracellular signaling cascades elicited by the ECM. Plating these cells on substrates of mechanical and biochemical properties similar to those in vivo allows us to understanding the key factors that control cell behavior.

In this paper we report the effect of the complex relationship of ECM adhesiveness and compliance on cell migration and cell-cell cohesion. We find there is an optimum where cells are highly motile and invasive and cell-cell adhesion is not observed. This optimum is a function of both ligand concentration and matrix stiffness. Further we show that cell-matrix and cell-cell adhesion are not inversely related, but in a more complex relationship, as increasing substrate adhesivity promotes cell-cell adhesivity but also can induce an increase in cell motility and thus cell dispersion. Increased duration of cell-cell contact decreases cell motility, dampened by increased mechanical and not biochemical properties of the ECM. Decreasing substrate elasticity to that of pre-malignant tissue maximizes cell-cell cohesion and leads to the formation of three dimensional aggregates. Our results thus show there exists a delicate balance between cell-matrix and cell-cell adhesion that is controlled through mechano-chemical alteration of the extracellular environment.

### **3.1 Biochemical and mechanical ECM cues dictate cell migration velocity**

Biochemical and mechanical properties and gradients in extracellular environment have been individually shown to affect cell behavior, specifically spreading, migration and interaction [5, 16, 18, 19, 24, 36]. However the extent of ECM dictating cell phenotype and directing cell motility, interaction and tissue formation has not been fully isolated, tested and understood. Here we explore the importance of the two ECM cues acting in concert in

a breast cancer model, without the influence of oncogenic or soluble factors.

Cells have been shown to exhibit biphasic velocity profile as a function of compliance [17]. Our further investigation of the combined effect of both cues on cell motility, we report novel findings that cell speed is a shifting biphasic function of both mechanical and biochemical cues, Fig. 3.1. Breast epithelial cells show a maximum in migration velocity with ligand concentration for each substrate compliance and with increasing gel stiffness at constant ligand density. The maximum velocity peak shifts as a function of both stiffness and ligand concentration with an inversely dependent relationship.

Cell migration goes through a maximum as a function of increasing ligand concentration at each compliance (Fig. 3.1A). The cell speed is biphasic on glass and polyacrylamide surface, and the FN concentration at which the cell speed reaches maximum increases as the substrate stiffness decreases. Thus velocity is dependent not only on mechanical but also on biochemical ECM conditions and to achieve maximum velocity, a higher concentration of ligand is required to compensate for the decrease in matrix stiffness. The inverse relationship between the substrate stiffness and ligand density supports the hypothesis that both mechanical and biochemical cues play important compensating roles in cell migration.

The interplay of the two cues is also seen in the data that shows on softer 2500 and 1250 Pa gels, at FN concentration below 0.01 mg/ml, the cells cannot adhere strongly to the substrate and therefore are not motile, as compared to either a stiffer 7900 Pa gel or a glass substrate. Also note the biphasic behavior is not observed on the ligand-saturated 1250 Pa gels, introducing a limit to how much ligand density can rescue motility on soft surface. Cell motility does not decrease even after the polyacrylamide surface has been saturated with ligand.

Further comparison of cell motility on gels of different stiffnesses was performed at three FN ligand concentrations, 0.01, 0.05 and 0.1 mg/ml (Fig. 3.1B). The cell speed goes through a maximum as the substrate stiffness increases and the maximum shifts to higher



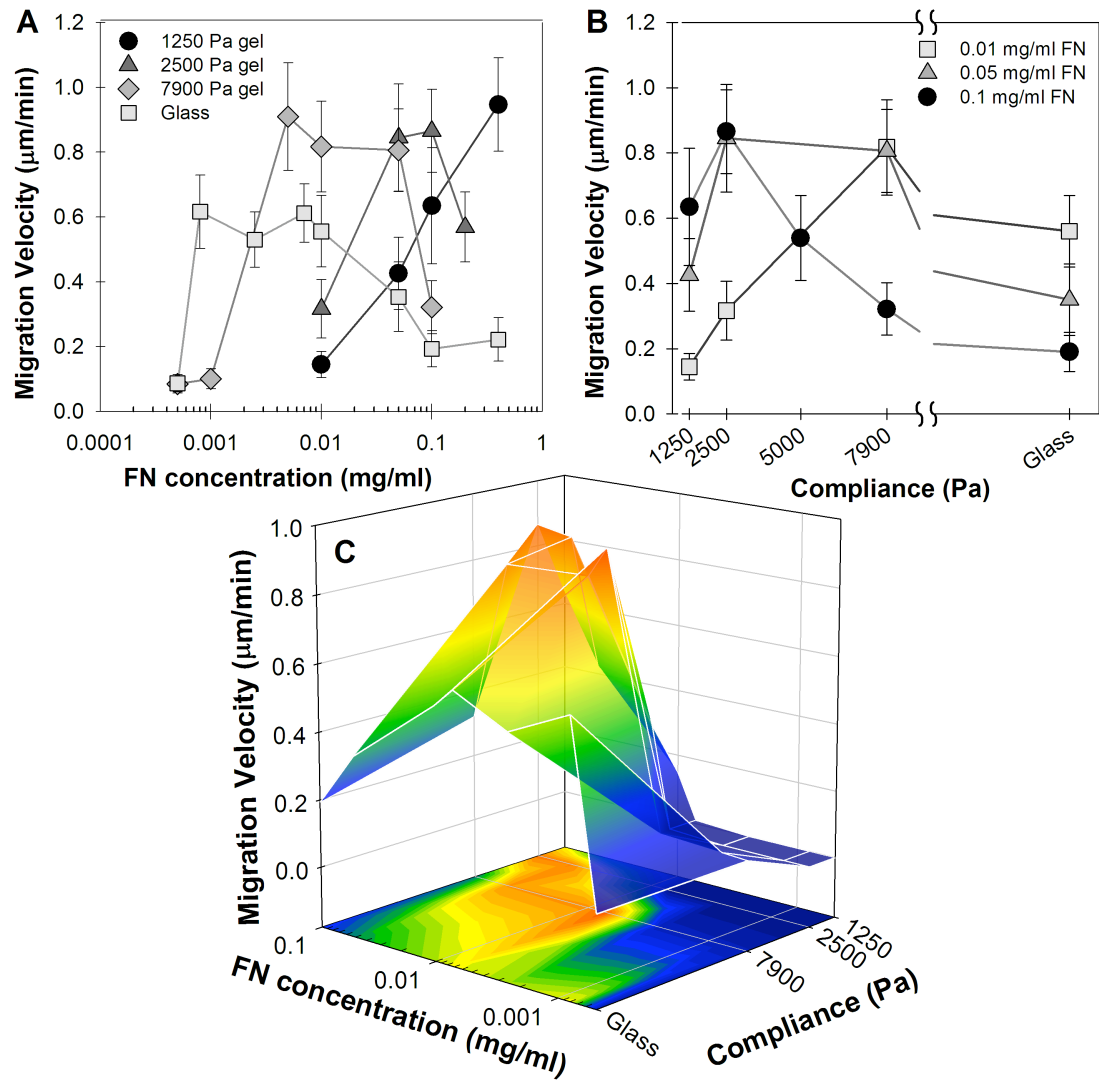


Figure 3.1: Cell migration velocity as a function of the ECM. MCF10A human breast epithelial single cell migration velocity is plotted as a function of both biochemical and mechanical cues of the extracellular matrix (ECM). Single cell velocity is observed on substrates with increasing fibronectin (FN) ligand concentration (A) on (■) glass, and polyacrylamide gels of (◆) 7900 Pa, (▲) 2500 Pa, (filled circle) 1250 Pa Young's elastic modulus. Velocity profile displays a shifting biphasic function of FN concentration. (B) Gel compliance also dictates single cell motility in a shifting biphasic manner, as seen on (■) 0.01 mg/ml, (filled circle) 0.05 mg/ml and (▲) 0.1 mg/ml FN bulk concentration gels with increasing stiffness. (C) 3D mesh plot and underlying 2D projection demonstrate the shifting maximum velocity peak as a function of FN concentration and gel compliance ECM parameters,  $\pm$  SEM

stiffness with decreasing ligand concentration. At lower FN concentration the stiffness of the matrix must be higher to achieve the same speed as at higher FN concentration and lower gel rigidity. Comparatively the effect of FN surface density and compliance is not the same on cell spread area, which is a monotonically increasing function of both cues (Fig. 3.2).

Fig. 3.1C is a three dimensional plot with the underlying heat map that shows how decreasing substrate rigidity from high to low and increasing substrate adhesiveness from low ligand density to high shifts the specific ECM conditions at which the cell is able to achieve maximum migration velocity, combining the results from Fig. 3.1A and B. The plot shows the maximum in migration velocity is reached at an intermediate value of both adhesion and compliance.

Spread area of MCF10A breast epithelial cells is found to be monotonically increasing with both ligand density and stiffness, Fig. 3.2, although cells on softer substrate of 1250 Pa reach a limit to spread area and can not spread as much as cells on higher stiffnesses.

## **3.2 ECM mediated cell-cell adhesion slows migration**

In this work we also investigated the role of cell-cell adhesion in cell motility. Previously, Reinhart-King and co-workers showed that cell-cell interactions between bovine aortic endothelial cells on compliant surfaces can decrease cell migration and dispersion [20]. We find mammary epithelial cell-cell interaction consistently decreases the velocity of the cells in contact on all substrate configurations.

To explore if cell-cell adhesion hinders cell migration, we compared the motility of individual cells and cells in contact (Fig. 3.3A). At higher FN concentration or softer compliance, we found the cell speed is always lower for cells in pairs than individual cells. The significant reduction of speed due to cell-cell interactions on 7900 and 2500 Pa gels occurs

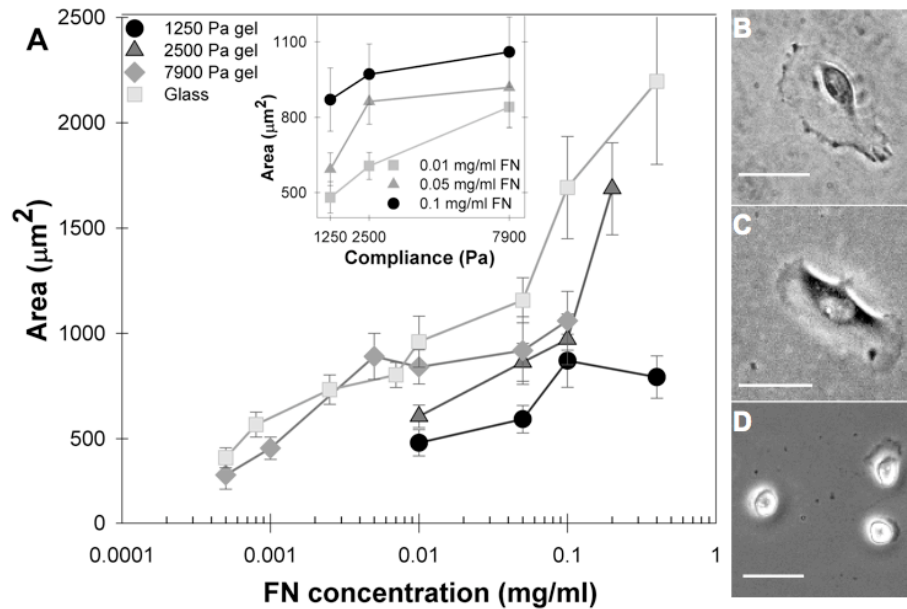


Figure 3.2: Cell spread area as a function of the ECM.

MCF10A human breast epithelial cells plated sparsely (see methods) on (■) glass and on polyacrylamide gels of varying stiffness (◆) 7900 Pa, (▲) 2500 Pa, (filled circle) 1250 Pa Young's modulus and coated with increasing Fibronectin (FN) ligand concentration. Single cell spread area (A) plotted as a function of increasing ligand concentration. Inset is cell area as a function of increasing gel stiffness on gels coated with (■) 0.01, (filled circle) 0.05 and (▲) 0.1 mg/ml FN,  $\pm$  SEM. Representative snapshots of cells plated on FN saturated surfaces at 0.1 mg/ml bulk concentration on glass (B), 0.2 mg/ml on 2500 Pa (C) and 0.4 mg/ml on 1250 Pa (D) compliant gel. Scale bar = 50  $\mu$ m

at values of FN concentration where maximum velocity had been observed for individual cells. At sufficiently high FN concentrations, migration velocity decreases for individual cells and those in contact. On softer 1250 Pa gels cell-cell interactions slow cell velocities at all FN concentrations. On these gels of elasticity similar to that of tumor adjacent stroma in human breast [5, 46], cell-cell interactions significantly reduce motility, suggesting a compliance threshold up to which cell-cell adhesion prevents cell invasiveness.

In Fig. 3.3B single cell motility and the motility of cells in pairs are compared for each FN concentration as a function of gel compliance. Again, interacting cells move more slowly than individual cells at gel rigidities where the single cell speed is maximal. For low FN density, 0.01 mg/ml, the difference is only significant on a 7900 Pa gel. However at high FN density, 0.1 mg/ml, the velocity of interacting cells is significantly slower on softer substrates of elastic moduli 1250 and 2500 Pa.

Further quantification of the effect of cell-cell interaction shows novel findings that cell migration depends on duration of cell-cell contact, Fig. 3.4A. Cell-cell interaction is represented by fraction of time the cells spend in contact. The migration velocity of cell pairs decreases linearly as a function of cell contact duration on FN coated gels. Best fit analysis the data also shows the magnitude of the negative slope of velocity versus contact fraction is increasing with increasing gel stiffness. It is evident cell-cell adhesion has a more pronounced effect and decreases cell motility more acutely on softer 1250 Pa substrate than on stiffer substrates. Thus although the magnitude of migratory reduction depends on ligand density and compliance of the ECM environment, it is the compliance of the ECM that dictates the extent of contact inhibited migration. Prolonged cell-cell contact decreases cell motility more appreciably as the substrate stiffness decreases.

Optimum cell migration is also uniquely a function of the cell spread area, evoked at multiple specific combinations of the two ECM conditions. The relationship between migration velocity and cell spreading area is quantified for isolated single cells (i) and cells

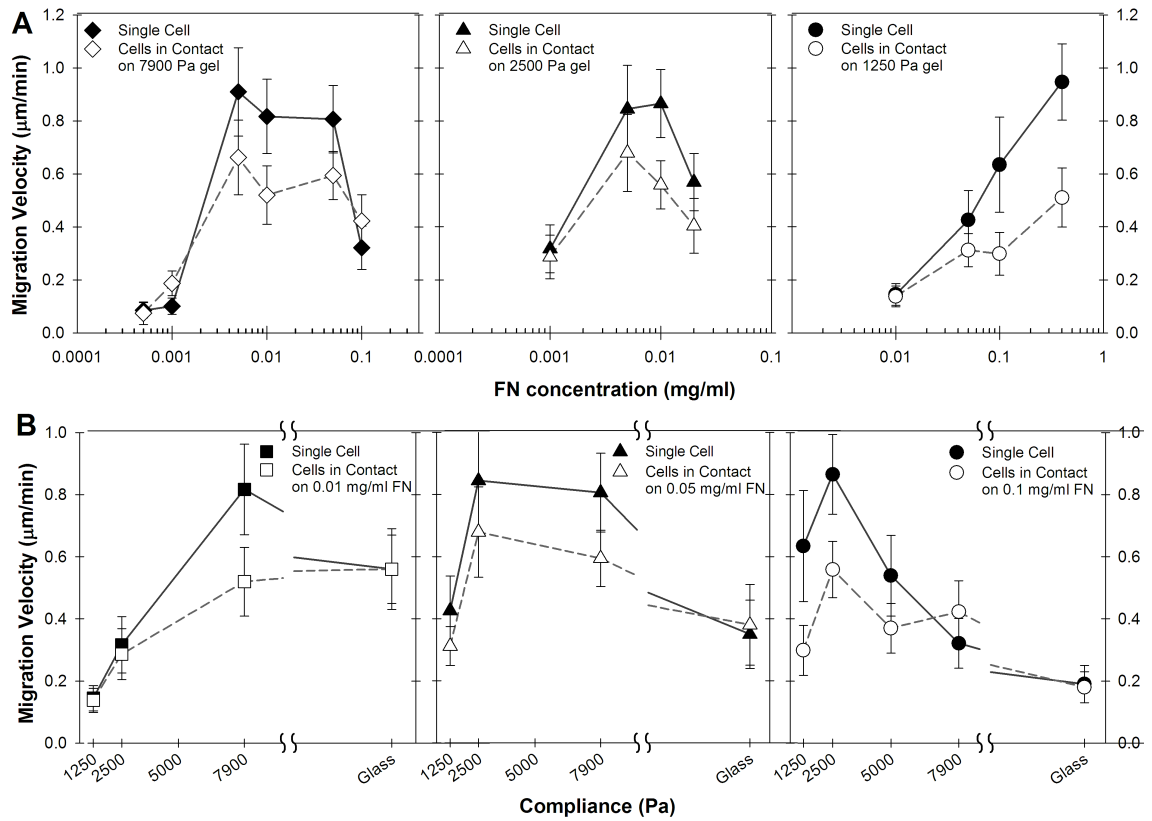


Figure 3.3: Cell velocity profile of single and adherent cells.

MCF10A cell migration velocity of single cells is compared to cells in contact. Velocity is plotted as a function of (A) increasing FN ligand concentration on gels of decreasing stiffness ( $\blacklozenge$ ) 7900 Pa, ( $\blacktriangle$ ) 2500 Pa, (filled circles) 1250 Pa Young's modulus and (B) as a function of compliance on ( $\blacksquare$ ) 0.01 mg/ml, (filled circles) 0.05 mg/ml and ( $\blacktriangle$ ) 0.1 mg/ml FN bulk concentration. Cell velocity ( $\mu\text{m}/\text{min}$ ) is plotted for single cells (filled markers) and cell pairs in contact (empty markers),  $\pm$  SEM

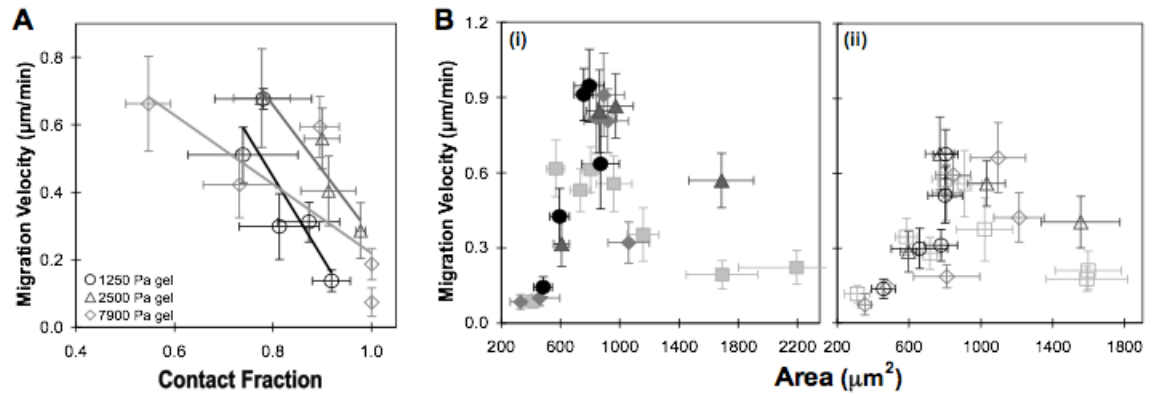


Figure 3.4: Cell-cell contact inhibits maximum velocity.

MCF10A cell migration velocity is a function of cell-cell contact fraction (A) and cell spread area (B). Cell pair motility decreases with increasing cell-cell adhesion duration (A). The slopes of the best fit lines are -1.0, -1.9, and -2.4 for 7900, 2500, and 1250 Pa gels respectively. The magnitudes of slopes are increasing with decreasing substrate stiffness, therefore cell-cell adhesion has a stronger affect on cell migration on more compliant gels. (B) Cell migration is a biphasic function of cell spread area for (i) single cells (filled markers) and (ii) cells in contact (empty markers). Maximum migration velocity is achieved by single cells in area range of 750 to 1000  $\mu\text{m}^2$ . However cells in contact do not exhibit same maximum migration velocity as do single cells. The cell velocity ( $\mu\text{m}/\text{min}$ ) is measured on ( $\blacksquare$ ) glass, ( $\blacklozenge$ ) 7900 Pa, ( $\blacktriangle$ ) 2500 Pa, (filled circles) 1250 Pa Young's modulus,  $\pm$  SEM

in pairs (ii) in Fig. 3.4B. For all cells, the migration velocity is a biphasic function of cell area, whereas area is a linearly increasing function of substrate adhesion and compliance (Fig. 3.2). The maximum velocity is observed for isolated cells at spread area of 750 to 1000  $\mu\text{m}^2$ . Cells outside this range of spread area are not able to migrate as fast, no matter the ECM stiffness or ligand density. Both cues of the ECM stimulate the cell to spread and dictate the optimum area where the cell can then achieve maximum migration. Cell-cell interaction also prevents cells in pairs from reaching the same maximum velocity as single cells at that same spread area (Fig. 3.4B).

Furthermore, it has been previously shown that the spread area is directly related to the cells ability to generate force [5, 37] and that maximum cell speed is related to intermediate level of force generation, for numerous integrin and ligand expression levels [38]. Thus we can elucidate the link between intermediate spread area and maximum velocity lies in the

cells ability to generate optimum traction with the substrate. Our results conclude that both mechanical and biochemical factors acting together evoke optimum spread area and force generation to achieve maximum velocity.

Video micrographs of pairs of cells and their persistent interactions indicate that adhesiveness and compliance of the surrounding matrix play a role in the dynamics of cell-cell interactions (Fig. 3.5). On a stiffer substrate of 7900 Pa, cell-cell contact is continuous at FN concentration of 0.05 mg/ml, Fig. 3.5A. The two cells do not lose contact, pull each other in all directions and are unable to migrate in unison nor independently. However on 0.05 mg/ml FN coated soft 1250 Pa gel, there is minimal interaction between cells. Two cells pictured in Fig. 3.5B collide, redirect themselves and move on. The cells slow down briefly upon collision, but do not form a lasting connection as they continue to migrate independently away from each other. However, when FN concentration is significantly increased to 0.4 mg/ml on the same soft gel, two cells pictured in Fig. 3.5C do not lose contact, but rather pull and push each other as they attempt to migrate together. The cells are unable to successfully move, just like the ones on gels in Fig. 3.5A. Thus inverse changes in substrate elasticity and adhesion result in the same cell-cell behavior.

### **3.3 ECM compliance promotes formation of 3D multicellular structures on 2D surface**

Cell-cell adhesion's significant affect on cell behavior on soft gels lead us to hypothesize that reduction in substrate compliance to 400 Pa stiffness, similar to pre-malignant breast tissue, would further promote cell-cell adhesiveness and increase cell assembly. Plating the cells at 0.1 mg/ml FN concentration on the 400 Pa gels greatly decreased cell motility and cell-cell contacts were persistent and permanent over a period of 3 days. Cells were unable to spread nor significantly migrate, however when in close proximity, cells did

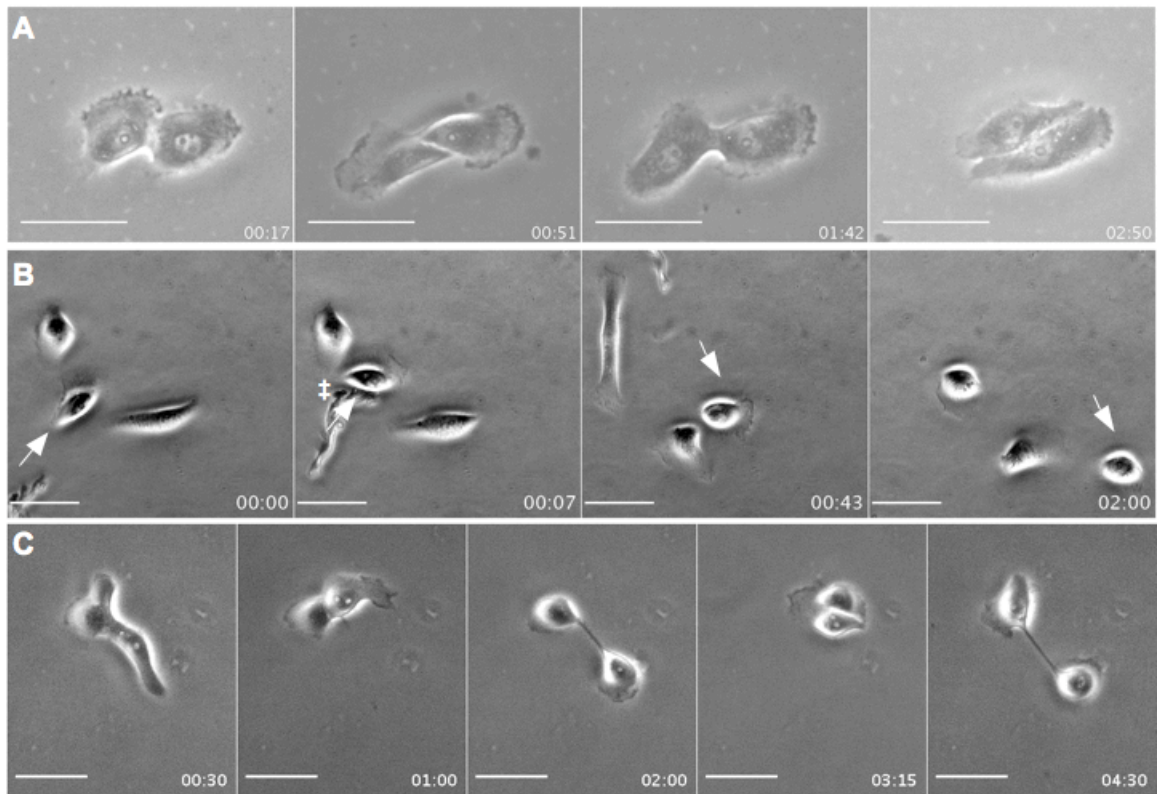


Figure 3.5: ECM mediated cell interactions visualized.

MCF10A cell pairs pictured at time points captured with phase microscopy. The cells are imaged on (A) 7900 Pa gel coated with 0.05 mg/ml FN, (B) 1250 Pa gel coated with 0.05 mg/ml and (C) 0.4 mg/ml FN bulk concentration. → follows the cell of interest and † denotes cells in brief contact. HH:MM. Scale bar = 50  $\mu$ m



come together and remain attached. With time they divided and rearranged themselves into spherical three dimensional structures even on two dimensional gels. Cell assembly was first observed after 24 hours of incubation on polyacrylamide gel, Fig. 3.6A. Cell division and re-arrangement into more spherical or ellipsoid aggregates was observed next, after 48 hours of incubation on these PA gels, as illustrated in Fig. 3.6B and C.

After 72 hours of incubation on 1250 and 400 Pa gels, cell aggregates were found on the two dimensional surfaces as illustrated in Fig. 3.7. On 1250 Pa gels, the cells formed islands of two dimensional aggregates, Fig. 3.7A. However on 400 Pa gels the aggregates were three dimensional as confirmed with phase microscopy z-axis focus that revealed cells at multiple heights of the aggregate. The third dimension of the aggregates was confirmed with staining of the nuclei and observing that some nuclei were residing on top of other, Fig. 3.7B.

In addition to the time lapse phase microscopy images, we further tested whether the aggregates assembled into the 3D structure or proliferated to form the structures. Prior to plating on 400 Pa gels, half of the cell population was incubated with cell tracker beads while the other half was not. The mixed final sample was plated and incubated for 72 hours. Some 3D aggregates were found to have both bead and no-bead containing cells, confirming cell assembly is involved in formation of 3D aggregates. In some 3D aggregates none of the cells had beads while in others all cells contained beads. These results imply that cells divided into these structures (Fig. 3.7C). Similar results were found on 140 Pa gels, which is the elasticity similar to that of normal breast tissue (data not shown).

It is further important to mention one important driver for the observed cell aggregation, which is the cell's ability to sense its neighbors. Cells can sense the deformation of the elastic substrate through durotaxis, as has been shown previously with NIH 3T3 fibroblasts on polyacrylamide gels [37]. These cells were able to sense and migrate toward the stretched and stiffer substrates. In our experiments on softer substrates, we find the MCF10A cells

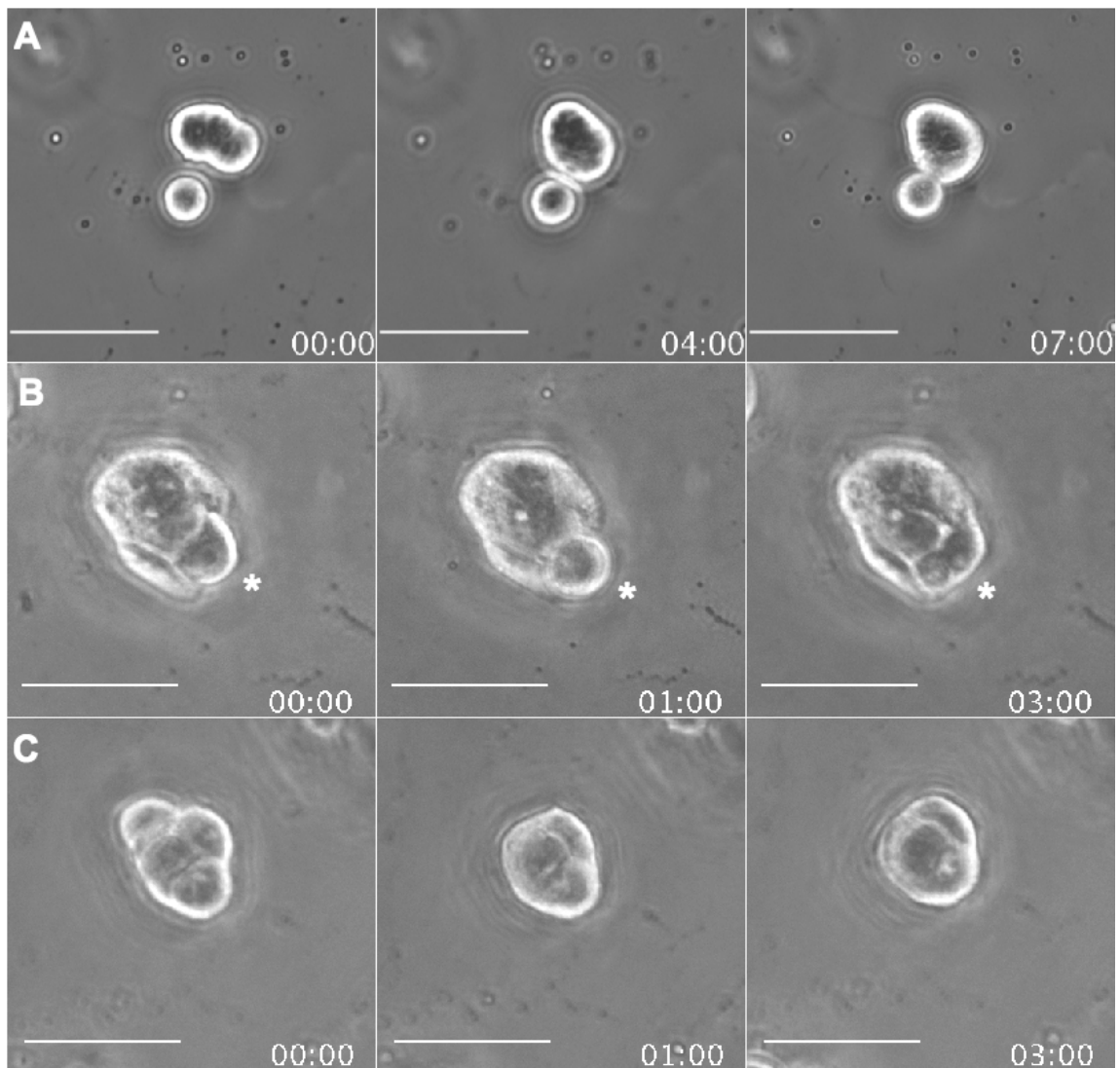


Figure 3.6: Cell assembly and aggregate initiation.

MCF10A cells assemble, divide and re-arrange into 3 dimensional aggregates on soft gels with elastic modulus similar to pre-malignant tissue. (A) 24 hrs after plating, MCF10A cells were imaged for 8 hours (see methods) and observed to assemble. 48 hours after plating the cells were observed to divide (B) and re-arrange (C) into spherical 3-dimensional aggregates on 2-dimensional FN coated polyacrylamide gels. All gels are 400 Pa and coated with 0.1 mg/ml FN. \* denotes a cell undergoing division. HH:MM. Scale bar = 50  $\mu$ m

are able to sense the mechanical substrate deformation due to forces applied by nearby cells and thus migrate toward each other. This phenomenon is demonstrated in Fig. 3.7, where cells migrate toward each other on the 1250 Pa gels and after 72 hours of incubation remain attached to each other forming 2D islands of cells on the gels. On more compliant substrates, these aggregates become spherical and three dimensional. Thus the flexible substrate induces tissue-like aggregation of MCF10A cells, similarly as the 3T3 cells studied [37]

Therefore the cells do not need a 3D environment, as they are mechanosensing the softness of the substrate which drives the formation of an energetically optimal spherical 3D aggregate. These aggregates may be the 2-dimensional analogues of the energetically favorable spherical acini structures these cells form in 3-dimensional gels [5]. Comparatively, cells on 1250 Pa gels cluster and stick together and form a 2D-aggregate of cells, but do not protrude in 3rd dimension (Fig. 3.7). Further increase in rigidity above 1250 Pa or decrease in ligand density do not produce similar tight-island like aggregates in two nor three dimensions (Fig. 3.8).

Furthermore we find the 3D aggregates in mouse mammary epithelial cells, EpH4-J3B1 [44], as well, Fig. 3.9. On 1250 Pa gels coated with GFOGER collagen peptide after 3 days of incubation cells form 2 dimensional tight islands and no 3 dimensional structures, Fig. 3.9A. Although we did find that after 6 days of incubation the cells formed tube like structures with very few but present 3 dimensional aggregates on the tip, as seen in Fig. 3.9B and the inset fluorescent nuclei staining which shows a few nuclei residing on top of other nuclei. This is similar to the observed EpH4-J3B1 behavior in 3D collagen culture as reported by Montesano et al. [44]. This structure is also similar to native in vivo breast tissue that consists of ducts leading into spherical lumen containing acini [6, 45]. On softer gels of 675 Pa 3D aggregates started developing 2 days and grew 3 days after plating as seen with inset nuclei staining, Fig. 3.9C and D.

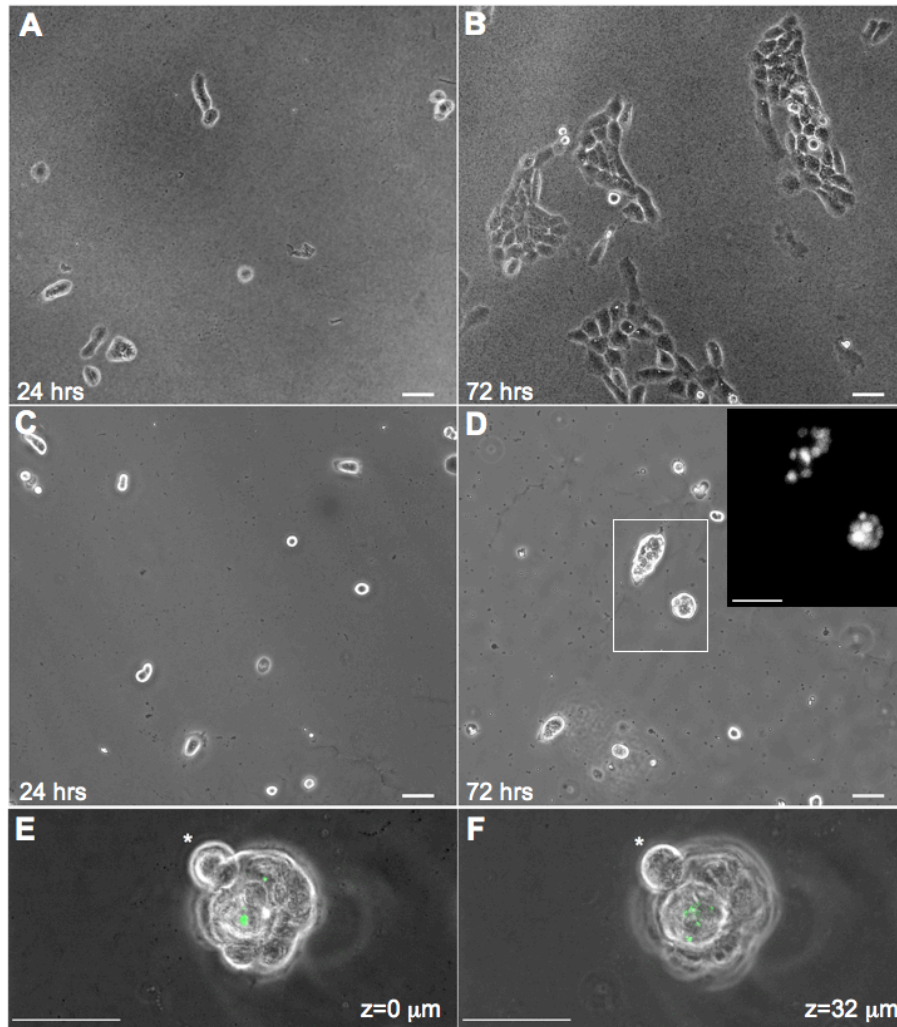


Figure 3.7: MCF10A 3D spherical aggregates on 2D substrates.

MCF10A cells on softer 2-dimensional FN coated polyacrylamide gels 24 hours after plating (A and C) and the respective aggregates 72 hours after plating (B, D-F). (A-B) 2D aggregates on 1250 Pa gels coated with 0.1 mg/ml FN. (C-D) On softer 400 Pa gels coated with 0.1 mg/ml FN, 3 dimensional aggregates are shown with inset fluorescent image of Hoechst dye stained nuclei in 3D locations (D). (E-F) Bottom to top view of a 3D aggregate 72 hrs after plating, with  $z=0 \mu\text{m}$  at the gel surface and slice  $32 \mu\text{m}$  above on 0.1 mg/ml FN coated 400 Pa gel. 72 hr snapshots with fluorescent beads were taken to test whether cells assemble or proliferate into 3D structures via pre-incubating half of the cells with fluorescent beads and mixing equally with unlabeled cells prior to plating. \* denotes a cell undergoing division. Scale bar =  $50 \mu\text{m}$

Califano and Reinhart-King showed that bovine aortic endothelial cells assemble into tubular structures on low compliance gels (at elasticity below 1250 Pa) [14]. Recently Saunders and Hammer further showed that the aspect ratio, useful metric for quantifying the propensity of cells to form networks, is not network conducive on substrates of stiffness greater than 1050 Pa for human umbilical vein endothelial cells [41]. Thus it may be that cells of all types are encoded with a mechanical sensitivity to substrate elasticity that drives them into multi-cellular structures appropriate to their phenotype. It is interesting to explore the universality of this 1 kPa compliance associated switch further. These extensive results beg to question other cell types to understand if all cells experience a universal compliance threshold.

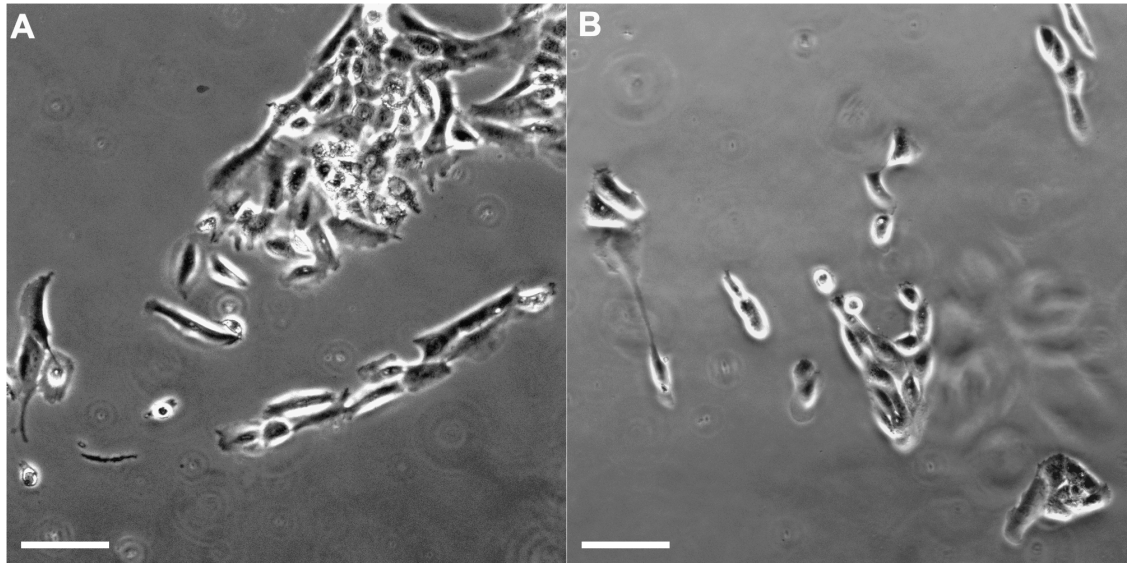


Figure 3.8: Absence of aggregates on stiffer substrates. MCF10A cells seeded at low density and imaged 72 hours after plating. (A) Cells plated on 2500 Pa gels and 0.01 mg/ml FN density. (B) Cells on 7900 Pa gels and 0.001 mg/ml FN. 3-dimensional aggregate formation is not observed at these ECM conditions. Scale bar = 50  $\mu$ m

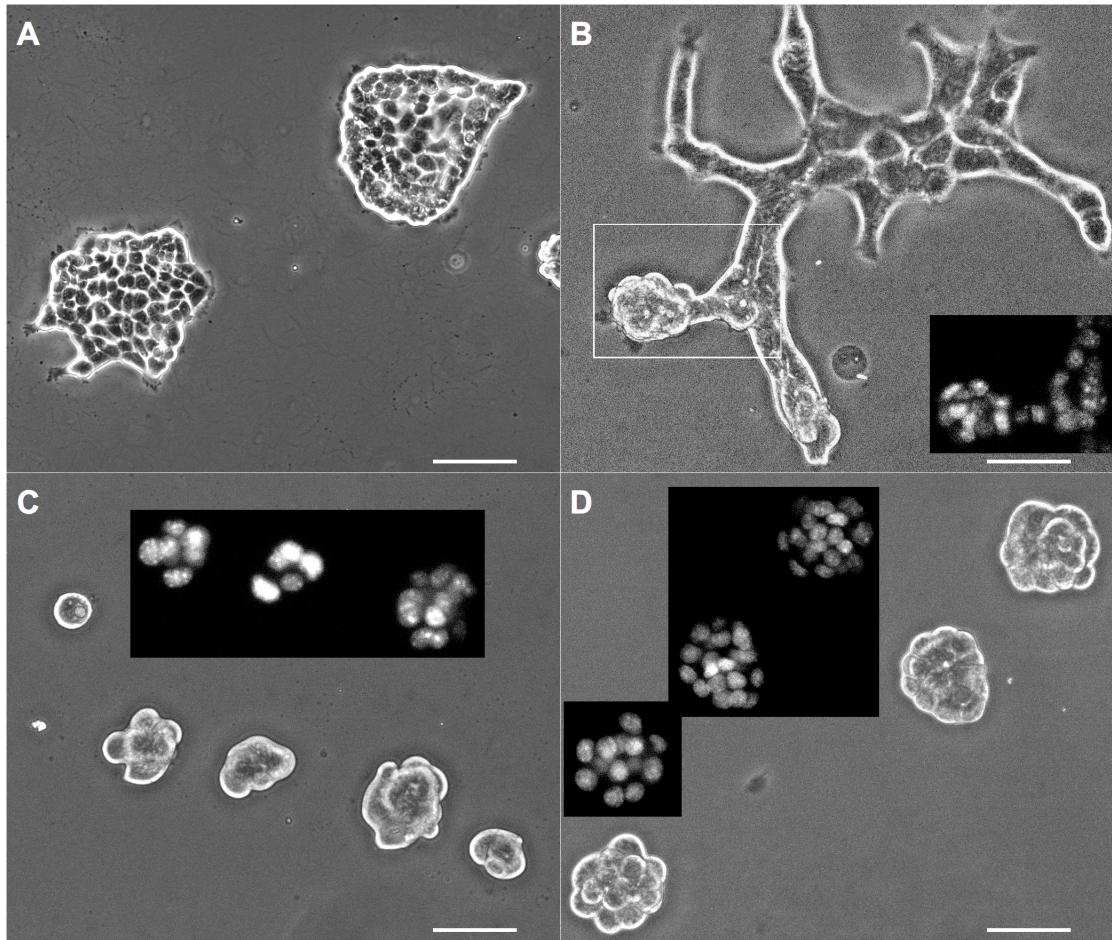


Figure 3.9: Mouse mammary epithelial cell aggregates.

Mouse mammary epithelial cells, EpH4-J3B1, on 0.05 mg/ml GFOGER collagen peptide saturated gels. EpH4 cells imaged (A) 3 days and (B) 6 days after plating on 1250 Pa gels. Cell aggregates on 675 Pa gels (C) 2 days and (D) 3 days after plating. Inset Hoecht dye stained nuclei. Scale bar = 50  $\mu$ m

### 3.4 Mechanical and Biochemical ECM model

These findings link extracellular environment to collective cell behavior through the intracellular connection between cell-matrix and cell-cell adhesions, as represented in schematic Fig. 3.10. It is clear from the data that increasing biochemical stimuli on gel surface activates stronger cell-cell adhesion through a cascade of intracellular molecular events. The activated cell adherens junctions (AJ) then maintain cells in continuous contact, and once adherent to each other the cells' migration is then inhibited. The cells would rather maintain contact than move independently. Increases in surface ligand concentration beyond the optimum amount on the specific rigidity, continue to strengthen cell-matrix adhesion and decrease cell motility for individual cells and cell pairs alike. The data further concludes that increasing the mechanical stimuli favors cell-matrix interaction over cell-cell interaction. Softer, more elastic matrices are unable to induce strong mature cell-matrix adhesion and cell-cell adhesion is more evident. The mechanical conditions of the environment increase the affinity and strength of cell-cell adhesion to such an extent that mammary epithelial cells further organize into 3 dimensional structures. Therefore, it is the mechano-driven ligand-integrin activation of proteins and molecular pathways inside the cell that promote stronger cell-cell adhesions, while the compliance of the matrix inhibits the formation of strong substrate adhesion.

The data suggests a link between ligand-integrin engagement and the formation of strong adherens junctions between cells. Integrin-cadherin crosstalk and connection has been previously explored [32, 39, 40] and our results suggest it plays a role in collective cell behavior. One possible interpretation of our findings is that focal adhesions are activated by biochemical and mechanical properties of the ECM, whereas AJs are activated by biochemical cues and inhibited by mechanical cues. Cell-cell interaction is activated and favored at high ligand density, but is reduced by the rigidity of the ECM. At high stiffness, the adhesion between two cells is not able to override the strength of cell-matrix adhesion



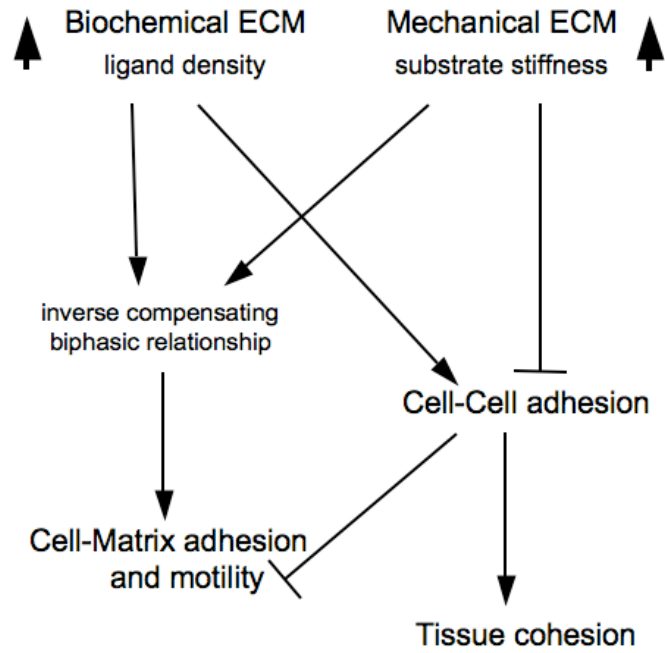


Figure 3.10: Schematic summary of effects of biochemical and mechanical cues of the ECM on cell-cell and cell-matrix interactions leading to cell motility and cell-cell assembly.

due to increasing mechanical cues of the ECM. But on softer gels cell-cell interaction is stronger and thus cell migration is limited and cell-cell assembly is promoted, summarized in Fig. 3.10.

### 3.5 Bibliography

1. Kass, L., et al., Mammary epithelial cell: influence of extracellular matrix composition and organization during development and tumorigenesis. *International Journal of Biochemistry and Cell Biology*, 2007. 39(11): p. 1987-94.
2. Tognon, C., et al., Expression of the ETV6-NTRK3 gene fusion as a primary event in human secretory breast carcinoma. *Cancer Cell*, 2002. 2(5): p. 367-376.
3. Weaver, V.M., et al., Reversion of the malignant phenotype of human breast cells in three-dimensional culture and in vivo by integrin blocking antibodies. *Journal of Cell Biology*, 1997. 137(1): p. 231-245.
4. Wolfe, J.N., Risk for Breast-Cancer Development Determined by Mammographic Parenchymal Pattern. *Cancer*, 1976. 37(5): p. 2486-2492.
5. Paszek, M.J., et al., Tensional homeostasis and the malignant phenotype. *Cancer Cell*, 2005. 8(3): p. 241-254.
6. Debnath, J. and J.S. Brugge, Modelling glandular epithelial cancers in 3-dimensional cultures. *Nat Rev Cancer*, 2005. 5(9): p. 675-88.
7. Debnath, J., S.K. Muthuswamy, and J.S. Brugge, Morphogenesis and oncogenesis of MCF-10A mammary epithelial acini grown in three-dimensional basement membrane cultures. *Methods*, 2003. 30(3): p. 256-268.
8. Li, T., et al., The association of measured breast tissue characteristics with mammographic density and other risk factors for breast cancer. *Cancer Epidemiology Biomarkers & Prevention*, 2005. 14(2): p. 343-349.
9. Brown, L.F., et al., Vascular stroma formation in carcinoma in situ, invasive carcinoma, and metastatic carcinoma of the breast. *Clinical Cancer Research*, 1999. 5(5):

p. 1041-1056.

10. Hao, X.S., et al., Differential gene and protein expression in primary breast malignancies and their lymph node metastases as revealed by combined cDNA microarray and tissue microarray analysis. *Cancer*, 2004. 100(6): p. 1110-1122.
11. Tawil, N.J., et al., Integrin alpha(3)beta(1) can promote adhesion and spreading of metastatic breast carcinoma cells on the lymph node stroma. *International Journal of Cancer*, 1996. 66(5): p. 703-710.
12. Duguay, D., R.A. Foty, and M.S. Steinberg, Cadherin-mediated cell adhesion and tissue segregation: qualitative and quantitative determinants. *Developmental Biology*, 2003. 253(2): p. 309-23.
13. Foty, R.A. and M.S. Steinberg, Cadherin-mediated cell-cell adhesion and tissue segregation in relation to malignancy. *International Journal of Developmental Biology*, 2004. 48(5-6): p. 397-409.
14. Califano, J.P., and C.A. Reinhart-King, A balance of substrate mechanics and matrix chemistry regulates endothelial cell network assembly. *Cellular and Molecular Bioengineering*, 2008. 1: p. 122-32.
15. Lauffenburger, D.A. and L.G. Griffith, Who's got pull around here? Cell organization in development and tissue engineering. *Proceedings of the National Academy of Sciences of the United States of America*, 2001. 98(8): p. 4282-4284.
16. Lo, C.M., et al., Cell movement is guided by the rigidity of the substrate. *Biophysical Journal*, 2000. 79(1): p. 144-152.
17. Peyton, S.R. and A.J. Putnam, Extracellular matrix rigidity governs smooth muscle cell motility in a biphasic fashion. *Journal of Cellular Physiology*, 2005. 204(1): p. 198-209.

18. Wong, J.Y., et al., Directed movement of vascular smooth muscle cells on gradient-compliant hydrogels. *Langmuir*, 2003. 19(5): p. 1908-1913.
19. Yeung, T., et al., Effects of substrate stiffness on cell morphology, cytoskeletal structure, and adhesion. *Cell Motility and the Cytoskeleton*, 2005. 60(1): p. 24-34.
20. Reinhart-King, C.A., M. Dembo, and D.A. Hammer, Cell-cell mechanical communication through compliant substrates. *Biophysical Journal*, 2008. 95(12): p. 6044-51.
21. Butcher, D.T., T. Alliston, and V.M. Weaver, A tense situation: forcing tumour progression. *Nat Rev Cancer*, 2009. 9(2): p. 108-22.
22. Chen, C.S., Mechanotransduction - a field pulling together? *Journal of Cell Science*, 2008. 121(20): p. 3285-3292.
23. Vial, E., E. Sahai, and C.J. Marshall, ERK-MAPK signaling coordinately regulates activity of Rac1 and RhoA for tumor cell motility. *Cancer Cell*, 2003. 4(1): p. 67-79.
24. Gaudet, C., et al., Influence of type I collagen surface density on fibroblast spreading, motility, and contractility. *Biophysical Journal*, 2003. 85(5): p. 3329-3335.
25. Dimilla, P.A., et al., Maximal Migration of Human Smooth-Muscle Cells on Fibronectin and Type-IV Collagen Occurs at an Intermediate Attachment Strength. *Journal of Cell Biology*, 1993. 122(3): p. 729-737.
26. Dimilla, P.A., K. Barbee, and D.A. Lauffenburger, Mathematical-Model for the Effects of Adhesion and Mechanics on Cell-Migration Speed. *Biophysical Journal*, 1991. 60(1): p. 15-37.
27. Zaman, M.H., et al., Computational model for cell migration in three-dimensional matrices. *Biophysical Journal*, 2005. 88(1): p. 516A-517A.

28. Zaman, M.H., et al., Migration of tumor cells in 3D matrices is governed by matrix stiffness along with cell-matrix adhesion and proteolysis. *PNAS*, 2006. 103(29): p. 10889-10894.
29. Chen, X. and B.M. Gumbiner, Crosstalk between different adhesion molecules. *Current Opinion in Cell Biology*, 2006. 18(5): p. 572-8.
30. Miyoshi, J. and Y. Takai, Structural and functional associations of apical junctions with cytoskeleton. *Biochimica et Biophysica Acta*, 2008. 1778(3): p. 670-91.
31. Yamada, S. and W.J. Nelson, Localized zones of Rho and Rac activities drive initiation and expansion of epithelial cell-cell adhesion. *Journal of Cell Biology*, 2007. 178(3): p. 517-27.
32. Tsai, J. and L. Kam, Rigidity-dependent cross talk between integrin and cadherin signaling. *Biophysical Journal*, 2009. 96(6): p. L39-41.
33. Wang, Y.L. and R.J. Pelham, Preparation of a flexible, porous polyacrylamide substrate for mechanical studies of cultured cells. *Molecular Motors and the Cytoskeleton*, Pt B, 1998. 298: p. 489-496.
34. Wong, J.Y., J.B. Leach, and X.Q. Brown, Balance of chemistry, topography, and mechanics at the cell-biomaterial interface: Issues and challenges for assessing the role of substrate mechanics on cell response. *Surface Science*, 2004. 570(1-2): p. 119-133.
35. Pless, D.D., et al., Specific Cell-Adhesion to Immobilized Glycoproteins Demonstrated Using New Reagents for Protein and Glycoprotein Immobilization. *Journal of Biological Chemistry*, 1983. 258(4): p. 2340-2349.
36. Engler, A., et al., Substrate compliance versus ligand density in cell on gel responses. *Biophysical Journal*, 2004. 86(1 Pt 1): p. 617-28.

37. Guo, W.H., et al., Substrate rigidity regulates the formation and maintenance of tissues. *Biophysical Journal*, 2006. 90(6): p. 2213-20.
38. Palecek, S.P., et al., Integrin-ligand binding properties govern cell migration speed through cell-substratum adhesiveness. *Nature*, 1997. 385(6616): p. 537-40.
39. Reinhart-King, C.A., M. Dembo, and D.A. Hammer, Endothelial cell traction forces on RGD-derivatized polyacrylamide substrata. *Langmuir*, 2003. 19(5): p. 1573-1579.
40. Fournier, A.K., et al., Rac-dependent cyclin D1 gene expression regulated by cadherin- and integrin-mediated adhesion. *Journal of Cell Science*, 2008. 121(Pt 2): p. 226-33.
41. Saunders, R.L., and D.A. Hammer, Assembly of human umbilical vein endothelial cells on compliant hydrogels. *Cellular and Molecular Bioengineering*, 2010. 3(1): p. 60-67.
42. Byfield, F.J., et al., Absence of filamin A prevents cells from responding to stiffness gradients on gels coated with collagen but not fibronectin. *Biophysical Journal*, 2009. 96(12): p. 5095-5102.
43. Park, S., K.D. Costa, and G.A. Ateshian, Microscale frictional response of bovine articular cartilage from atomic force microscopy. *Journal of Biomechanics*, 2004. 37(11): p. 1679-1687.
44. Montesano, R. et al, Isolation of EpH4 mammary epithelial cell subpopulations which differ in their morphogenetic properties. *In Vitro Cellular Developmental Biology*, 1998. 34: p. 468-477.
45. Ewald, A.J. et al, Collective epithelial migration and cell rearrangements drive mammary branching morphogenesis. *Cell*, 2008. 14: p. 570-581.

46. Levental, I. et al., A simple indentation device for measuring micrometer-scale tissue stiffness. *Journal of Physics: Condensed Matter*, 2010. 22: p. 194120-194129.

## **Chapter 4**

# **Force profile in breast cancer invasiveness and adhesiveness**

Mechanosensing and cellular mechanotransduction are important areas of research in early tissue development and disease progression, such as cancer. Force exerted by cells on the matrix is an important part of cell spreading, migration, invasion and aggregation, and is a function of the biochemical and mechanical properties of the extracellular environment. Recent research on forces cells exert onto neighboring cells shows the importance of cell-cell mechanics in tissue integrity and homeostasis [11]. Therefore mechanical strength of both cell-matrix and cell-cell adhesions dictate cell behavior, specifically migration in cancer invasion and metastasis. However the inter-connected and complicated relationship between these forces and motility has yet to be fully explored.

In previous chapter our results showed motility increasing biphasically with increasing substrate stiffness and ligand density. These findings point to the existence of a substrate adhesivity optimum for maximum migration. This highly motile cellular behavior was found to be inhibited by cell-cell interaction, as adherent cell pairs were unable to reach the same maximal velocity as single cells on all extracellular matrix (ECM) mechanical



and biochemical conditions. Furthermore the invasive phenotype was reverted on a two-dimensional gel by decreasing the substrate stiffness to that of pre-malignant tissue. We found that mammary epithelial cells can assemble, divide, re-arrange and crawl on top of each other to form 3D tissue-like aggregates on 2D soft gels of 400 Pascals (Pa) Young's elastic modulus. This three-dimensional assembly is favored by strong cell-cell adhesion and is not observed on substrates of 1250 Pa or stiffer. The mechanical softness of the gel drives the cells to form permanent connections and adhere to each other preferentially versus the surrounding matrix. This data suggests that cells are able to mechanosense not only the matrix, but each other as well.

All of these novel findings of cell-cell mechanical linkage are supported by reported motility and force traction data of cells plated on cadherin coated glass and elastomer pillars [11, 6, 7]. Additionally the reported cross-talk between cell-matrix and cell-cell adhesions, via intracellular integrin and cadherin mediated adhesion pathways [8, 10, 13], all serve as our motivation for further research in the cross-linked cellular force mechanics.

Our findings are first to relate average cell motility to average traction force. Our data of MCF10A cell motility reveal novel dynamics of an intermediate force that elicits maximum migration of single cells but not in adherent cell pairs. We report data of maximum cell stresses on soft and stiff substrates coated with a range of ligand densities. The maximum stresses a cell is able to exert onto the underlying substrate are consistently and significantly higher in adherent cells versus single cells, although the spread area of adherent cells on average is smaller. This finding is slightly different than that reported by a study of forces exerted by sheets of cells on micropillars. Findings concluded that the cells on the periphery exerted highest forces onto the substrate and those on the inside of the sheet, much lower [2]. The possible missing links could be the number of neighbors, density of the cell packing, size and ability of the cell to spread at the edge versus the inside of the sheet. Even cell cycle of the cell can influence the force exerted onto the ECM. It would also be

interesting to find the intercellular forces in the sheet - if these forces are higher on the inside of the sheet versus the periphery.

We are also first to report cell-cell tension data of adherent cell pairs as a function of matrix stiffness and ligand density. In these experiments we find a novel linear relationship between cell-cell and cell-matrix force. The ratio of cell-cell to cell-matrix force is found linearly decreasing with cell spread area, which points to competition between the two adhesions. With increased fibronectin ligand density and gel stiffness, the cell spreads more on and adheres stronger to the substrate than that to its neighboring cell. The affect is then observed to be opposite on cell motility. Velocity decreases with increasing cell-cell to cell matrix force ratios. Which means with stronger cell-cell over cell-matrix adhesions, cell motility is decreased. It is a regulated balance and competition between cell-cell and cell-ECM adhesion that dictate motile behavior of the cells.

Adhesion complexes have been identified to connect two cells biochemically and mechanically, similarly as focal adhesions connect cells to the underlying matrix [3, 9, 14, 12]. To better understand the strength of cell-cell adhesion we further focused on  $\beta$ -catenin, a key protein that links Adheren Junctions (AJ) and intracellular mechanical actomyosin machinery.  $\beta$ -catenin is found bound to cytoplasmic domain of E-cadherin in AJ [5]. Phosphorylated E-cadherin cytoplasmic domain is found to interact directly with a hydrophobic patch of  $\beta$ -catenin [5]. Therefore  $\beta$ -catenin links intercellular adhesion to intracellular force sensing and generating proteins and therefore plays an important role in the force dependant pathway of cell-cell interaction.

Furthermore if E-cadherin bound  $\beta$ -catenin serves a supportive role in cell-cell adhesion and tissue connectivity and integrity, the unbound intracellular  $\beta$ -catenin serves an antagonistic role. Tumor cells with nuclear accumulation of  $\beta$ -catenin have also been found to undergo loss of E-cadherin expression and epithelial-mesenchymal transition, a phenomenon describing transformation events to invasive epithelial cancers [4]. Therefore we

conducted force experiments on MCF10A transfected cells with dominantly expressing  $\beta$ -catenin binding site mutant of E-cadherin. These cells are over-expressing the GFP-tagged mutant E-cadherin that is missing a  $\beta$ -catenin binding domain. As expected the mutant cells could not exert high forces onto each other, but furthermore we found they could not exert high forces onto the matrix either. Importantly the cell-cell force did not increase with matrix stiffness nor as cell-matrix force increased, thus decoupling the cross-linked pathways.

## **4.1 Motility is a function of cell-matrix traction force mediated through cell-cell adhesion**

Adhesion strength and traction forces exerted by cells onto the extracellular matrix (ECM) drive cells motility in cancer metastasis. We report novel findings of mammary epithelial cell force generation and motility as a function of cell-matrix and cell-cell adhesion. MCF10A cells are plated on soft and stiff polyacrylamide gels, 1250 and 7900 Pa respectively. The gels are coated with a range of fibronectin (FN) concentrations from low 0.001 to saturated 0.1 mg/ml.

Average traction forces increase for single and adherent cell pairs with increasing matrix stiffness and ligand density, Fig. 4.1A. There is no statistical difference between average forces of single and adherent epithelial cells. However the maximum stresses the adherent cells in pairs are able to apply onto the underlying substrate are much higher, Fig. 4.1C. On 7900 Pa stiff gels the difference between maximum stresses of single and adherent cells is statistically significant with a p value  $< 0.05$ . On softer substrate of 1250 Pa this difference is even more significant with a p value  $< 0.002$ . Therefore cell-cell adhesion activates and engages the cellular cytoskeleton to elicit higher cell-matrix stresses than a single cell is able to exert.

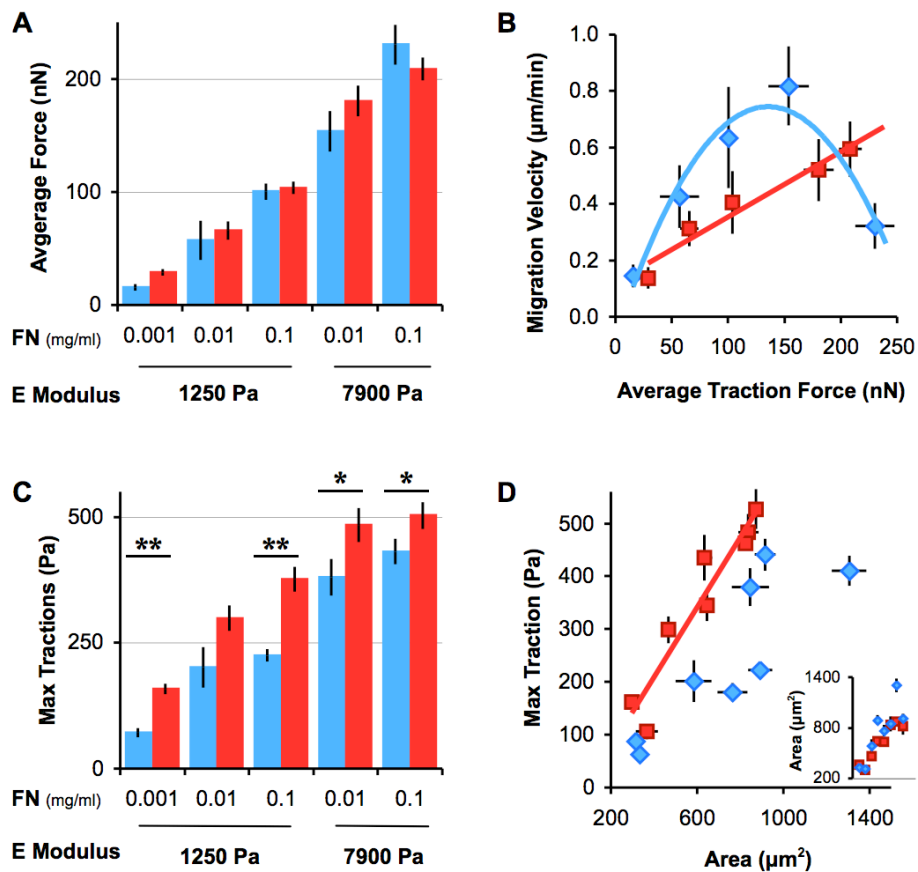


Figure 4.1: Traction forces and stresses dictate motility.

MCF10A human mammary epithelial cell traction forces are compared for single cells (blue) and adherent cell pairs (red) on physiologically soft and stiff gels, 1250 and 7900 Pa Elastic Modulus. (A) Average traction forces increase with increasing Fibronectin (FN) ligand and increasing substrate stiffness. (B) Migration velocity is plotted as a function of average traction force cells exert for single cells (◆) and adherent cell pairs (■). (C) Maximum traction stresses exerted by single cells and adherent cell pairs. \*p value < 0.05 and \*\*p value < 0.002 (D) Maximum tractions increase linearly with increasing cell area. Inset is plot of cell spread area of single and adherent cells linearly increasing with the biochemical and mechanical cues. ±SEM

The calculated average traction force on each substrate is plotted in relationship to the cell motility reported at the corresponding ECM condition previously. A novel correlation is found between single cell motility and average traction force. The speed goes through a maximum as a function of cell-matrix traction forces, Fig. 4.1B, where an intermediate force elicits the optimum single cell motility. However, this biphasic maximum is not observed in adherent cell pairs. Cells in pairs do not reach the maximum velocity at all over the range of calculated forces.

Furthermore for the similar spread areas, adherent cell pairs exert consistently higher maximum stresses onto the underlying substrate. Even though the single cells are able to spread to higher areas on some substrates, the maximum traction stresses are still lower, Fig. 4.1D. This novel data means cytoskeletal contraction is higher in adherent cells and therefore is activated by cell-cell adhesion in addition to cell-matrix adhesion. It is a novel link to cell-matrix stresses enhanced by cell-cell adhesion.

To better understand cell-cell adhesion, tension between adherent cell pairs was calculated through the matrix traction force balance (see Theory section of Chapter 1). Although cell-cell force,  $|F_{21}|$ , is increasing with increasing stiffness and ligand density, the increase is only statistically significant on softest gel and lowest FN density of 0.001 mg/ml,  $p$  value  $< 0.002$ , Fig. 4.2A. An interesting linear increasing relationship between average traction force and cell-cell force is observed, Fig. 4.2B. Furthermore to shed understanding of affect of ECM mediated spread area on the cell-cell adhesion versus cell-matrix adhesion, we find that cell-cell to cell-matrix force ratio is decreasing with increasing cell spread area. Especially on stiff 7900 Pa substrates (purple markers) force of cell-cell to cell-matrix adhesion is much lower than on soft 1250 Pa gels (green markers), Fig. 4.2C.

Since in previous work we found that cell migration velocity is slowed by cell-cell interaction, we further tested if the strength of cell-cell versus cell-matrix adhesion affects cell migration velocity. The new findings of a linearly decreasing cell migration velocity of

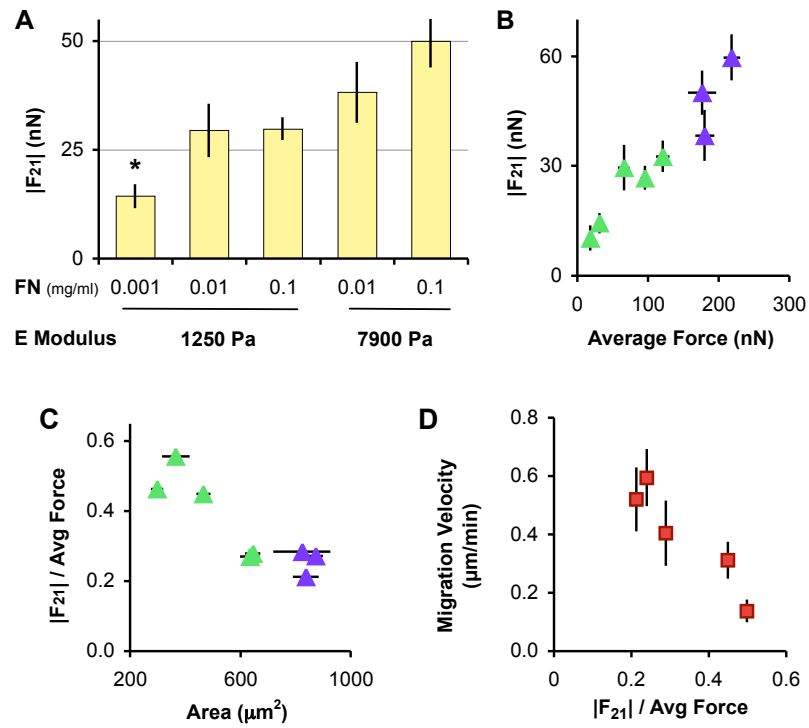


Figure 4.2: Cell-cell tension and average force relationships.

(A) Cell-cell tension,  $|F_{21}|$ , is plotted as a function of substrate stiffness, E Modulus 1250 and 7900 Pa, and FN ligand density (mg/ml). \*p value < 0.002 Further comparison of calculated traction forces is done on 1250 (green) and 7900 (purple) gels. (B)  $|F_{21}|$  is plotted versus cell-matrix average traction force. (C) Ratio of  $|F_{21}|$  to average traction force is a function of cell spread area. (D) Cell velocity is plotted as a function of  $|F_{21}| / \text{average traction force}$  ratio.  $\pm$ SEM

adherent cell pairs was found to correlate to increasing cell-cell over cell-matrix force ratio, Fig. 4.2D. This data sheds light on understanding cell-cell adhesion role in cell motility and invasiveness. We find it is not the absolute strength of the cell-cell adhesion that decreases cell motility, but rather a correlation to that of strength of cell-matrix adhesion. A cell must exert enough cell-matrix force to overcome the cell-cell tension to reach high velocity. The speed and invasiveness of adherent cells thus depends on this ratio and not on absolute cell-cell tension value. Therefore we report significant cell-cell and cell-matrix cross talk in force dynamics.

## 4.2 Role of $\beta$ -catenin in cell force profile

To better understand cell-cell force we focused on an intracellular player involved in the connection between cell-cell adhesion and cytoskeleton engagement.  $\beta$ -catenin is an important player at cell-cell junctions that mediates cytoskeletal engagement connection to E-cadherin cell-cell junctions. In normal cells it is found at AJ but in metastatic cells in cytoplasm and nucleus [1]. Furthermore assembly of new AJ has been found aided by presence of integrins [10, 9, 13], which is also observed in our staining colocalization (yellow) of  $\beta$ 1 integrin (green) and  $\beta$ -catenin (red), Fig. 4.3. Therefore we decided to further test the impact of  $\beta$ -catenin in cell force generation profile.

A dominantly expressing plasmid with mutant E-cadherin that is missing the  $\beta$ -catenin binding domain was transfected into MCF10A cells. The mutant allowed us to test the role of E-cadherin and  $\beta$ -catenin binding in adherens junctions (AJ) and activation of the actomyosin cytoskeleton in force transduction. As expected the data finds the cell-cell tension,  $|\mathbf{F}_{21}|$ , is significantly lower in mutant cells versus un-transfected cells on 1250 Pa soft and 7900 Pa stiff gels, Fig. 4.4B. The  $|\mathbf{F}_{21}|$  is not only lower but doesnot increase with increasing substrate stiffness, as observed in normal cells.

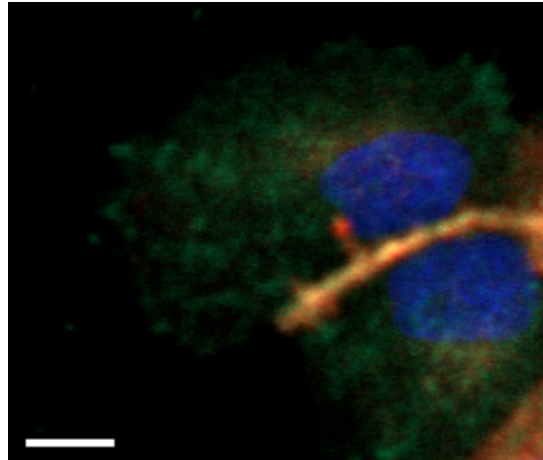


Figure 4.3: MCF10A cells fluorescent staining.

MCF10A cells on 14 kPa stiff 0.1 mg/ml fibronectin coated polyacrylamide gels were fixed and stained with Hoechst dye nuclei (blue), Alexa488  $\beta$ 1 integrin (green) and Cy5  $\beta$ -catenin (red). Yellow color at cell-cell junction is evident due to overlay of green and red, integrin and catenin staining respectively. Scale bar = 10  $\mu$ m

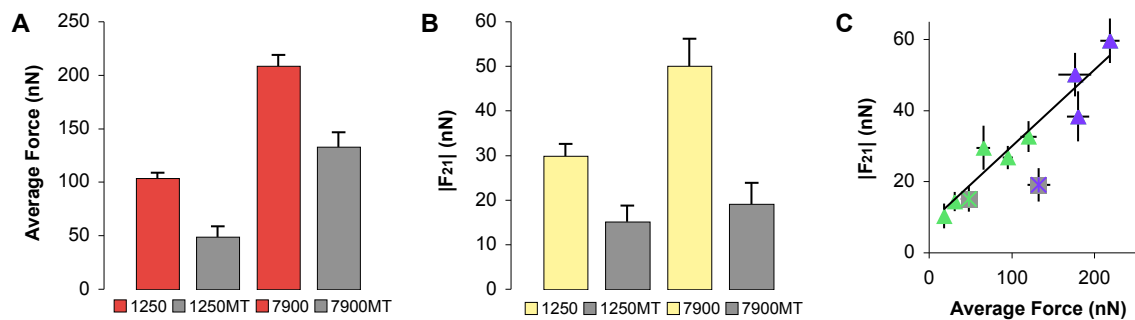


Figure 4.4: E-cadherin mutant force profiles.

Traction forces of MCF10 E-cadherin mutant transfected cell pairs (grey) are compared to normal adherent cell pairs (color). (A) Average traction force and (B) cell-cell tension,  $|F_{21}|$ , are compared on 1250 and 7900 Pa 0.1 mg/ml FN coated gels. (C) Cell-cell tension is plotted as a function of average traction force. Cells on soft 1250 Pa gels are green and on stiff 7900 Pa gels are purple and mutant cell data is shaded with grey markers (■).  $\pm$ SEM



Surprisingly the average force exerted by the mutant adherent cells is also lower than normal on both substrates, Fig. 4.4A, although it is increasing with increasing substrate stiffness. There is no significant change in cell spread area, data not shown. Furthermore mutant cell-cell force plotted in relationship to average traction force does not follow the previously reported linearly increasing relationship in normal EpH4 cells, Fig. 4.4C. Increasing substrate stiffness increases average force, but cell-cell tension remains unchanged in mutant cells. The inability of the mutant cells'  $\beta$ -catenin to bind to E-cadherin and engage the cellular cytoskeleton at the AJ prevents it from exerting strong  $|\mathbf{F}_{21}|$  forces. Therefore we report novel findings that  $\beta$ -catenin E-cadherin binding is necessary in cell-cell force transduction pathway and cross-talk.

### 4.3 Bibliography

- [1] Rodriguez-Sastre M.A., Gonzalez-Maya L., Delgado R., Lizano M., Tsubaki G., Mohar A., and Garcia-Carranca A. Abnormal distribution of e-cadherin and beta-catenin in different histologic types of cancer of the uterine cervix. *Gynecologic Oncology*, 97(2):330–336, May 2005.
- [2] A. Saez, A. Buguin, P. Silberzan, and B. Ladoux. Is the mechanical activity of epithelial cells controlled by deformations or forces? *Biophysical Journal*, 89(6):52–4, Dec 2005.
- [3] M. Lambert, O. Thoumine, J. Brevier, D. Choquet, D. Riveline, and R.M. Mege. Nucleation and growth of cadherin adhesions. *Experimental Cell Research*, 313(19):4025–40, 2007.
- [4] R. Fodde and T. Brabletz. Wnt beta-catenin signaling in cancer stemness and malignant behavior. *Current Opinion in Cell Biology*, 19(2):150–8, Apr 2007.

- [5] A H Huber and W I Weis. The structure of the beta-catenin/e-cadherin complex and the molecular basis of diverse ligand recognition by beta-catenin. *Cell*, 105(3):391–402, May 2001.
- [6] E. Kardash, M. Reichman-Fried, J.L. Maitre, B. Boldajipour, E. Papusheva, E.M. Messerschmidt, C.P. Heisenberg, and E. Raz. A role for rho gtpases and cell-cell adhesion in single-cell motility in vivo. *Nature Cell Biology*, 12(1):47–53, Jan 2010.
- [7] J. Silvestre, P. J. A. Kenis, and D. E. Leckband. Cadherin and integrin regulation of epithelial cell migration. *Langmuir*, 25(17):10092–9, Sep 2009.
- [8] N. Borghi, M. Lowndes, V. Maruthamuthu, M. L. Gardel, and W. J. Nelson. Regulation of cell motile behavior by crosstalk between cadherin- and integrin-mediated adhesions. *Proceedings of the National Academy of Sciences*, 107(30):13324–13329, 2010.
- [9] W. J. Nelson. Regulation of cell-cell adhesion by the cadherin-catenin complex. *Biochem Soc Trans*, 36:149–55, 2008.
- [10] X. Chen and B. M. Gumbiner. Crosstalk between different adhesion molecules. *Current Opinion in Cell Biology*, 18(5):572–8, 2006.
- [11] A. Ganz, M. Lambert, A. Saez, P. Silberzan, A. Buguin, R. M. Mege, and B. Ladoux. Traction forces exerted through n-cadherin contacts. *Biologie Cellulaire*, 98(12):721–30, 2006.
- [12] B. Ladoux, E. Anon, M. Lambert, A. Rabodzey, P. Hersen, A. Buguin, P. Silberzan, and R. M. Mege. Strength dependence of cadherin-mediated adhesions. *Biophysical Journal*, 98(4):534–42, 2010.
- [13] J. Tsai and L. Kam. Rigidity-dependent cross talk between integrin and cadherin signaling. *Biophysical Journal*, 96(6):L39–41, 2009.

- [14] S. Yamada and W. J. Nelson. Localized zones of rho and rac activities drive initiation and expansion of epithelial cell-cell adhesion. *Journal of Cell Biology*, 178(3):517–27, 2007.

# Chapter 5

## Force dynamics of cell-cell interactions

Cellular ability to sense mechanical stimuli and exert stress on the extracellular matrix and on its neighbors is important in tissue development and destabilization in disease progression. Numerous diseases are associated with defects in mechanotransduction [36]. In breast cancer especially, where cell metastasis is the leading cause of lethality, forces play important role in motility and invasiveness. Strength and disturbance of epithelial cell adhesions to the surrounding matrix and to its neighbors is the hallmark of the invasive metastatic phenotype. We have thus set out to understand the dynamic mechanical connection of cell-cell adhesions through cell-matrix interaction in a breast cancer model.

The role of the extracellular matrix (ECM) in force sensing and generation to cell spreading and motility has been studied in diverse cell systems. Cells are able to exert traction stresses onto the ECM through intracellular focal adhesion components connected to the cellular actin cytoskeleton [15, 16, 20, 31, 45]. Furthermore substrate mechanical stimuli have been shown to increase size, number, composition, and strength of focal adhesions and the force cells exert [45, 18, 19, 21, 34, 37].

Published data has also shown cell are able to sense mechanical stimuli and exert force through cadherin mediated adherens junctions. These experiments have been conducted

in cadherin coated polyacrylamide and polydimethylsiloxane micropillar substrates that mimicked cell surface [11, 12, 13]. Cadherin mediated cell-cell adhesion has been found connected to the cellular cytoskeleton via intracellular molecular players [26, 32, 35, 42, 43, 53, 52] and to actomyosin contractility, implicated with myosin motors [30, 40, 50]. However this unique and interesting mechanical connection involved in cell-cell adhesion is not fully understood.

Furthermore, cell-cell and cell-matrix mechanotransduction intracellular pathways are not mutually exclusive, as connection and cross-talk between them have been proposed to exist [8, 10, 13]. Cell-cell cohesion and cell-matrix adhesion were found as connected but competing pathways in the differential adhesion hypothesis [28, 29, 48]. However, vascular endothelial cadherin and cell-cell adhesion have been shown to promote cell-matrix adhesion through increase in focal adhesion size and number [44]. Whereas, ECM rigidity acts to inhibit cadherin mediated cell-cell adhesion and promote cell scattering and invasiveness [45, 51, 23]. Therefore the complicated cross-talk and connection of cell-cell and cell-matrix interaction remains unclear in mechanical dynamics and strengths of the adhesion.

In our work we analyze both cell-cell and cell-matrix forces co-currently in time for a range of interactive dynamics to understand the cellular mechanotransduction on both fronts. Experiments of breast epithelial cell pairs in contact or retracting, with some cyclically repeating the interaction, revealed novel dynamics of their interactions. The mechanical properties of the substrate gels was varied from an elastic modulus of 1250 Pascals (Pa), to 2500 and 7900 Pa, which represents the range of stiffness of pre-malignant to invasive tumor breast cancer environments [45, 17, 39]. Analysis was performed with traction force microscopy (TFM) [24]. Novel mechanics were found and quantified through cell exerted force orientation, magnitude and residual error on the extracellular substrate and on adherent cell.

Inspired by single cell polarization and orientation perpendicular to externally applied stress fields modeled and experimentally tested [22, 33, 49, 54], we performed cell polarization and orientation experiments in cell pairs. Our experimental set up has no outside source of substrate deformation. Our findings report that cells exert force onto the extracellular matrix anti-parallel to each other when they are in contact. The cells orient their force fields anti-parallel only when the two cells are in direct contact and a mechanical connection exists between the pair. This polarization is not observed prior or post contact nor for cells in close proximity, less than a cell diameter distance apart.

Furthermore we find the alignment is also dependant on the strength of the cell-cell interaction. The orientation angle begins to deviate from anti-parallel alignment and becomes random when cell-cell force is too weak, below 50 nN on all substrates. Therefore we find in adherent cell pairs, the anti-parallel orientation of force is directly a function of cell-cell adhesion, not due to substrate stiffness, nor substrate deformation or ligand type. This interesting finding is further supported by intracellular molecular biology work that shows cell-cell adhesion induces polarity and directed anti-parallel migration [25]. Most recent publication by Nelson lab found that in presence of E-cadherin, on collagen patterned surface, the cells orient their migration and traction forces[98], which supports our findings as well.

We further find cell-cell force magnitude is a function of the ECM stiffness and is dynamic in time. Average intercellular force increases with increasing ECM stiffness. Force magnitude and residual error analysis yield dynamic quantitative results of mechanical strength and signal to noise magnitude of the cell-cell adhesion in time. The temporal mechanics are a fascinating insight into strength of adhesions between the cells and the matrix, validated by analysis of error in signal. This powerful assay can predict the breaking of cell-cell bond mechanically before it is visually confirmed. Such an assay can be used in combination with biological essays to test the presence, absence as well as concen-

trations of molecular players involved strong, weak and retracting cell-cell adhesions.

Finally, we find that a mechanical connection and correlation exists between the strength of cell-cell and cell-matrix interactions, which further supports the intracellular connection and cross-talk of molecular players and pathways between focal adhesions and adherens junctions. We report experimental data that shows when adherent cell pair force increases, cell-matrix force decreases, and when the cell-cell mechanical bond weakens, the cells exert stronger stresses onto the substrate. Indicating a mechanical tug of war exists within the cell, via actomyosin contraction preferentially occurring either at cell-cell or at cell-matrix adhesion. It will be interesting to test how one adhesion's mechanical bond preferentially drives the strength of the other or if it is a random cause and effect relationship.

It is finally important to note that all the studies of cell-cell mechanical interactions were studied as a function of the ECM. Our experimental system interpolates cues from both sources. This experimental system is only possible with TFM and is ideal in identifying whether molecular players differentially prefer mechanical strength of cell-matrix over cell-cell adhesions or cross-talk to increase and decrease each simultaneously.

## **5.1 Cell-cell interaction quantified through substrate deformation**

Dynamics of cell-cell mechanotransduction of mouse mammary epithelial cell pairs elegantly tell a story through their surroundings. The interactions were captured with time-lapse microscopy and traction force calculations [24, 41]. Two single cells were observed coming together, forming a visual contact, then breaking the adhesion and retracting away from each other, for some cell pairs a repetitive cycle. Fig. 5.1A phase images provide the visual confirmation of such a cell pair in time. The interaction between the cells is reflected through the deformation of the underlying elastic polyacrylamide substrate. The

cell-deformed substrate corresponding to each phase image was tracked with fluorescent bead movements, embedded at the surface of the gel, Fig. 5.1B. In this figure, the displacement vectors are exaggerated for better visualization for a cell pair on 1250 Pa collagen coated gel.

The displacement fields of cells not in contact, at time 00:00 and 01:20, show bead movement concentrated in two or three small areas under the cell with inward stresses. Each cell thus strains the substrate at a few localized centers. These force centers either create two dipoles within the cell or co-localize in the direction of movement. In this cell pair the two dipoles persist as the cells come into contact initially, Fig. 5.1C. However as the two cells form a strong adhesion with each other they rearrange to have only one force center each, opposing to that of its partner, as seen at time 01:00 in Fig. 5.1B. The individual cells now act together as one and their anti-parallel displacement fields show the cell pair develops two dipoles as one entity. The substrate displacement vectors are larger in magnitude as each cell concentrates all of its forces to oppose the other.

Furthermore, in substrate deformation, small displacement vectors can be seen pointing perpendicular to the anti-parallel force dipoles at the cell-cell adhesion boundary. These vectors represent the substrate being ‘squeezed out’ at the site of cell junction, further illustrating the absence of force onto the substrate at this site and the presence of a mechanical bond between the two cells. An analogy can be drawn to a ‘tug of war’ between the two cells – each cell anchors itself into the substrate anti-parallel to its partner as it pulls on the other through a metaphorical rope. Thus the gel is strained on opposite ends of each cell and pushed out at the middle.

Using the traction vector definitions and Newton’s laws discussed in the Theory section, we calculated the cell traction force maps corresponding to each time point, Fig. 5.1C. The maps reflect the calculated stress magnitude and direction each cell must exert to elicit the observed deformation of the substrate. Inset is a simplified cartoon representation of the



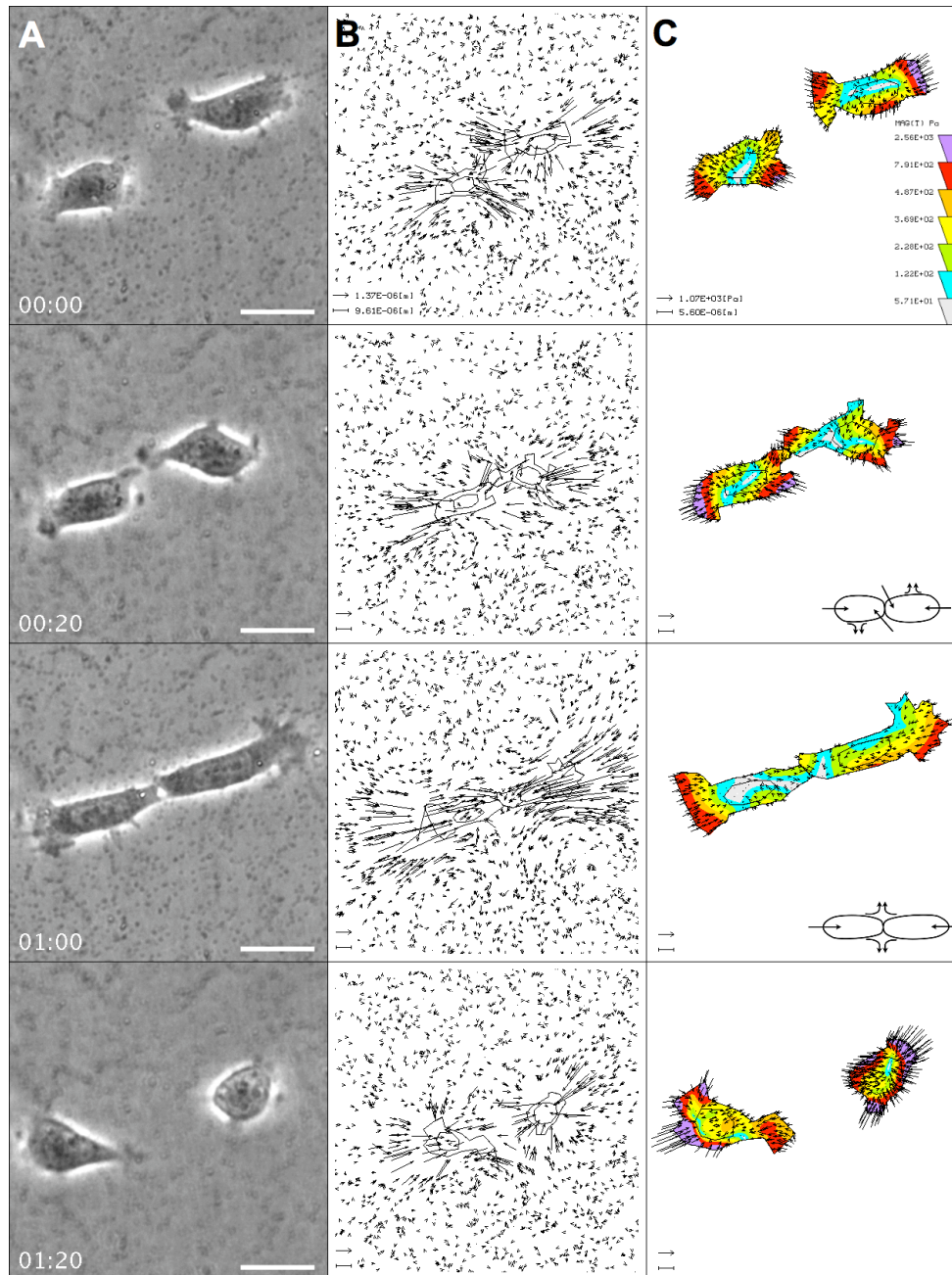


Figure 5.1: EpH4 two cell interaction visualized.

Mouse breast epithelial cell interaction is captured with time lapse microscopy on 1250 Pa substrates. (A) Phase images show two cells on collagen coated polyacrylamide gel with embedded fluorescent beads. HH:MM. Scale bar = 50  $\mu\text{m}$  (B) Displacement vectors of the fluorescent beads correspond to the phase images at each time point. The vector fields represent the substrate deformation due to force exerted by the cells. (C) Calculated traction force maps show the cell stress fields and centers as the two cells come into contact and separate. Inset cartoons depict the directionality of the gel deformation due to the stress applied by the adherent cells.

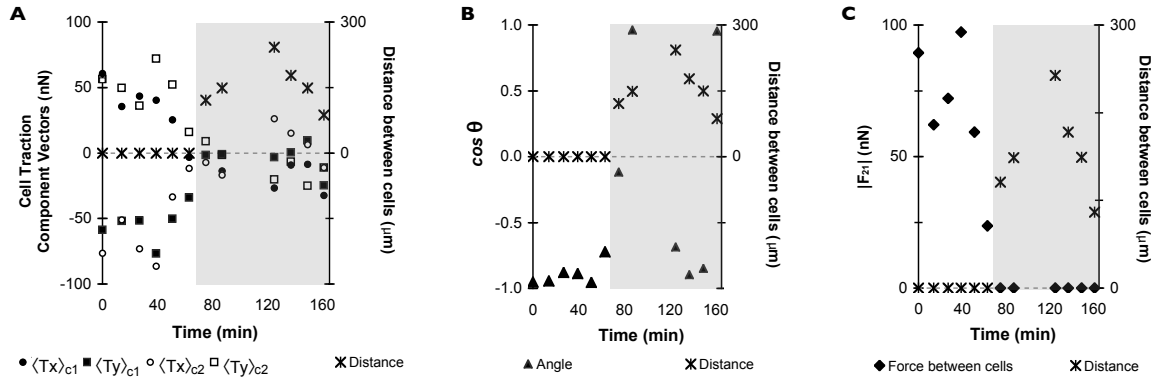


Figure 5.2: Temporal force vectors of cell-cell interactions.

Quantitative temporal results of interacting cell pair depict the cells initially in contact and then retracting (shaded area). The cells were plated on collagen coated 7900 Pa polyacrylamide gel. On all plots values for distance between the cells (\*) are on the right y-axis. (A) x and y traction integral component vectors of each cell in the pair are represented with  $\langle T_x \rangle_{c1}$  and  $\langle T_y \rangle_{c1}$  for cell 1 (black symbols) and  $\langle T_x \rangle_{c2}$  and  $\langle T_y \rangle_{c2}$  for cell 2 (white symbols). (B) The angle between the traction vectors ( $\blacktriangle$ ) of cell 1 and cell 2 is reported with  $\cos \vartheta$ , where  $\cos \vartheta = -1$  represents anti-parallel traction vector alignment, seen for cells in contact. (C) Magnitude of the force ( $\blacklozenge$ ) each cell exerts onto the other in an adherent pair is calculated in accordance with Newton's Laws, described in Definition and Theory section and represented with  $|F_{21}|$ .

anti-parallel alignment of force centers and substrate deformations observed in mechanically adherent cell pairs on all substrates.

Quantitative analysis of the cell pairs substantiated these novel dynamics and mechanics of cell interaction. Traction calculations provided new data of adherent cell force component vectors, angles and magnitudes, Fig. 5.2. Computed x and y components of the traction vectors of each cell ( $\langle T_x \rangle$  and  $\langle T_y \rangle$ ) are plotted as a function of time for a pair of cells on 7900 Pa gel, Fig. 5.2A. The data shows the x and y vectors of each cell are opposite in direction when the cells are in physical contact. The force exerted onto the substrate in x and y direction for cell 1 and cell 2 are mirror images of each other, equal and opposite. These vectors become random as soon as the two cells brake the physical connection, retract and separate (shaded area). Calculated angles between these traction vectors support the substrate displacements seen in Fig. 5.2B, the cells exert force anti-parallel (represented with  $\cos \vartheta \approx -1$ ) to each other when they are in contact, Fig. 5.2B. The orientation becomes

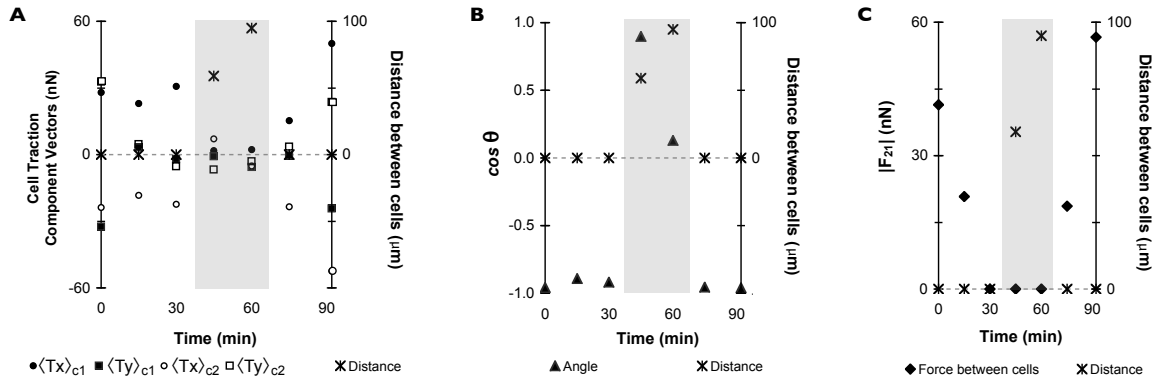


Figure 5.3: Temporal cyclic interaction dynamics.

Quantitative results of interacting cell pair in time depict the cells in contact retracting (shaded area) and then coming back together. The cells were plated on collagen coated 1250 Pa polyacrylamide gel. On all plots values for distance between the cells (\*) are on the right y-axis. (A) x and y traction integral component vectors of each cell in the pair are represented with  $\langle T_x \rangle_{c1}$  and  $\langle T_y \rangle_{c1}$  for cell 1 and  $\langle T_x \rangle_{c2}$  and  $\langle T_y \rangle_{c2}$  for cell 2. (B) The angle between the traction vectors ( $\blacktriangle$ ) of cell 1 and cell 2 is reported with  $\cos \theta$ , where  $\cos \theta = -1$  represents anti-parallel traction vector alignment, seen for cells in contact. (C) Magnitude of the force  $|F_{21}|$  ( $\blacklozenge$ ) each cell exerts onto the other in an adherent pair is plotted versus time.

random when the cells retract.

Applying 1st law of motion to the component vectors, we calculated the magnitude of force ( $|F_{21}|$ ) the cells exert onto each other throughout the time of interaction, Fig. 5.2C. Constrained by Newton's laws, that global force and torque integrated over the entire system must be zero, the force between two physically separated cells equals zero, as seen in the shaded area of Fig. 5.2C. For two cells in contact,  $|F_{21}|$  is plotted on the order of nN and interestingly decreases prior to the visual separation of the contact between the two cells. The decrease can be similarly observed in the magnitudes of the component vectors in Fig. 5.2A. These novel finding suggest that the mechanical strength of the interaction between two cells decreases prior to visual separation of the adhesion junction, a concept we'll discuss further in the following sections. Furthermore these results are not stiffness dependant and are repeatable occurrences that retract and come back together as supported by data on 1250 Pa, Fig. 5.3.

## 5.2 Adherent cells exert anti-parallel forces

The quantitative analysis of individual cell pairs on 1250 and 7900 Pa gels was averaged and quantified to represent universal dynamics of cell-cell interaction on both soft and stiff substrates, Fig. 5.4. As defined by the Newton's laws of motion we calculated magnitude of cell-cell force,  $|\mathbf{F}_{21}|$ , for each interacting cell pair and the angle between the forces exerted by cells onto the substrate ( $\cos \vartheta$ ). On both soft and stiff substrate the adherent cell pairs exerted anti-parallel forces, where as separated cells exhibited a random alignment distribution, Fig. 5.4A. The anti-parallel orientation for adherent cell pairs was found on all substrate stiffnesses coated with both collagen and collagen peptide (GFOGER collagen binding domain[27, 38, 47]), Fig. 5.5. Any affect of stiffness or ligand contribution to the orientation angle was thus ruled out.

This is a significant finding because cells are able to align their force centers anti-parallel to the neighboring cell only when the two are in contact, indicative of the strain that the cells feel from each other and not through the substrate. The anti-parallel alignment has been previously observed in response to substrate strain from outside stress field [22, 33, 49, 54]. Our data show that the cells align to the strain they feel from each other and not the substrate. Furthermore the angle of alignment of adherent cell pairs depends on the strength of the cell-cell bond, Fig. 5.4C. On a range of substrate stiffness, 1250, 2500 and 7900 Pa, there is a minimum force cells must exert on each other to align anti-parallel. At  $|\mathbf{F}_{21}| < 50$  nN the orientation of the forces is still in opposite directions, but some of the cell pairs are not anti-parallel with  $-0.75 < \cos \vartheta < -1.0$ , as seen in the inset of Fig. 5.4C. And at  $|\mathbf{F}_{21}| < 20$  nN the alignment is random. The data shows there is a minimum strain cells must sense from each other to align anti-parallel.

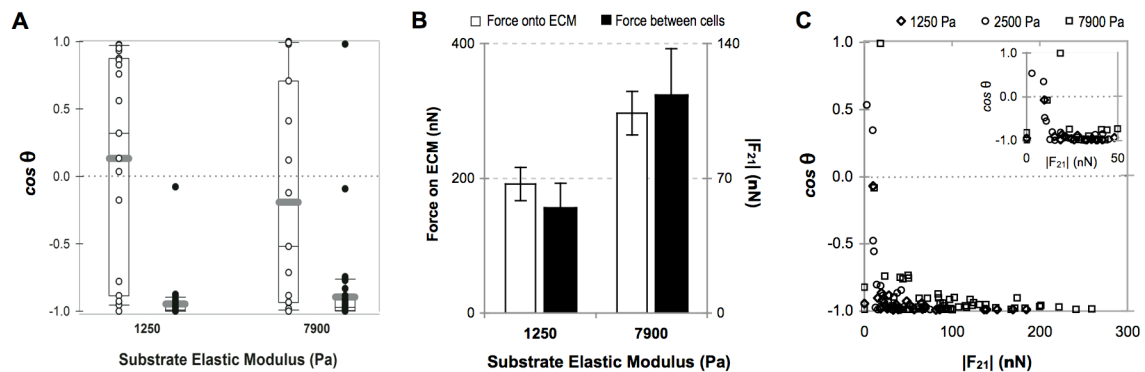


Figure 5.4: Two cell anti-parallel alignment and average force.

Traction vector alignment and force are calculated and averaged for cells on 1250 and 7900 Pa gels. (A) Box and whiskers plots with overlaying angle data ( $\cos \vartheta$ ) are plotted for single cells (empty circles) and adherent cell pairs (filled circles). Thick grey bar represents the mean value. (B) Average force a cell exerts onto the extracellular matrix (ECM) is plotted with white bars ( $p < 0.02$ ). Average force at the cell-cell junction exerted onto the adherent cell,  $|F_{21}|$ , is plotted with black bars with corresponding values on the right Y axis ( $p < 0.03$ ).  $\pm$ SEM (C) Anti-parallel orientation angle ( $\cos \vartheta$ ) of adherent cell pairs is graphed as a function of strength of the cell-cell adhesion on 1250 ( $\diamond$ ), 2500 ( $\circ$ ) and 7900 ( $\square$ ) Pa gels. Inset is a zoom at low  $|F_{21}|$  cell-cell force values.

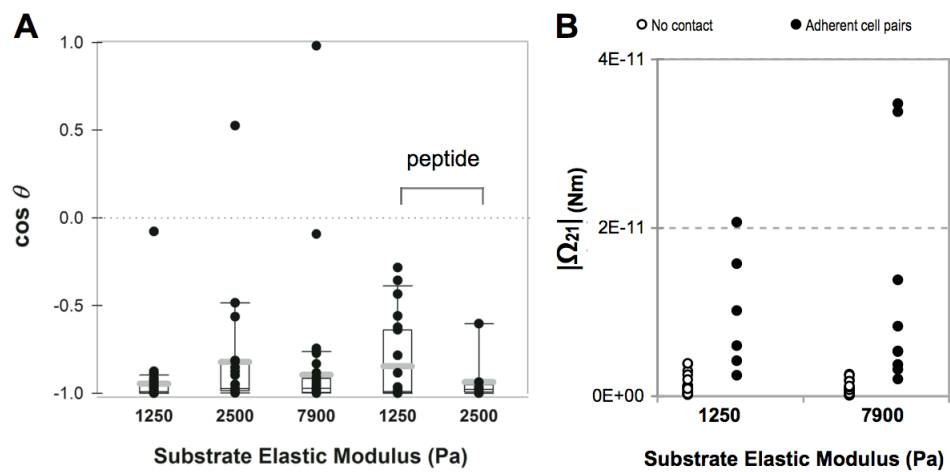


Figure 5.5: Cell pair angles and torques.

(A) Traction vector alignment was averaged for cells on 1250, 2500 and 7900 Pa gels coated with 0.1 mg/ml collagen and 0.05 mg/ml GFOGER peptide concentrations. Box and whiskers plots with overlaying angle data is plotted for adherent cell pairs. Thick grey bar represents the mean value. (B) Intercellular torque magnitudes,  $|\Omega_{21}|$ , are plotted for each adherent cell pair (filled circles) and compared to separated cells (empty circles) for which the values are due to error and  $\approx 0$ . The non-zero adherent cell-cell torques confirms existence of intricate mechanical mechanisms in cell-cell communications.

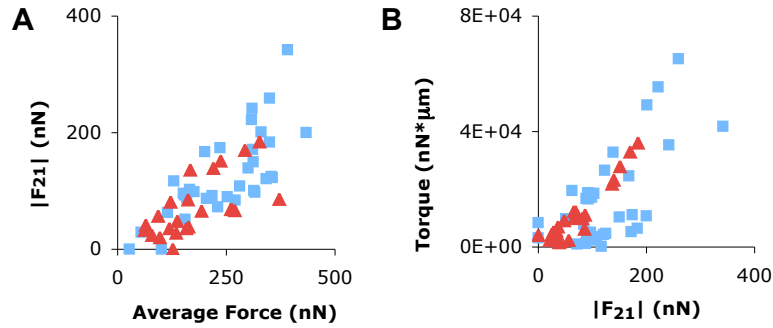


Figure 5.6: MCF10A force and cell-cell tension relationship.

Cell-matrix and cell-cell force relationship plotted for cells on soft 1250 Pa ( $\blacktriangle$ ) and stiff 7900 Pa ( $\blacksquare$ ) gels. (A) Cell-cell force,  $|F_{21}|$  is plotted as a function of cell-matrix force and (B) cell-cell torque,  $|\Omega_{21}|$ , is plotted as a function of cell-cell force,  $|F_{21}|$ .

We also averaged forces exerted onto the substrate by each cell and the force the cells exerted onto each other  $|F_{21}|$ , Fig. 5.4B. The average force cells exerted onto the substrate increased with increasing substrate stiffness as expected. The difference was statistically significant between 1250 and 7900 Pa gels with p value  $< 0.02$ . The force cells exerted on each other increased as a function of the stiffness of the substrate as well, with p value  $< 0.03$ . Furthermore the data shows that the force cells exert onto the ECM is only about two fold larger than the force the cells exert on each other. This unique finding shows that cells are able to exert strong forces on each other within an order of magnitude of those they exert on the substrate. Although strong adheren complexes similar to focal adhesions have not been fully identified in adhesion junctions between the cells, our data implies that intracellular pathways must exist to allow for such high forces at cell-cell adhesions.

From the mechanical data of cell-cell adhesion strength, we went further to test if there is a torque component in cell-cell adhesion, since there exists a rotational contribution of force in cell-matrix adhesion. Interestingly we find non-zero torque exists between adherent cells, Fig. 5.5B. In addition to linear tension between cells, this new concept of cells rotating against each other like gears is very unique and needs to be pursued further.

A further relationship between cell-matrix and cell-cell forces was found linear when plotted as a function of each other, Fig. 5.6. On soft and stiff substrates, 1250 and 7900 Pa respectively, cell-cell tension increases with increasing cell-matrix force, Fig. 5.6(A). Additionally cell-cell torque was found linearly increasing with the cell-cell force, Fig. 5.6(B). All of the analysis was performed on significant signal data, as determined by the dimensionless  $C_- > 0.2$  statistic discussed in the next section.

### 5.3 Statistical interpretation of cell-cell adhesion strength and retraction

In our analysis we further wanted to understand the error of the calculated data versus the real data. Error analysis supplements our average reported values with statistics on the dynamic cell-cell interaction, Fig. 5.7. Scaled non-dimensional residual ( $C_+$  and  $C_-$  discussed in Theory section of Chapter 1) calculations serve to distinguish the noise due to error, from the detectable signal. These residuals proved to be significant statistical determinants and in most instances predictors of cell-cell adhesion retraction.

Fig. 5.7A tracks the cell pair analyzed in Figs. 5.2. The shaded area represents the visual separation observed with phase microscopy. The traction residuals for separated cells represent purely error and therefore both are of low magnitude and  $C_+ \approx C_-$ . Since the  $C_+$  term represents only the error term, it remains relatively unchanged throughout the entire experiment. The  $C_-$  term is a sum of both error term and the  $|\mathbf{F}_{21}|$  cell interaction force term, therefore for two cells in mechanical contact this residual is expected to be significantly higher. In fact this significance is observed for cells in contact  $C_+ < C_-$ .

Furthermore  $C_-$  (dashed line) residual values decrease prior to visual retraction. Both, these statistical results and the cell-cell force magnitude calculations in Fig. 5.2C, serve as a clear predictor and indicator of cell pair retraction prior to and even with out the need for



visual confirmation. The decrease in intercellular force signal is in fact seen in adherent cell pairs on all substrates prior the cell-cell adhesion is visually broken, Fig. 5.7C. Retracting cell pairs are analyzed and plotted on rescaled to time x-axis, with 0 corresponding to the first visual separation of the cell-cell adhesion. Negative time identifies cell pairs in contact and positive time is after cells retracted and remained separated. There is statistical difference between  $C_+$  and  $C_-$  for cells in contact (t-test at each time point gives  $p < 0.03$ ), but no statistical difference for separated cells. And  $C_-$  decreases for all cell pairs prior to visual separation. Therefore the mechanical strength of the cell-cell adhesion decreases prior to visual retraction of that adhesion.

The residuals can thus serve as a test for the mechanical signal strength versus error of the cell-cell adhesion junction. When the phase images confirm physical contact between the two cells over a period of an hour, the  $C_-$  statistic attests to the strength and significance of their bond, Fig. 5.7B. In this figure the cells are plated on 2500 Pa gels and start out physically separated initially, denoted with shaded area. After 30 minutes the cells come into contact and remain visibly adherent to each other as they push and pull on each other. The inset phase images show the visibly attached cells at time points denoted with arrow heads. Although visual adhesion is never broken, the  $C_-$  values fluctuate and serve as the gauge meter for the mechanical signal strength versus noise. Such analysis can provide crucial insight into studies of molecular players involved in the mechanosensing and mechanotransducing pathways of adherens junctions.

## **5.4 Mechanical dynamics of cross-talk between cell-matrix and cell-cell adhesions**

Cell-matrix and cell-cell adhesions have been linked through common inter-cellular molecular cytoskeleton players, here we report new data supporting the mechanical connection

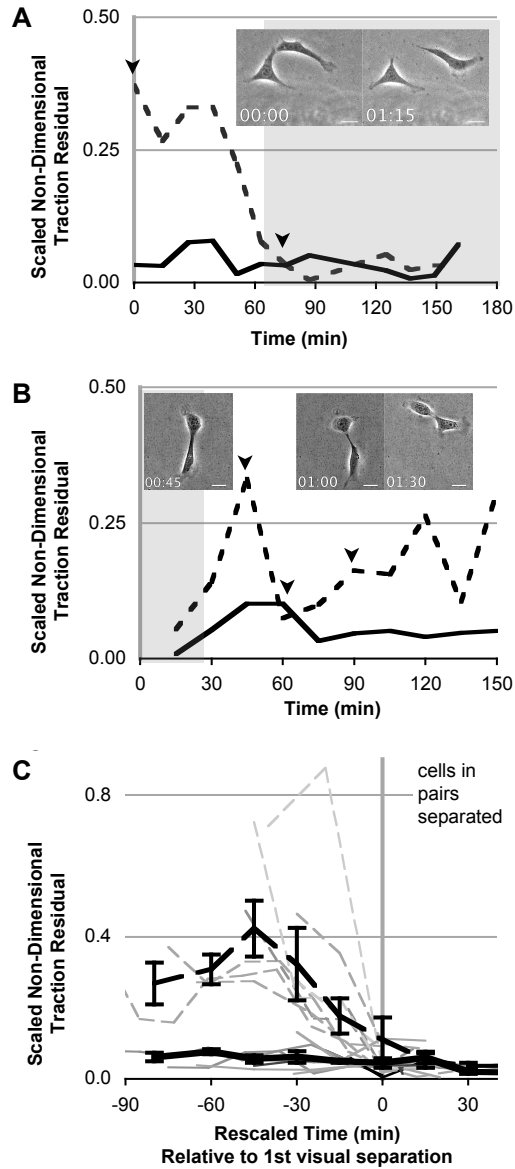


Figure 5.7: Statistical analysis of cell-cell force interactions.

Scaled non-dimensional traction residuals,  $C_+$  (solid line) and  $C_-$  (dashed line), were calculated as discussed in Chapter 1. Corresponding phase images are inset for the cell pairs with the time points marked by black arrowheads. (A) Two cells on 7900 Pa gels are in contact at time 00:00 and retract at 01:15. The cells stay separated as highlighted by the gray area. HH:MM. (B) Two cells initially captured separate on 2500 Pa gels come into contact after 30 minutes. The cell pair remains in contact for the remainder of the experiment, however  $C_-$  fluctuates. (C) Cell pair temporal interaction on 1250, 2500 and 7900 Pa gels was rescaled to time 0 corresponding to the first visual separation of the cell-cell adhesion. Negative time identifies cells in contact with each other and positive time is after cells retracted and remained separated.  $C_+$  (solid line) and  $C_-$  (dashed line) were averaged over 10 cell pairs. Statistical difference observed for cells in contact  $C_+ < C_-$  (t-test  $p$  value  $< 0.03$  at each time point), but for separated cells  $C_+ \approx C_- \pm \text{SEM}$

with force and traction stress result. Direct comparison of maximum traction stresses the cells exert onto the ECM over 95% of their area and the force the cells exert onto each other shows a correlation in the dynamics, Fig. 5.8. The cell pair plated on 2500 Pa substrate pictured in Fig. 5.7B was analyzed for a correlation between the oscillating cell-cell force pattern and cell-matrix force. Fig. 5.8A shows the anti-phase oscillatory behavior of both forces with time. As the cells come into contact the force between them increases, then as they migrate the force between the two cells decreases, and so on. The stress exerted onto the substrate follows the opposite cycle, at first decreasing then as the cells move the cell-matrix adhesion strengthens. There is an inverse linear relationship between the maximum stress onto the substrate exerted by the adherent cells and the force between them, Fig. 5.8B.

The cell-cell versus cell-matrix inverse relationship is seen for non-oscillating force behavior too, as in Fig. 5.8C. For this cell pair, after initial contact, the stress onto the substrate remains high as a mechanical bond is formed between the two cells. The force between the cells decrease to the lowest value but the stress onto the substrate remains high. However as the cell-cell force increases, the cell-matrix stress drops to a low value, pointed with the red arrow. Both values seem to then equilibrate for the rest of the experiment. The force dynamics of cell-cell adhesion are thus correlated to the dynamics of cell-matrix adhesion, shown by inset graph. The magnitude of force a cell applies onto its neighbor is inversely related to the force it applies onto the surrounding matrix.

This new-found mechanical link between cell-cell and cell-matrix adhesion is also observed in cell-cell torque. Intercellular torque increases as the stress applied on the gel decreases, Fig. 5.8D, confirming a correlation between cell-cell and cell-matrix mechanics. Furthermore an interesting cell-cell force relationship is found. The torque data implies that the cells are not only pulling and pushing on each other, but in addition to a contractile cell-cell adhesion there also must exist a shearing component to the interaction.

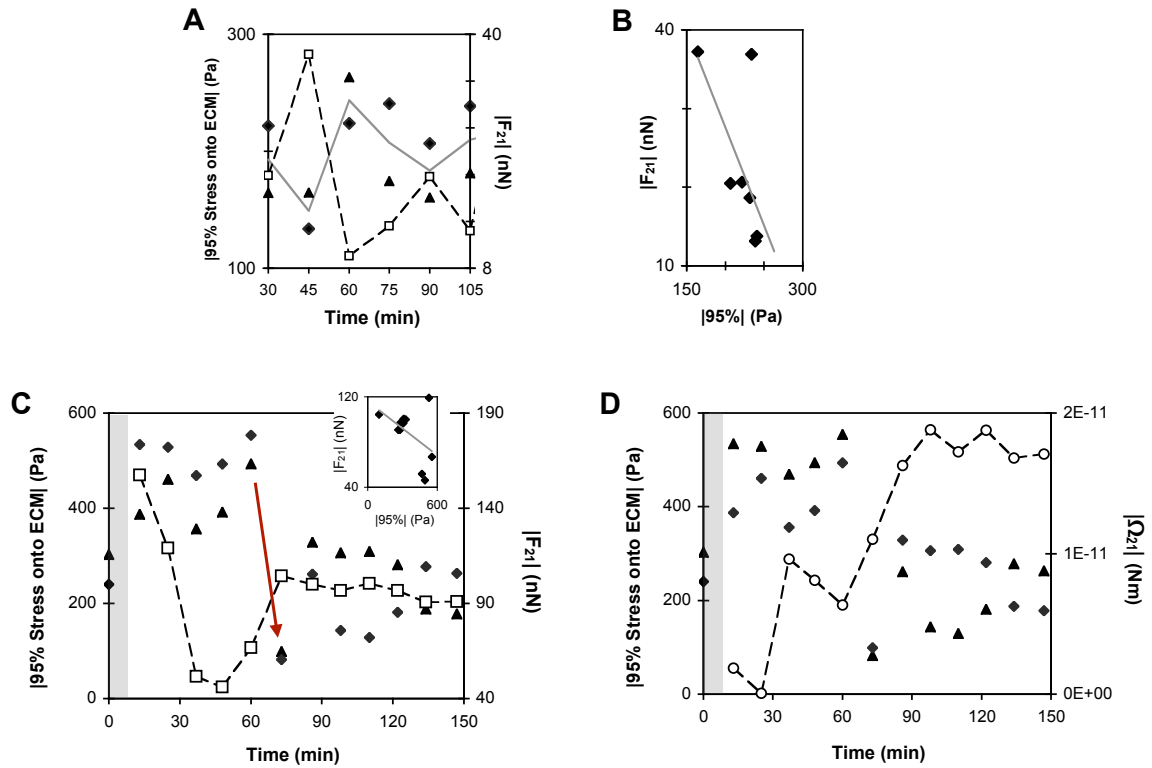


Figure 5.8: Mechanical cell-matrix and cell-cell crosstalk.

Existence of cross talk between cell-matrix and cell-cell adhesion is explored in traction stress and force dynamics. Maximum traction stresses exerted by each cell over 95% of its area ( $\blacktriangle$  and  $\blacklozenge$  on left y-axis) and magnitude of force between the two cells,  $|F_{21}|$  ( $\square$ ) on right y-axis are plotted as time series. (A) Mechanical interaction in cell-matrix and cell-cell adhesions is calculated for a cell pair on 2500 Pa gels pictured in Fig. 4b. The stress each cells exert onto the ECM ( $\blacktriangle$  and  $\blacklozenge$ ) oscillates with time, decreasing after the initial contact. The solid line represents the average between the maximum stresses of two cells. The force between the cells  $|F_{21}|$  ( $\square$ ) oscillates anti-phase compared to cell-matrix dynamics, increasing initially and then decreasing. (B) The relationship between the two forces is linearly dependant with a negative slope, for increasing cell-matrix stresses (maximum 95% stress) the cell-cell force decreases ( $|F_{21}|$ ). (C) Force dynamics were plotted for cells on 7900 Pa gels that come and remain in contact. The red arrow points to a sharp decrease in stress cells exert onto the substrate at exact time there is an increase in force cells exert on each other. Inset shows the inverse linear relationship of the cell-matrix and cell-cell forces. (D) The stress cells exert onto the ECM is compared to the intercellular torque  $|\Omega_{21}|$  ( $\circ$ ), magnitude values on the right y-axis. Shaded area represents the two separated cells prior to contact.

Our findings of mechanotransduction in cell-cell adhesion mediated by cell-matrix adhesion show that cells polarize during contact with minimal force requirement, exert greater force on each other on higher stiffness extracellular substrates, and exhibit ‘tug of war’ dynamics between the two adhesion sites. The dynamics not only show a mechanical bond between two cells disappearing before the visual confirmation, but attest to the strength of the interaction during cell motility and the strength of the mechanical interaction is inversely related to the stresses the cell exerts onto its environment. The present study is the first to show that measurement of cell-cell forces is feasible, significant and temporally dynamic. In the future it will be necessary to study the molecular mechanisms generating inter-cell forces and the role of such forces in physiology and pathology. There are numerous important questions raised. Could the inter-cell forces be part of signaling pathways that have some role in tissue morphogenesis? Could defects in the control or production of such forces be associated with pathological processes like cancer? In short, when one considers the ramifications, the present work represents the threshold of a really revolutionary and seminal series of developments.

## 5.5 Bibliography

- [15] N. Q. Balaban, U. S. Schwarz, D. Riveline, P. Goichberg, G. Tzur, I. Sabanay, D. Mahalu, S. Safran, A. Bershadsky, L. Addadi, and B. Geiger. Force and focal adhesion assembly: a close relationship studied using elastic micropatterned substrates. *Nat Cell Biol*, 3(5):466–72, 2001.
  
- [16] K. A. Beningo, M. Dembo, and Y. L. Wang. Responses of fibroblasts to anchorage of dorsal extracellular matrix receptors. *Proceedings of the National Academy of Sciences of the United States of America*, 101(52):18024–9, 2004.

- [17] D. T. Butcher, T. Alliston, and V. M. Weaver. A tense situation: forcing tumour progression. *Nature Reviews of Cancer*, 9(2):108–22, 2009.
- [18] J. P. Califano and C. A. Reinhart-King. Substrate stiffness and cell area predict cellular traction stresses in single cells and cells in contact. *Cellular and Molecular Bioengineering*, 3(1):68–75, 2010.
- [19] C. E. Chan and D. J. Odde. Traction dynamics of filopodia on compliant substrates. *Science*, 322(5908):1687–91, 2008.
- [20] C. S. Chen. Mechanotransduction - a field pulling together? *Journal of Cell Science*, 121(20):3285–3292, 2008.
- [21] D. Choquet, D. P. Felsenfeld, and M. P. Sheetz. Extracellular matrix rigidity causes strengthening of integrin-cytoskeleton linkages. *Cell*, 88(1):39–48, 1997.
- [22] R. De and S. A. Safran. Dynamical theory of active cellular response to external stress. *Phys Rev E Stat Nonlin Soft Matter Phys*, 78(3):031923, 2008.
- [23] J. de Rooij, A. Kerstens, G. Danuser, M. A. Schwartz, and C. M. Waterman-Storer. Integrin-dependent actomyosin contraction regulates epithelial cell scattering. *Journal of Cell Biology*, 171(1):153–64, 2005.
- [24] M. Dembo, T. Oliver, A. Ishihara, and K. Jacobson. Imaging the traction stresses exerted by locomoting cells with the elastic substratum method. *Biophysical Journal*, 70(4):2008–22, 1996.
- [25] R. A. Desai, L. Gao, S. Raghavan, W. F. Liu, and C. S. Chen. Cell polarity triggered by cell-cell adhesion via e-cadherin. *Journal of Cell Science*, 122(7):905–11, 2009.

- [26] F. Drees, S. Pokutta, S. Yamada, W. J. Nelson, and W. I. Weis. Alpha-catenin is a molecular switch that binds e-cadherin-beta-catenin and regulates actin-filament assembly. *Cell*, 123(5):903–15, 2005.
- [27] J. Emsley, C. G. Knight, R. W. Farndale, M. J. Barnes, and R. C. Liddington. Structural basis of collagen recognition by integrin alpha2beta1. *Cell*, 101(1):47–56, 2000.
- [28] R. A. Foty and M. S. Steinberg. Cadherin-mediated cell-cell adhesion and tissue segregation in relation to malignancy. *International Journal of Developmental Biology*, 48(5-6):397–409, 2004.
- [29] R. A. Foty and M. S. Steinberg. The differential adhesion hypothesis: a direct evaluation. *Developmental Biology*, 278(1):255–63, 2005.
- [30] A. Ganz, M. Lambert, A. Saez, P. Silberzan, A. Buguin, R. M. Mege, and B. Ladoux. Traction forces exerted through n-cadherin contacts. *Biologie Cellulaire*, 98(12):721–30, 2006.
- [31] M. L. Gardel, B. Sabass, L. Ji, G. Danuser, U. S. Schwarz, and C. M. Waterman. Traction stress in focal adhesions correlates biphasically with actin retrograde flow speed. *Journal of Cell Biology*, 183(6):999–1005, 2008.
- [32] J. Gavard, M. Lambert, I. Grosheva, V. Marthiens, T. Irinopoulou, J. F. Riou, A. Bershadsky, and R. M. Mege. Lamellipodium extension and cadherin adhesion: two cell responses to cadherin activation relying on distinct signalling pathways. *Journal of Cell Science*, 117(2):257–70, 2004.
- [33] A. M. Goldryn, B. A. Rioja, J. P. Spatz, C. Ballestrem, and R. Kemkemer. Force-induced cell polarisation is linked to rhoa-driven microtubule-independent focal-adhesion sliding. *Journal of Cell Science*, 122(20):3644–51, 2009.

- [34] W. H. Guo, M. T. Frey, N. A. Burnham, and Y. L. Wang. Substrate rigidity regulates the formation and maintenance of tissues. *Biophysical Journal*, 90(6):2213–20, 2006.
- [35] A. Hartsock and W. J. Nelson. Adherens and tight junctions: structure, function and connections to the actin cytoskeleton. *Biochimica et Biophysica Acta*, 1778(3):660–9, 2008.
- [36] D. E. Jaalouk and J. Lammerding. Mechanotransduction gone awry. *Nat Rev Mol Cell Biol*, 10(1):63–73, 2009.
- [37] B. Z. Katz, E. Zamir, A. Bershadsky, Z. Kam, K. M. Yamada, and B. Geiger. Physical state of the extracellular matrix regulates the structure and molecular composition of cell-matrix adhesions. *Molecular Biology of the Cell*, 11(3):1047–60, 2000.
- [38] C. G. Knight, L. F. Morton, A. R. Peachey, D. S. Tuckwell, R. W. Farndale, and M. J. Barnes. The collagen-binding  $\alpha$ -domains of integrins  $\alpha(1)\beta(1)$  and  $\alpha(2)\beta(1)$  recognize the same specific amino acid sequence, gfo $\alpha$ , in native (triple-helical) collagens. *Journal of Biological Chemistry*, 275(1):35–40, 2000.
- [39] K. R. Levental, H. Yu, L. Kass, J. N. Lakins, M. Egeblad, J. T. Ertler, S. F. Fong, K. Csiszar, A. Giaccia, W. Weninger, M. Yamauchi, D. L. Gasser, and V. M. Weaver. Matrix crosslinking forces tumor progression by enhancing integrin signaling. *Cell*, 139(5):891–906, 2009.
- [40] M. P. Maddugoda, M. S. Crampton, A. M. Shewan, and A. S. Yap. Myosin vi and vinculin cooperate during the morphogenesis of cadherin cell cell contacts in mammalian epithelial cells. *Journal of Cell Biology*, 178(3):529–40, 2007.
- [41] W. A. Marganski, M. Dembo, and Y. L. Wang. Measurements of cell-generated deformations on flexible substrata using correlation-based optical flow. *Methods in Enzymology*, 361:197–211, 2003.



- [42] R. M. Mege, J. Gavard, and M. Lambert. Regulation of cell-cell junctions by the cytoskeleton. *Current Opinion in Cell Biology*, 18(5):541–8, 2006.
- [43] J. Miyoshi and Y. Takai. Structural and functional associations of apical junctions with cytoskeleton. *Biochimica et Biophysica Acta*, 1778(3):670–91, 2008.
- [44] C. M. Nelson, D. M. Pirone, J. L. Tan, and C. S. Chen. Vascular endothelial-cadherin regulates cytoskeletal tension, cell spreading, and focal adhesions by stimulating rhoa. *Molecular Biology of the Cell*, 15(6):2943–53, 2004.
- [45] M. J. Paszek, N. Zahir, K. R. Johnson, J. N. Lakins, G. I. Rozenberg, A. Gefen, C. A. Reinhart-King, S. S. Margulies, M. Dembo, D. Boettiger, D. A. Hammer, and V. M. Weaver. Tensional homeostasis and the malignant phenotype. *Cancer Cell*, 8(3):241–254, 2005.
- [46] C. A. Reinhart-King, M. Dembo, and D. A. Hammer. Cell-cell mechanical communication through compliant substrates. *Biophysical Journal*, 95(12):6044–51, 2008.
- [47] C. D. Reyes and A. J. Garcia. Engineering integrin-specific surfaces with a triple-helical collagen-mimetic peptide. *J Biomed Mater Res A*, 65(4):511–23, 2003.
- [48] P. L. Ryan, R. A. Foty, J. Kohn, and M. S. Steinberg. Tissue spreading on implantable substrates is a competitive outcome of cell-cell vs. cell-substratum adhesivity. *Proceedings of the National Academy of Sciences of the United States of America*, 98(8):4323–7, 2001.
- [49] S. A. Safran and R. De. Nonlinear dynamics of cell orientation. *Phys Rev E Stat Nonlin Soft Matter Phys*, 80(6):060901, 2009.
- [50] A. M. Shewan, M. Maddugoda, A. Kraemer, S. J. Stehbens, S. Verma, E. M. Kovacs, and A. S. Yap. Myosin 2 is a key rho kinase target necessary for the local concentra-

tion of e-cadherin at cell-cell contacts. *Molecular Biology of the Cell*, 16(10):4531–42, 2005.

- [51] J. Tsai and L. Kam. Rigidity-dependent cross talk between integrin and cadherin signaling. *Biophysical Journal*, 96(6):L39–41, 2009.
- [52] S. Yamada and W. J. Nelson. Localized zones of rho and rac activities drive initiation and expansion of epithelial cell-cell adhesion. *Journal of Cell Biology*, 178(3):517–27, 2007.
- [53] S. Yamada, S. Pokutta, F. Drees, W. I. Weis, and W. J. Nelson. Deconstructing the cadherin-catenin-actin complex. *Cell*, 123(5):889–901, 2005.
- [54] A. Zemel, F. Rehfeldt, A. E. X. Brown, D. E. Discher, and S. A. Safran. Optimal matrix rigidity for stress-fibre polarization in stem cells. *Nature Physics*, pages 1–6, March 2010.

## **Chapter 6**

# **Cell division and cytokinesis through Extracellular Matrix**

Rapid and uncontrolled cell division with failed cytokinesis are a hallmark of growing tumors. Final stages of abscission failure creating chromosomally unstable cells have been linked to tumorigenic progression of cancer [78]. Inherently a mechanical process, it is hypothesised that cytokinesis is not a simple intracellular constriction step but additionally an anchorage dependant mechanosensing and mechanotransducing abscission in adherent mammalian cells.

The first and most widely accepted theory in cytokinesis progression is that an actin contractile ring formed at the equator is constricted by myosin II motors [72, 83]. Force profiles of dividing sea urchin egg have demonstrated that initially in the elongated cell, high forces are localized to opposite pole regions and to the equator where the furrow establishes and grows. As the furrow grows highest force is located in the region and aligned parallel to the furrow [73]. These findings indicate that although initially force is observed on opposing poles, it then co-localizes to the contractile ring region.

Contractile ring research has identified key mechanical components of the region as

the actomyosin network. Current detailed observations by numerous microscopical techniques such as 3D-EM, Pt-TEM, TIRF and 3D-deconvolution, show actin-myosin network in Anaphase of *Dictyostelium* does not form a uniform contractile ring [75]. Embryonic research on actin fibre alignment and myosin II localization have shown highly ordered bundles [72]. But in fibroblast cells, a substrate adherent mammalian cell, an organizational bias for an orientation perpendicular to the spindle axes has been found [66].

Another active division driver found is RhoA, the contractile GTPase found in stress fibres. Although localization nor gradients of RhoA have ever been detected, it is known that Rac is able to limit RhoA dependant contractility. Therefore RhoA contractility is muted in the polar cortical regions by Rac and actively pronounced in the equatorial region, where its role in ROCK activated myosin II drives constriction of the contractile ring [83, 61]. Further studies of actin cytoskeleton dynamics in the division cycle show actin localization at the contractile ring region as early as Telophase in addition to aggregating to the periphery to provide the cortical cell rigidity prior to cytokinesis[56]. The actin, myosin and Rho research of substrate independent cell division yielded different mechanisms of intracellular mechanical division. The three mechanisms involved in the contraction of the ring: purse string, orthogonal filament, isotropic, anisotropic, parallel and traction contraction [67, 71].

In addition to alignment, concentration of these active components has been found important. Data from Yu-li Wang group also shows that higher accumulation of actin filaments, caused by  $\alpha$ -actinin over-expression and loss of actin turn over, actually results in cytokinetic failure. Where as decrease in actin filaments at the cleavage furrow, brought on by siRNA knock down of  $\alpha$ -actinin, speeds up cytokinesis [59]. Myosin II is unaffected in all of the experiments. This finding suggests that for adherent cells lower concentration of filamentous actin at the contractile ring is desired for successful cytokinesis.

However the concentration, order or disorder of the contractile ring actin organization differ between different organisms, especially in adherent animal cells [76]. Spreading,

mechanosensing and stress dynamics onto the underlying substrate have been identified as necessary and determinant in attached cells. Inhibition of cell spreading and increased matrix elasticity decrease cell proliferation and increased *in vivo* tissue stiffening has been found at sites of increased proliferation[58]. Identification of mechanotransducing molecular players such as ROCK [72], RhoA, Rac and Rho opposing gradients [83], FAK, vinculin [56], Crk and paxillin[80] during cytokinesis has lead some groups to implicate presence and participation of focal adhesion complexes in cytokinesis [69].

Important and intricate intracellular roles are played by Rac GTPases. Rac1 localization to the cortical poles during cytokinesis and cell spreading is found important in myosin light chain kinase phosphorylation and thus inactivation of myosin II. It is proposed that Rac is involved in the mechanics of cytokinesis through a passive equatorial tearing that divides two daughter cells via polar protrusion and traction force generation. This theory is supported by experimental results of myosin II null and blebbistatin inhibited adherent cells that are able to undergo complete division and cytokinesis on ligand coated glass substrates [57, 83]. This myosin II contraction independent scission has been called as cytokinesis B or passive cytokinesis, which is dependant on the presence and adhesivity of the Extracellular matrix [60].

Specific link between extracellular matrix (ECM) adhesion and cytokinesis was further established when cells with impaired  $\beta 1$  integrin signaling went into cytokinetic block [62]. Biochemical ECM was found to affect division in fibronectin ligand ability to rescue cytokinesis failures in serum-free unattached rat epithelial cells [72]. Mechanical ECM affect on increasing proliferation has been observed *in vitro* and *in vivo* [58]. Overall increased cell-matrix adhesivity due to biochemical or mechanical ECM cues increases cell mitogenic activity[84].

With all this supportive mechanical data, it is interesting to find that only a few studies have been published on the forces of cell division and cytokinesis. One such study was

performed on substrate-independent division of mold cells. Calculations of force at the equator region were based on the amount of fluorescent myosin II present and applied to Hooke's Law [77].

$$\begin{aligned}\mathbf{F} &= -k * \mathbf{x} \\ \gamma &= 2S_c \cos\theta * \mathbf{R}_f.\end{aligned}\tag{6.1}$$

The elastic force, which is the minimal contraction force ( $\gamma$ ), is proportional to extent of furrow progression ( $\mathbf{R}_f$ ) and related to measured cell stiffness constant ( $2S_c \cos\theta$ ). These calculations indicated maximum force of about 5nN exerted at the furrow region during initial stages of elongated unattached cell cytokinesis before the dividing cell takes on the dumbbell shape of late cytokinesis [77]. This force data of substrate independent division has shown the highest contractile force between two daughter cells is exerted in the initial stages of cytokinesis, prior to midbody formation and not during the ingression. Published myosin-dependant equatorial cytokinesis model estimates a generation of maximal contractile force of 1 to 100 nN range in the contractile ring [79]. Further mechanical calculations and force determinants have been gathered through non-substrate experiments, like micropipette aspiration, atomic force microscopy, and laser tracking micro-rheology [74].

The only force data of substrate attached cells was conducted on silicone sheets through measurements of the wrinkles, which were observed highest at the furrow region in early cleavage formation and then at the polar regions during cell separation [68]. These results pave the way for more unanswered division and cytokinesis force questions, that we explore in our studies.

In our work on cell division, we are first to show the mechanics and force profile of

the dynamic process of adherent mammalian cell division. We find a cell completely lifts off the substrate as it rounds up into a mitotic body and is unable to stress the substrate. These findings are supplemented with cantilever force detachment experiments of cells in different stages of the cell cycle showed cells in G2M/mitotic to maintain a much lower number of cell-matrix bonds and therefore faster release of the matrix adhesion than the cells in other stages of the mitotic cycle. However these few adhesions required higher force to break. Thus the cell is tethered to the substrate with very few but very strong bonds during the rounded lift off stage of the cycle [85].

Then in Anaphase and Telophase the two visible but not yet separate daughter cell bodies slowly spread onto the underlying substrate, exerting very low forces still similarly to spreading cells. As the cell undergoes cytokinesis we find the force profile is similar to that of two retracting interacting cells. However the interesting and different dynamic is found in the tension between daughter cells through the early and late stages of cytokinesis. Our data show that in early stages the cell-cell force and torque rise and hit a maximum. Although this maximum is observed in calculated equator force values of unadherent cells with Hooke's Law approximation by Robinson et al., we find our data derived from cell-matrix traction force are an order of magnitude higher for the adherent epithelial cells. Furthermore averaged data for each stage of the cycle force dynamics reveals two linearly dependant relationships, that between cell force and spread area, and between cell-cell tension and cell-matrix force. Overall the area and force dynamics are similar on a range of substrate stiffnesses, as normalized comparison data revealed.

Upon further investigation of the role of the ECM in the mechanotransduction of cytokinesis, we used chemical inhibitors to inhibit strength and contractility in cell-matrix adhesion. Inhibition of ROCK, which has been hypothesised to drive myosin II mediated contractile ring constriction [83, 61], showed normal completion of cytokinesis. Although lower percentage of cells was found continuing cell division cycle past Metaphase, all cells

formed two complete and separate daughter cells. In addition to this finding, the force data of the division cycle retained the force-area and maximum cell-cell tension patterns observed in normal cell division. However the forces the cells were able to exert onto the substrate and therefore onto each other were on the order of magnitude lower. These findings show that strength of cell-matrix adhesion makes a decision point for cell to enter or not to enter the division cycle, but does not affect active nor passive cytokinesis of the cell.

However inhibition of myosin II directly with blebbistatin resulted in completely different outcome. None of the inhibited cells were able to complete abscission and form two daughter cells in cytokinesis, although all cells entered and continued through the division cycle. After division cells remained binucleate and a few were furthermore observed entering division again and forming trinucleate cells. We further find that inhibition of contractility also decreased cell-matrix and cell-cell forces by an order of magnitude, but furthermore the linear force-area and maximum cell-cell tension force dynamics are lost as well. Therefore on physiologically stiff gel substrates, unlike published data on functionalized stiff glass [57], passive cytokinesis of two cells pulling apart cannot rescue the lack of myosin II mediated active cytokinesis.

## **6.1 Temporal force profile of cell division and cytokinesis**

Extracellular environment is imperative for successful cell division and cytokinesis in adherent cells, such as epithelial cells. Most of our knowledge of cell division comes from non-adherent ECM independent egg and yeast studies. In our experiments to understand cell division, an important event in cancer progression, we study the process through its relationship and adhesion to the ECM. The mechanics and ECM role in cytokinesis have only been studied briefly through the extracellular environment [68], but are still poorly understood. Here we are the first to show force dynamics of cell division of adherent cells.



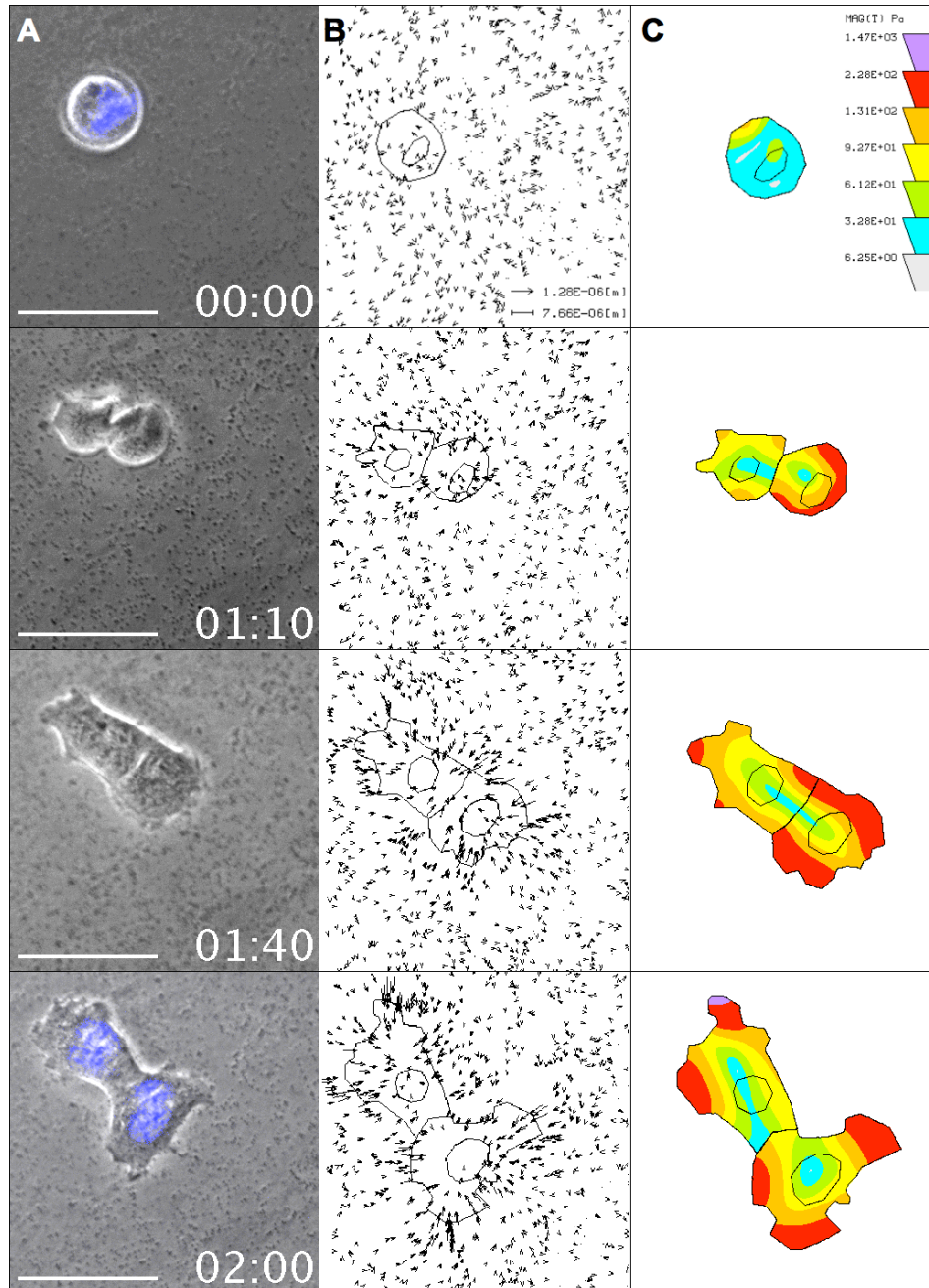


Figure 6.1: Temporal force profile of EpH4 mouse mammary epithelial cell division. Cell division is observed on 0.05 mg/ml collagen functionalized 2500 Pa gels. (A) Rounded cell entering Metaphase is captured in time with phase microscopy as it divides into two daughter cells. Nuclei stained with Hoecht fluorescent dye to confirm Metaphase and two daughter cell nuclei. HH:MM. Scale bar = 50  $\mu\text{m}$  (B) Displacement vectors of the fluorescent beads correspond to the phase images at each time point. The vector fields represent the substrate deformation due to force exerted by the cells. (C) Calculated traction force maps show the cell stress fields and centers. Size not to scale.

Normal mouse mammary epithelial cells, EpH4, were captured dividing on 2500 Pa, stiffness physiologically similar to a mouse mammary tumour [55], and the forces calculated, Fig. 6.1. Nuclear staining and phase images confirm the stage of the division cycle, Fig. 6.1A. At time 0 the cell is pictured in Metaphase, then the two daughter cells are evident and at 2 hours the daughter cells are spread and pictured separating in the final stages of cytokinesis. Bead displacements of the underlying stressed substrate, Fig. 6.1B, are used to calculate the traction force fields of the division process, Fig. 6.1C. At time 0 the cell is rounded and detached from the substrate with one small force center tethering it to the substrate. Temporal resolution then shows the mechanical dynamics of spreading and separation of the two daughter cells.

Quantitative analysis of this dividing cell are plotted in Fig. 6.2. Cell area during Metaphase remains constant while the cell is detached and rounded, but as the daughter cells spread their area increases, Fig. 6.2A. Average cell force follows the similar behavior. The force of the detached rounded mother cell is almost zero as the cell completely detaches from the substrate to undergo Metaphase and Anaphase. The daughter cells exert increasing force as they spread on the substrate and pull away from each other. Therefore force-area relationship is linearly increasing with division cycle progression, Fig. 6.2B.

However the tension between the daughter cells does not follow the linear relationship. Force between two cells,  $|\mathbf{F}_{21}|$ , increases initially but goes through a maximum and decreases as the two cells pull away from each other, Fig. 6.2C. The torque,  $|\mathbf{\Omega}_{21}|$ , between the two cells also goes through a sharp maximum. The maximum corresponds to phase image at 01:40 in Fig. 6.1A. The maximum phenomenon is unique because it has not been previously observed in interacting cells, Chapter 4. This maximum therefore has to be related exclusively to the process of cell division. It has been previously estimated with Hooke's Law approximation published by Robinson et al. However we find our magnitude of cell-cell tension and maximum are an order of magnitude higher than the previously

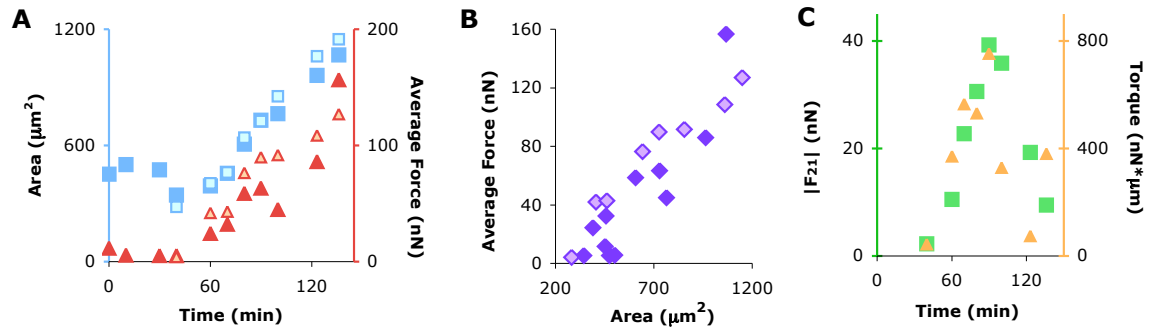


Figure 6.2: Quantitative analysis of dividing cell mechanics.

(A) Cell area (■) and average force per cell (▲), of cells pictured in Fig. 6.1, are plotted in time. Single mother cell divides into two daughter cells. (B) Average cell force is plotted as a function of cell area (◆). Dark and light markers represent cell1 and cell2 respectively. (C) Cell-cell force  $|F_{21}|$  (■) and torque  $|\Omega_{21}|$  (▲) between the two daughter cells are plotted in time.

published data [77]. This maximum could further represent the intracellular contractile ring constriction at the final point of active cytokinesis, after which it is the cell-matrix adhesion and anchoring that pulls the cells apart in the late stage of cytokinesis also referred to as passive cytokinesis.

In addition to cytokinesis, where the ECM plays an important role in the interesting force dynamics, the mechanics of the division process can also be divided into initial lift off and cell adhesion and spreading of the two daughter cells. Starting in the beginning, the analysis of dividing cells prior to entrance into Metaphase show no deviation in force from normal S phase behavior. The cell simply rounds up and lifts off the substrate when it enters Metaphase, breaking most of its adhesions with the substrate, Fig. 6.3A. Cell area and force dramatically drop when the cell rounds up. Interestingly the cell-matrix adhesion force drops to almost zero, Fig. 6.3B, which signifies a rapid disassembly of focal adhesions and complexes. Adhesion to and force exerted on the substrate remains insignificant as the cell divides into two daughter cells. At which time the cells begin to adhere and spread on the substrate exerting increasing forces. Force is a linearly decreasing function of area as the cell enters division, Fig. 6.3C, similar to that of a spreading cell.

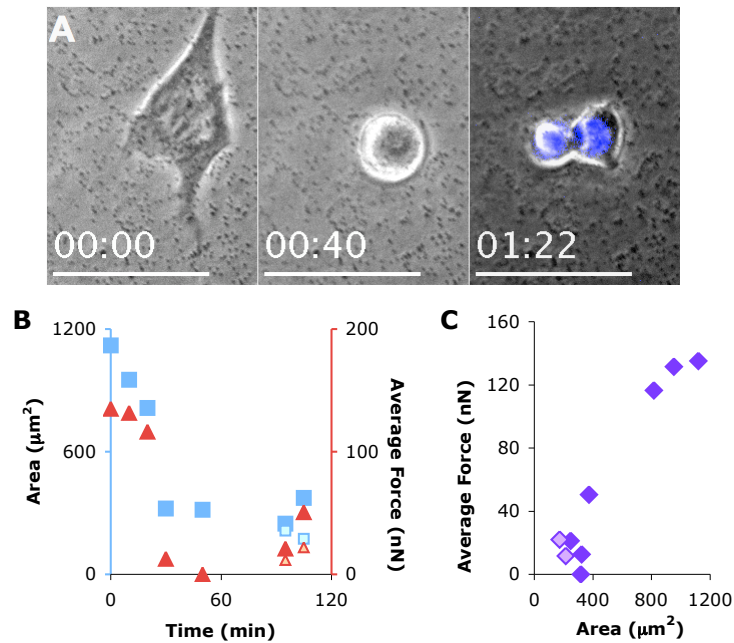


Figure 6.3: Force profile of cell entering division.

(A) Temporal phase micrographs of an EpH4 mouse mammary epithelial cell entering division cycle with Hoechst dye labeled nuclei. Cell is plated on 2500 Pa 0.05 mg/ml collagen coated gel. (B) Corresponding quantitative data of cell area (■) and average cell force (▲) in time. (C) Average cell force is plotted as a function of cell area (◆). Dark and light markers represent cell1 and cell2 respectively. Scale bar = 50  $\mu\text{m}$

In the spreading stage of the daughter cells, the cell spread area and average force dynamics of the dividing daughter cells are very similar to that of a single cell, Fig. 6.4. Quantitative analysis of a single EpH4 cell spreading show that the force on the extracellular environment increases as the cell spreads. Force is a linearly increasing function of the cell area, Fig. 6.4C. The linear spreading force-area relationship has also been published in other cell types by Reinhart-King lab, [65, 46].

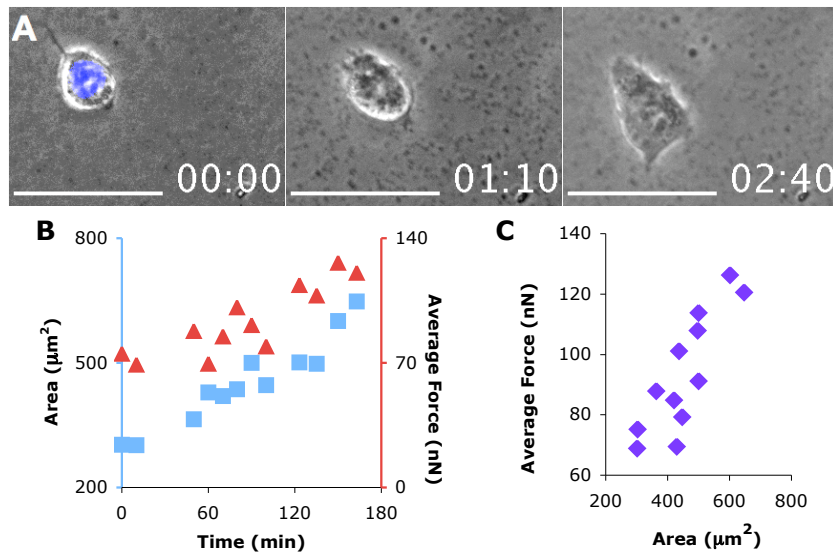


Figure 6.4: Force profile of cell spreading.

Quantitative analysis of a single non-dividing mouse mammary epithelial cell spreading on 0.05 mg/ml collagen functionalized 2500 Pa gels. (A) Phase images with fluorescent labeled nuclei depict the single cell as it spreads. (B) Cell area (■) and average force (▲) are plotted in time. (C) Average cell force is plotted as a function of cell area (◆). Scale bar = 50 μm

## 6.2 Traction force analysis at each stage of the cell division cycle

Individual cell analysis was applied and averaged to bring quantitative understanding of cell division at each stage of the division cycle. EpH4 cell division stages were distinguished by nuclear staining and physically visible morphological changes. Normal non-dividing single cell data is labeled as S phase. The visible distinctions of division stages are: Metaphase when the cells is rounded and detached; Anaphase with an elongated and oval shaped cell; Telophase with visible two rounded daughter cells; early cytokinesis observed in initial spreading of two daughter cells; and the separation of the two fully spread daughter cells in final late stages of cytokinesis as they break their connection.

All quantitative data points of the 15 dividing EpH4 cells on 0.05 mg/ml collagen functionalized 2500 Pa gels are plotted in Fig. 6.5 to capture the relationship of the dynamics of cell force. We observe the linearly increasing force-area relationship, Fig. 6.5A. The cell-cell tension analysis shows that cell-cell force  $|\mathbf{F}_{21}|$  is increasing linearly with increasing cell-matrix adhesion force, Fig. 6.5B. This linear relationship is also reminiscent of that found in interacting cell pairs in Fig. 5.6. However this linearly increasing pattern is not observed in the torque between the two cells,  $|\mathbf{\Omega}_{21}|$ , Fig. 6.5C. All of the analysis was performed on significant signal data, as determined by the dimensionless  $C_- > 0.2$  statistic.

The significant cell cycle force dynamics are further revealed in force averages at each phase of the cell cycle, Fig. 6.6. Average area and average cell force are at absolute minimum in Metaphase, Anaphase and Telophase. The cells are observed lifted and not strongly attached to the underlying substrate during these stages. The two metrics increase as the cells adhere to the substrate, spread and strengthen their anchorage to the matrix and proceed with cytokinesis, Fig. 6.6A and B. The increasing force-area relationship is maintained in all observed cells, Fig. 6.6C.

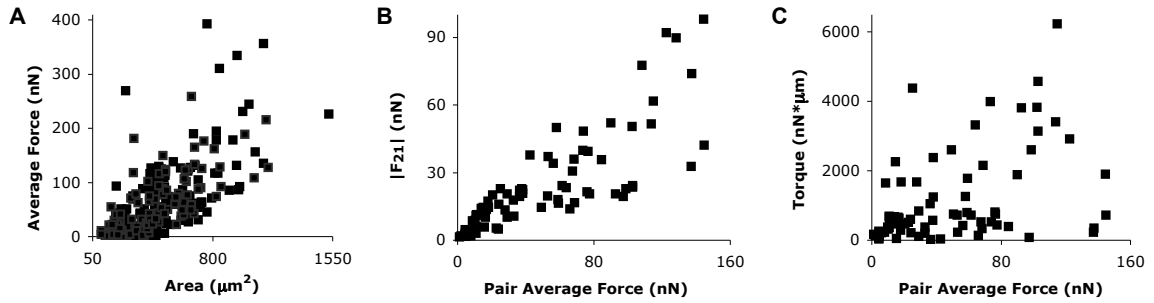


Figure 6.5: EpH4 force and cell-cell tension relationship.

Quantitative data for 15 dividing EpH4 cells on 0.05 mg/ml collagen functionalized 2500 Pa gels illustrates a linear force - area relationship (A). For significant signal, as determined by dimensionless  $C_{-} > 0.2$  statistic, cell-cell (B) force  $|\mathbf{F}_{21}|$  and (C) torque  $|\mathbf{\Omega}_{21}|$  are plotted as a function of increasing average force a daughter cell pair exerts onto the underlying matrix.

The tension between two daughter cells initiated in Anaphase/Telophase increases as cell division progresses, but then decreases in the final steps of cytokinesis, Fig. 6.6D. The tension between two daughter cells thus goes through a significant maximum in all cells observed. This data supports existence of two different mechanical mechanisms in early and late cytokinetic abscission. A significantly clear relationship is not found in cell-cell torque, Fig. 6.6E. All of this data is statistically significant as seen in the high signal to noise ratio, presented as dimensionless  $C_{-}$  and discussed in Introduction Theory section, Fig. 6.6F. This statistic is useful to show the significance of the signal and for distinguishing the signal from noise for further analysis in Fig. 6.5.

Furthermore the trends in area and average cell force are conserved on a range of substrate compliance, 1250, 2500 and 7900 Pa gels, Fig. 6.6G and H. Data from each substrate stiffness is normalized for the maximum on that substrate and averaged over the three conditions. The pattern of decreasing cell spread area and average force is maintained, similar to that on 2500 Pa gels. The linear increasing relationship of force versus cell spread area is conserved as well, Fig. 6.6I. Note the force drops close to zero in Meta, Ana and Telophase on all substrates, indicating the role of the ECM during these stages is minimal. Therefore we shift the focus of further research onto cytokinesis - a substrate dependant process.

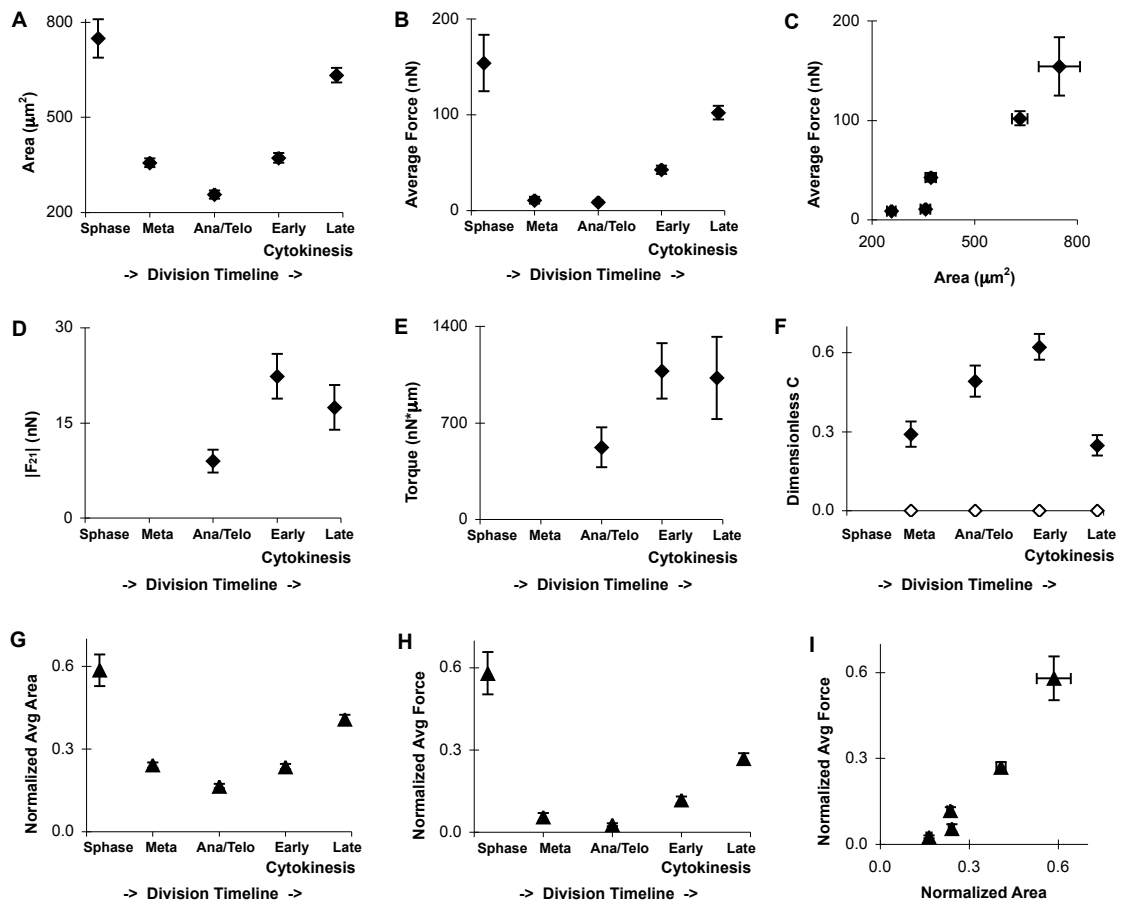


Figure 6.6: Force profile at each cell cycle stage.

EpH4 mouse mammary epithelial cell division analysis at S phase, Metaphase, Anaphase/Telophase and Early and Late Cytokinesis stages of cell cycle. Cells are plated on 2500 Pa 0.05 mg/ml collagen coated gels. (A) Area, (B) average cell force, cell-cell (D) force  $|\mathbf{F}_{21}|$  and (E) torque  $|\mathbf{\Omega}_{21}|$ , and (F) dimensionless signal to noise statistic  $C$  are all plotted as a function of the cell cycle stages. The dimensionless  $C_-$  ( $\blacklozenge$ ) confirm statistically significant signal of the results compared to noise  $C_+$  ( $\diamond$ ). (C) Average cell force is plotted as a function of area at each stage of division. EpH4 cell division is normalized over a range of substrate stiffnesses. (G) Cell area and (H) average cell force are plotted at each stage of the division cycle for cells on 1250, 2500 and 7900 Pa gels functionalized with 0.05 mg/ml collagen. (I) The average cell force is a function of cell spread area, normalized over all substrates.  $\pm$  SEM



## **6.3 Myosin II motor and Rho-associated kinase roles in cytokinesis**

The final part of the cell division cycle is the cytokinesis - complete abscission and separation of the two daughter cells. Cytokinesis has been widely studied in eggs, fission yeast and slime mold but not in mammalian cells. Therefore most of the findings on cytokinesis implicate active abscission process involving a contractile ring / cleavage furrow, consisting of acto-myosin contraction and components. Specifically non-muscle myosin II motor and RhoA GTPase provide and direct the force for furrow ingression. Myosin II has been found to localize to the furrow region in the final stages of cytokinesis, implicating that it is the dynamics and timing of the myosin II that drive ring constriction in cytokinesis [70, 75, 77, 86]. Blebbistatin inhibition of myosin II was found to arrest furrow ingression without blocking its assembly and disrupt the uniform distribution and localization to the furrow in dividing HeLa cells. Thus blebbistatin disrupts spatial organization of the cytokinesis motor machinery and inhibits contraction of the cleavage furrow, without disrupting mitosis or contractile ring assembly [81]. Interestingly Straight et al. also found that further inhibition of ROCK (Rho-kinase) following blebbistatin treatment delocalized myosin II over the entire mitotic cell body [81]. Although hypothesised to drive myosin II mediated contractile ring constriction [83, 61], in published studies ROCK inhibition has not been shown to disrupt equatorial myosin II localization in cell division, where as Rho inhibition has [86]. However ROCK has a big role in disrupting cell-matrix focal adhesions [82], therefore should be in important player in later stages passive cytokinesis.

In adherent mammalian cell lines the passive cytokinetic pathway has been defined as important, because cells cannot finish cytokinesis without adhering to ECM. Cell-matrix adhesion allows for the daughter cells to pull apart to complete the division. The passive pathway was identified when myosin II-null and inhibited cells underwent complete di-

vision cycle on ligand coated substrates [57]. ROCK inhibition did not inhibit complete cytokinesis either in these studies [57]. However all these studies were conducted on glass substrates. Therefore we wanted to further test the role of physiologically relevant ECM adhesion in dynamic force mechanics of cell division and cytokinesis with myosin II and ROCK inhibition.

We find that treatment of adherent mammary epithelial cells with myosin II inhibitor blebbistatin (blebbi [64, 63]) greatly reduced the force generation ability of the cells. Although cells were able to spread to much larger areas than normal on the 0.05 mg/ml collagen coated 2500 Pa gels, they were unable to contract and apply force onto the substrate, Fig. 6.7. Cellular polarization of forces as daughter cells spread and pull apart was lost as well, Fig. 6.7B. The linear relationship between cell-matrix force and spread area was not conserved, Fig. 6.7C and D. Although much smaller in magnitude, cell-cell tension was present. Cell-cell force and torque was calculated to go through somewhat of a maximum, Fig. 6.7D. However this was calculated in a hypothetical daughter cell division plane, as none of the blebbi treated cells were able to complete cytokinesis and form two separate daughter cells.

These results of completely inhibited cytokinesis are drastically different from the published data of 30  $\mu$ M blebbistatin treated normal rat kidney epithelial cells observed on fibronectin coated glass [57]. The difference is most likely due to substrate compliance affecting the contractile ability of the matrix adherent cell that was observed to rescue myosin inhibited cytokinesis. Our experiments are conducted on physiologically stiff, but compared to glass very soft, 2500 Pa gels. The implication draws even further attention to the role of ECM mechanics in cell division and cytokinesis.

Therefore we went further to study if the strength of cell-matrix adhesion in addition of contractility inhibits cytokinesis in the later stage of the passive abscission. Y-27632 selective chemical inhibitor was used to inhibit ROCK (Rho-associated kinase) that has

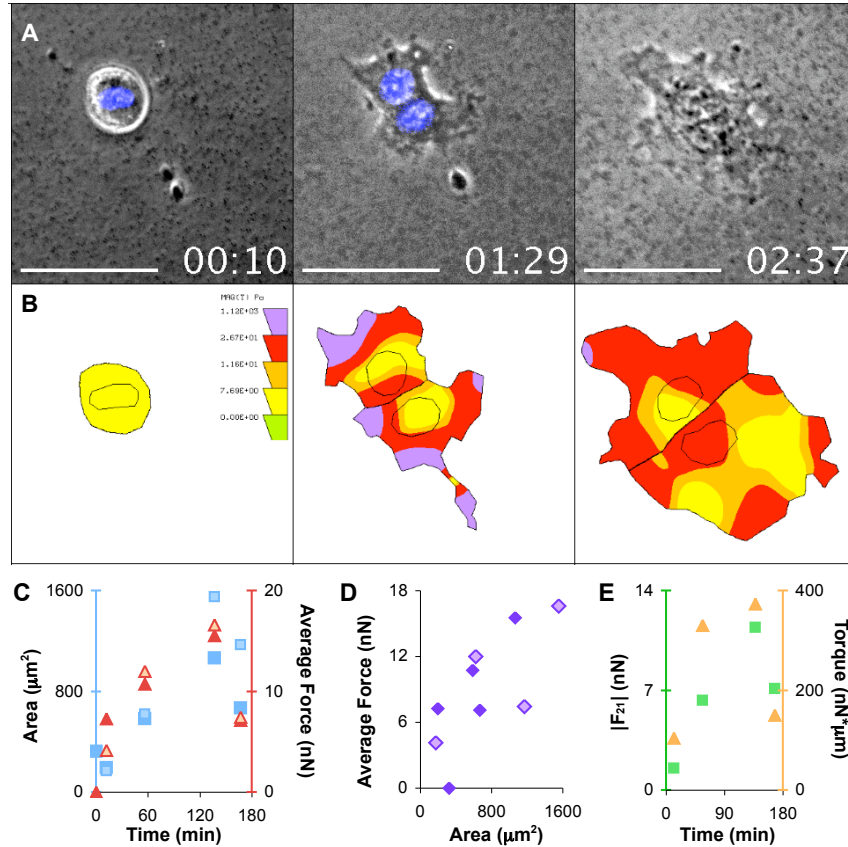


Figure 6.7: TFM results of blebbistatin treated cells.

Traction force profile of 30  $\mu\text{M}$  blebbistatin treated EpH4 cell division on 0.05 mg/ml collagen functionalized 2500 Pa gels. (A) Rounded cell entering Metaphase is captured in time with phase microscopy as it divides into two daughter cells. Nuclei stained with Hoecht fluorescent dye to confirm Metaphase and two daughter cell nuclei. HH:MM. Scale bar = 50  $\mu\text{m}$  (B) Calculated traction force maps show the cell stress fields. Size not to scale. (C) Quantitative analysis of dividing cell pair mechanics. Cell area ( $\blacksquare$ ) and average force per cell ( $\blacktriangle$ ) are plotted in time. (D) Average cell force is plotted as a function of cell area ( $\blacklozenge$ ). Dark and light markers represent cell1 and cell2 respectively. (E) Cell-cell force  $|F_{21}|$  ( $\blacksquare$ ) and torque  $|\Omega_{21}|$  ( $\blacktriangle$ ) between the two daughter cells are plotted in time.

been found to inhibit strong focal adhesions and reduce cell-matrix force [45, 82]. The treated EpH4 cells did exert lower forces onto the underlying substrate, but were observed to undergo complete division and cytokinesis, Fig. 6.8. The traction force maps show the cells polarize and exert anti-parallel forces as they pull apart, Fig. 6.8B. Furthermore the quantitative analysis of cell spread area and cell-matrix force increase and maintain a linear relationship similar to observed in normal division, Fig. 6.8C and D. Cell-cell tension too goes through a sharp maximum, Fig. 6.8E. Therefore disruption of ROCK mediated cell-matrix adhesion did not inhibit normal cytokinesis nor normal cell-matrix and cell-cell force dynamics of the dividing cells.

The observed behavior leads to decoupling of two different mechanical processes of passive cytokinesis: ROCK mediated substrate adhesion and myosin II substrate dependant cell contractility. Inhibition of ROCK and myosin II results in two completely different cytokinetic outcomes. These novel findings distinguish that it is only the inhibition of the myosin II contractility that results in adherent cell cytokinesis failure.

Direct average comparison of the inhibited division is summarized in Fig. 6.9. In normal cell division observed in 21 dividing cells, all of the cells that entered Metaphase continued with division and 20 successfully underwent cytokinesis to form two separate daughter cells. In comparison, out of the 23 observed blebbistatin (blebbi) treated cells 90% continued with cell division and none of them completed cytokinesis. All blebbi treated cells formed a binucleate single cell at the end of division. 35 cells were observed in Y-27632 ROCK inhibition (Yrock) experiment. Only 70% of the cells that entered Metaphase continued through the division cycle and of those 100% successfully finished the abscission into two daughter cells in cytokinesis. These results, summarized in Fig. 6.9A, bring novel understanding to ECM mediated cell division process.

Whereas myosin II inhibition prevents the cell from forming two complete daughter cells, this inhibition of cell contractility does not stop cells from going through the division

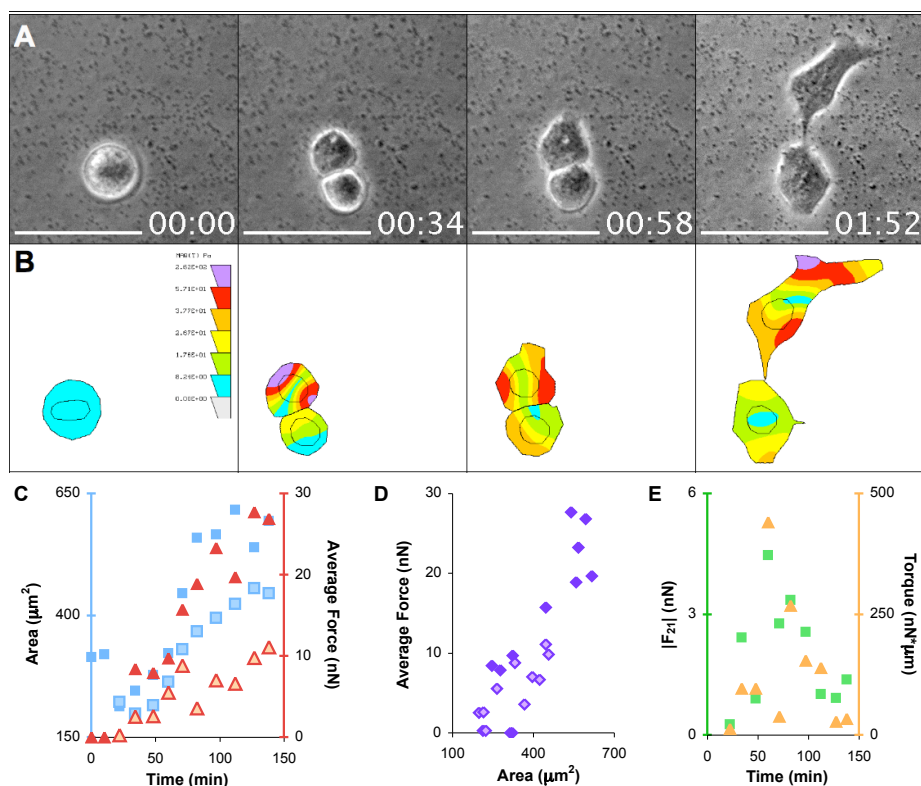


Figure 6.8: TFM results of Y-27632 treated cells.

Traction force profile of EpH4 cell division on 0.05 mg/ml collagen functionalized 2500 Pa gels, treated with 40  $\mu\text{M}$  Y-27632 ROCK inhibitor. (A) Phase microscopy of single cell dividing into two daughter cells. HH:MM. Scale bar = 50  $\mu\text{m}$  (B) Cell stress onto the extracellular environment represented with calculated traction force maps. Size not to scale. (C) Cell area ( $\blacksquare$ ) and average force per cell ( $\blacktriangle$ ) are plotted in time. (D) Average cell force is plotted as a function of cell area ( $\blacklozenge$ ). Dark and light markers represent cell1 and cell2 respectively. (E) Cell-cell force  $|F_{21}|$  ( $\blacksquare$ ) and torque  $|\Omega_{21}|$  ( $\blacktriangle$ ) between the two daughter cells are plotted in time.

cycle. However, Yrock disruption of the strength of cell-matrix adhesion influences the cell decision to enter the division cycle. Although the cell is able to completely divide and undergo cytokinesis, 30% of the cells decide to abort division early due to lack of strong cell-matrix adhesion. The strength of adhesion can also be decreased with decreasing matrix stiffness and in fact lower division numbers have been reported in cells plated on softer substrates versus increased division on stiffer substrates, where cells adhere and spread better [58]. These published division results further support our findings that ROCK mediated cell-matrix adhesion strength dictates cell decision to enter division, but we further find that it does not inhibit division completion and cytokinesis.

Cell spread area of Yrock treated cells is similar to that of normal cells (red line) throughout the cell division cycle, but not in blebbi treated cells, Fig. 6.9B. Blebbi treated cells are able to spread twice as much as the normal EpH4 cells on 2500 Pa gels. However neither inhibition allows for the cells to exert strong forces onto the ECM, Fig. 6.9C. In fact all the forces onto the ECM and the tension between the daughter cells are an order of magnitude lower than that of the normal cells, Fig. 6.9C-E. These results are significant signals and not noise, as quantified by the high values of dimensionless  $C_{-}$  statistic, Fig. 6.9F.

Furthermore quantifying the cell-matrix force as a function of cell spread area in division dynamics, it is observed that the linear force-area relationship is conserved only in the Yrock inhibited cells and not in the blebbi treated cells, Fig. 6.9D. The maximum cell-cell tension is also conserved in Yrock inhibited cells, but not for blebbi, Fig. 6.9E. Myosin II inhibited cells are able to spread to much greater area but the size does not linearly correlate to the amount of force they can exert onto the underlying gel. It is also published that RhoA activation of ROCK in cell division further phosphorylates and activates myosin [61]. However since our results show complete cytokinesis in ROCK inhibited cells, it is reasonable to suspect there has to be another myosin activation pathway that compensates

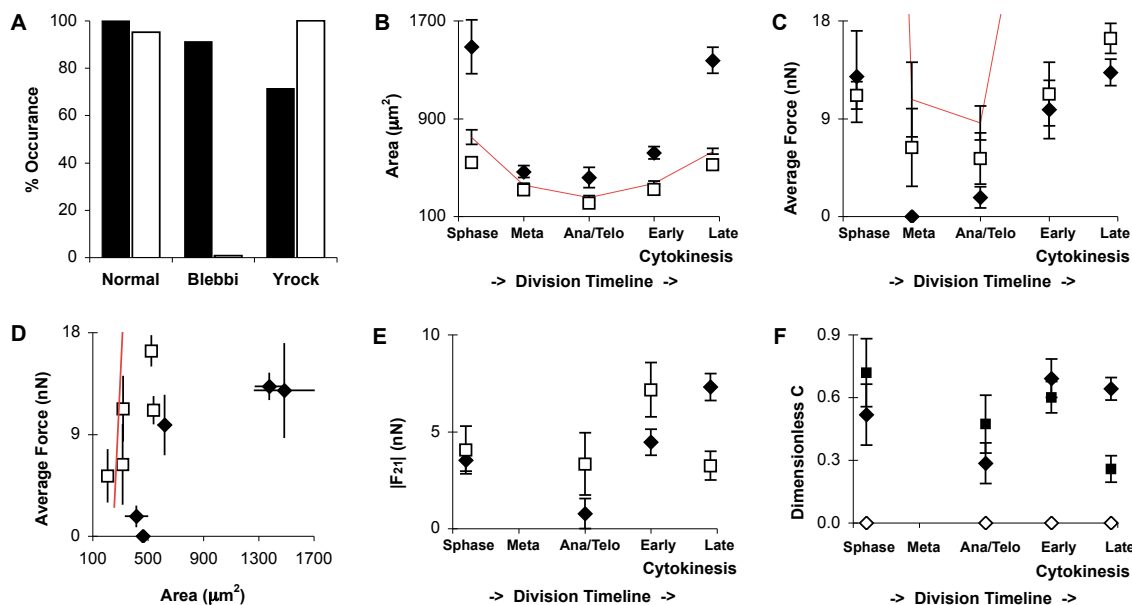


Figure 6.9: Summary of inhibited division and forces at each stage of cell cycle.

(A) EpH4 mouse mammary epithelial cell division percentages compared between untreated cells and those treated with blebbistatin (blebbi) and Y-27632 (Yrock). Black bars represent percent of cells undergoing division cycle after rounding up in Metaphase. White bars represent percent of cells that successfully underwent cytokinesis after entering division cycle. (B-F) Blebbistatin ( $\blacklozenge$ ) and Y-27632 ( $\square$ ) treated EpH4 cells are analyzed at S phase, Metaphase, Anaphase/Telophase and Early and Late Cytokinesis stages of cell cycle and compared to untreated EpH4 data (red line, see Fig. 6.6). (B) Area, (C) average cell force, (E) cell-cell force  $|F_{21}|$  and (F) dimensionless signal to noise statistic  $C$  are all plotted as a function of the cell cycle stages. (F) The dimensionless  $C_-$  ( $\blacklozenge$  blebbi and  $\blacksquare$  Yrock) confirm statistically significant signal of the results compared to noise  $C_+$  ( $\diamond$ ). (D) Average cell force is plotted as a function of area at each stage of division. All cells were plated on 2500 Pa 0.05 mg/ml collagen coated gels.  $\pm$  SEM

in ROCK inhibited case.

The detailed temporal mechanics of adherent mammalian cell division shed light on the force dynamics of the process, stressing the significance of the extracellular matrix in the division cycle. The maximum peak data of cell-cell tension in cytokinesis further implicates the importance of ECM in this process. The active intracellular equatorial contraction is supplemented by cell-matrix adhesion to finish cytokinetic division into two daughter cells, termed passive cytokinesis. Force data of the chemical inhibition experiments further separate and define the contractile and adhesion pathways of passive cytokinesis. Myosin II mediated contractility is necessary for completion of cytokinesis, where as ROCK mediated strength of cell-matrix adhesivity serves as a check point to enter into the division cycle but does not inhibit abscission of the two daughter cells.

## 6.4 Bibliography

- [55] K. R. Levental, H. Yu, L. Kass, J. N. Lakins, M. Egeblad, J. T. Erler, S. F. T. Fong, K. Csiszar, A. Giaccia, W. Weninger, M. Yamauchi, D. L. Gasser, and V. M. Weaver. Matrix crosslinking forces tumor progression by enhancing integrin signaling. *Cell*, 139(5):891–906, 2009.
- [56] Y. W. Heng and C. G. Koh. Actin cytoskeleton dynamics and the cell division cycle. *International Journal of Biochemistry and Cell Biology*, 2010.
- [57] M. Kanada, A. Nagasaki, and T. Q. P. Uyeda. Adhesion-dependent and contractile ring-independent equatorial furrowing during cytokinesis in mammalian cells. *Molecular Biology of the Cell*, 16(8):3865–3872, 2005.
- [58] Eric A Klein, Liqun Yin, Devashish Kothapalli, Paola Castagnino, Fitzroy J Byfield, Tina Xu, Ilya Levental, Elizabeth Hawthorne, Paul A Janmey, and Richard K Assoian.



Cell-cycle control by physiological matrix elasticity and in vivo tissue stiffening. *Current Biology*, 19(18):1511–8, Sep 2009.

- [59] S. Mukhina, Y. L. Wang, and M. Murata-Hori. Alpha-actinin is required for tightly regulated remodeling of the actin cortical network during cytokinesis. *Dev Cell*, 13(4):554–65, 2007.
- [60] A. Nagasaki, M. Kanada, and T. Q. P. Uyeda. Cell adhesion molecules regulate contractile ring-independent cytokinesis in dictyostelium discoideum. *Cell Research*, 19(2):236–246, 2009.
- [61] Alisa Piekny, Michael Werner, and Michael Glotzer. Cytokinesis: welcome to the rho zone. *Trends in Cell Biology*, 15(12):651–8, Dec 2005.
- [62] Elena N Pugacheva, Fabrice Roegiers, and Erica A Golemis. Interdependence of cell attachment and cell cycle signaling. *Current Opinion in Cell Biology*, 18(5):507–15, Oct 2006.
- [63] Cristina Lucas-Lopez, John S Allingham, Tomas Lebl, Christopher P A T Lawson, Ruth Brenk, James R Sellers, Ivan Rayment, and Nicholas J Westwood. The small molecule tool (s)-(-)-blebbistatin: novel insights of relevance to myosin inhibitor design. *Organic and Biomolecular Chemistry*, 6(12):2076–84, Jun 2008.
- [64] M. Kovacs, J. Toth, C. Hetenyi, A. Malnasi-Csizmadia, and J. R. Sellers. Mechanism of blebbistatin inhibition of myosin ii. *Journal of Biological Chemistry*, 279(34):35557–63, Aug 2004.
- [65] Cynthia A. Reinhart-King, Micah Dembo, and Daniel A. Hammer. Endothelial cell traction forces on rgd-derivatized polyacrylamide substrata. *Langmuir*, 19(5):1573–1579, 2003.

- [66] D J Fishkind and Y L Wang. Orientation and three-dimensional organization of actin filaments in dividing cultured cells. *Journal of Cell Biology*, 123(4):837–48, Nov 1993.
- [67] Ulrike S. Eggert, Timothy J. Mitchison, and Christine M. Field. Animal cytokinesis: From parts list to mechanisms. *Annual Review of Biochemistry*, 75(1):543–566, 2006.
- [68] K. Burton and D. L. Taylor. Traction forces of cytokinesis measured with optically modified elastic substrata. *Nature*, 385(6615):450–4, 1997.
- [69] E. H. Danen and K. M. Yamada. Fibronectin, integrins, and growth control. *Journal of Cellular Physiology*, 189(1):1–13, 2001.
- [70] J. C. Effler, Y. S. Kee, J. M. Berk, M. N. Tran, P. A. Iglesias, and D. N. Robinson. Mitosis-specific mechanosensing and contractile-protein redistribution control cell shape. *Current Biology*, 16(19):1962–7, 2006.
- [71] D. J. Fishkind and Y. L. Wang. New horizons for cytokinesis. *Current Opinion in Cell Biology*, 7(1):23–31, 1995.
- [72] M. Glotzer. Animal cell cytokinesis. *Annual Review of Cell and Developmental Biology*, 17:351–86, 2001.
- [73] H. Miyoshi, S. K. Satoh, E. Yamada, and Y. Hamaguchi. Temporal change in local forces and total force all over the surface of the sea urchin egg during cytokinesis. *Cell Motility and the Cytoskeleton*, 63(4):208–21, 2006.
- [74] E. M. Reichl, J. C. Effler, and D. N. Robinson. The stress and strain of cytokinesis. *Trends in Cell Biology*, 15(4):200–6, 2005.
- [75] E. M. Reichl, Y. Ren, M. K. Morphew, M. Delannoy, J. C. Effler, K. D. Girard, S. Divi, P. A. Iglesias, S. C. Kuo, and D. N. Robinson. Interactions between myosin and

- actin crosslinkers control cytokinesis contractility dynamics and mechanics. *Current Biology*, 18(7):471–80, 2008.
- [76] E. M. Reichl and D. N. Robinson. Putting the brakes on cytokinesis with alpha-actinin. *Dev Cell*, 13(4):460–2, 2007.
- [77] D. N. Robinson, G. Cavet, H. M. Warrick, and J. A. Spudich. Quantitation of the distribution and flux of myosin-ii during cytokinesis. *BMC Cell Biol*, 3:4, 2002.
- [78] A. P. Sagona and H. Stenmark. Cytokinesis and cancer. *FEBS Letters*, 584(12):2652–61, 2010.
- [79] J. M. Scholey, I. Brust-Mascher, and A. Mogilner. Cell division. *Nature*, 422(6933):746–52, 2003.
- [80] S. H. Shafikhani, K. Mostov, and J. Engel. Focal adhesion components are essential for mammalian cell cytokinesis. *Cell Cycle*, 7(18):2868–76, 2008.
- [81] A. F. Straight, A. Cheung, J. Limouze, I. Chen, N. J. Westwood, J. R. Sellers, and T. J. Mitchison. Dissecting temporal and spatial control of cytokinesis with a myosin ii inhibitor. *Science*, 299(5613):1743–7, 2003.
- [82] M. Uehata, T. Ishizaki, H. Satoh, T. Ono, T. Kawahara, T. Morishita, H. Tamakawa, K. Yamagami, J. Inui, M. Maekawa, and S. Narumiya. Calcium sensitization of smooth muscle mediated by a rho-associated protein kinase in hypertension. *Nature*, 389(6654):990–4, 1997.
- [83] T. Q. Uyeda, A. Nagasaki, and S. Yumura. Multiple parallelisms in animal cytokinesis. *International Review of Cytology*, 240:377–432, 2004.

- [84] J. L. Walker, A. K. Fournier, and R. K. Assoian. Regulation of growth factor signaling and cell cycle progression by cell adhesion and adhesion-dependent changes in cellular tension. *Cytokine and Growth Factor Reviews*, 16(4-5):395–405, 2005.
- [85] G. Weder, J. Voros, M. Giazzon, N. Matthey, H. Heinzelmann, and M. Liley. Measuring cell adhesion forces during the cell cycle by force spectroscopy. *Biointerphases*, 4(2):27–34, 2009.
- [86] M. Zhou and Y. L. Wang. Distinct pathways for the early recruitment of myosin ii and actin to the cytokinetic furrow. *Molecular Biology of the Cell*, 19(1):318–26, 2008.

# Chapter 7

## Conclusions and Future Directions

### 7.1 Force cross-talk

In this research of a vital quest in understanding breast cancer invasiveness and metastasis, we explored the pivotal role of the extracellular matrix (ECM). Our experimental results have shown single cell motility is a biphasic function of both biochemical and mechanical properties of the ECM. It is at intermediate and inversely related biochemical and mechanical stimuli that cells reach maximum velocity. Cell-cell adhesion, which inhibits the maximum migration rate, is also found to be a function of the ECM. Furthermore we find there is a compliance switch, around 1000 Pa, when cell-cell adhesions overcome cell-matrix adhesion and mammary epithelial cells, both human and mouse, form three dimensional aggregates on two dimensional gels. However, force profile calculations show that it is not the absolute values of cell-cell force, but the increasing ratio of cell-cell tension to that of cell-matrix force that linearly decreases cell motility. Therefore the next interesting questions to follow would be what cell-cell adhesion components inhibit or enhance this linear function.

We tested out one of the important components, which is  $\beta$ -catenin binding to E-

cadherin mediated cell-cell junctions. Over-expression of the E-cadherin mutant that lacks the  $\beta$ -catenin binding domain does inhibit cell-cell tension. The linearly increasing relationship between average traction force and cell-cell tension is lost in these mutant cells. Overall cells are unable to exert higher cell-cell forces even on stiffer substrates, as observed in normal cells. Of course testing a wider range of mechanical and biochemical substrates will paint a more complete picture of the ECM affect on  $\beta$ -catenin deficient interactions and if the cross-dependence of the cell-cell and cell-matrix force pathways will be decoupled. It will be further interesting to test the motility of these mutant cells, single and interacting. Since the mutant decreases average traction force as well as cell-cell tension and since optimum motility we observed at intermediate cell force and low cell-cell tension, our hypothesis is that the motility of even single cells will increase and cell-cell interaction will not significantly inhibit this invasive phenotypic behavior. But this would be an interesting question to pursue.

Further key players to test, that are involved in cell-cell adhesions and mechanotransduction that are also implicated in cross talk with cell-matrix adhesions, would be vinculin, myosin II and myosin IV. Since these proteins are very important in cell-matrix adhesions as well, the best approach would be from simulating and plating the cells on a cell surface mimetic gel. This can be achieved with coating the polyacrylamide gels with protein A followed by an E-cadherin FC chimera, as described in Chapter 2. Traction force microscopy can then be a great tool to see the differences in the forces the mutant cells exert on the E-cadherin coated surface. Furthermore plating  $\beta$ -catenin mutant cells on the cell mimetic surface will add to understanding of its role in promoting cell-cell adhesion and force generation.

These experimental ideas will apply the engineered surface and TFM computational model to understand E-cadherin mediated cell-cell interaction dynamics of mammary epithelial cells. Our hypothesis is that mammary epithelial cells are able to sense and exert

force on neighboring cells through myosin VI driven actomyosin contraction. This mechanotransduction at cell-cell junctions is dependent on initial clustering of surface E-cadherins through myosin II action and the cluster is associated with the cytoskeleton via  $\alpha$ -catenin and vinculin interaction.

Recent in vitro studies of cellular force generation have shown that cells are able to spread, migrate, and exert forces on cadherin coated substrates [98, 97, 96]. Motor proteins including myosin VI have also been identified as key drivers of mature cell-cell interactions [95], which is furthermore the only motor protein found localized at the site of tight adheren junctions (AJs). Implications of these new findings point to cellular cytoskeleton engagement and actomyosin contraction at cell junctions. TFM can be used to test the role of myosin VI in E-cadherin junctions through cellular ability to sense and generate force at AJs. Forces exerted by siRNA myosin VI knock down (KD) mammary epithelial cells can be measured and compared with control and exogenous myosin VI rescue experiments. Increase the mechanical stiffness of the surface will test if myosin VI also acts as a mechanosensor at AJ.

Myosin II directed surface E-cadherin clustering is found necessary for cell-cell force generation. Maturation of nascent cell-cell contacts to strong cadherin adhesions involves cadherin clustering that depends on myosin II driven cytoskeleton re-organization [94]. Myosin II was directly implicated in E-cadherin clustering through photobleaching and chemical inhibitor experiments conducted by Shewan et al [93]. Furthermore myosin II supports cadherin-based actin bundles [93]. By inhibiting myosin II with pharmacological inhibitors, it will be interesting to see if E-cadherin clustering and actin bundle formation are necessary for AJ force generation with the powerful tool of traction force microscopy.

$\alpha$ -catenin and vinculin interaction are found increase force generation through engaging the cytoskeleton at the cell-cell adhesion sites. To fully understand how myosin mediated force generation is exerted at cell-cell junctions, vinculin is the perfect protein to test be-

cause it connects the cytoskeleton to the E-cadherin junctions. Vinculin contains F-actin and  $\alpha$ -actin binding sites [91, 92]. Furthermore head and tail vinculin fragments fused to  $\alpha$ -catenin rescued cell-cell junction integrity of myosin VI-KD cells [95]. Therefore, it is reasonable to suspect that E-cadherin complex bound  $\alpha$ -catenin also binds vinculin, which further interacts with actin and therefore serves as the force transducer between the cytoskeleton and the cell-cell junction. Force generation role of  $\alpha$ -catenin-vinculin-actin binding with biological constructs of vinculin head or tail fused to  $\alpha$ -catenin would shed light on this important connection. Specifically, if over-expression of membrane bound vinculin head or tail domain will enhance or decrease force generation at cell-cell junctions.

All these experiments can be taken further to look at the cross-talk between cell-cell and cell-matrix adhesions by plating the mutant and knock down or inhibited cells on ECM coated polyacrylamide gels. However care should be taken in interpreting this data, because all three proteins are involved in cell-matrix adhesions as well.

## **7.2 Cell division mechanics**

Moving onto role of division in cancer progression, we looked at force dynamics of cell cycle progression. Such studies have never been performed in detail before and mechanical force data gathered. Therefore our detailed temporal results of normal cell division and cytokinesis are the important starting point to study mechanics of the ECM dependant process. It is especially in cytokinesis we find the important role the ECM plays. It has been published that blebbistatin inhibited myosin II cells are able to undergo complete abscission on glass substrates [90]. However our experimental results on physiologically stiff gels, 2500 Pa, did not yield any blebbistatin inhibited cells that formed two separate daughter cells. Furthermore our results show the area-force and cell-cell maximum tension relationships, observed in normal and in ROCK-inhibited cells, were lost. Therefore it



is interesting to ask if increasing the substrate stiffness further will rescue the cytokinetic failure, just like published results on glass.

Further interesting division mechanics questions arise in tumourigenic cells, where division rates are higher and cytokinetic failures are more frequent. Therefore force dynamics of tumourigenic cell lines like MCF7 and MDA-MB-231 can shed light on differences in division between normal and cancerous cells. Can ECM compliance also rescue normal division mechanics of these malignant cell lines?

There are numerous questions to ask when it comes to forces of ECM mediated cell division and cytokinesis - since this is a very poorly studied arena, but a very important phenomenon in tumour development and cancer progression. The role of RhoA and spatial inhibition of myosin II directly at the furrow can be explored beyond the work done in this thesis. Furthermore over-expression of these two contractile ring components will yield interesting force dynamic results as well. Inhibition of lamellipodial protrusion proteins, such as Rac1, or other focal adhesion components such as vinculin and talin would shed light on importance of cell's ability to spread and exert force on the ECM in cytokinesis. The degree of cytoskeleton crosslinking required for cytokinesis can be tested via  $\alpha$ -catenin protein inhibition or knock down.

### **7.3 ECM role in chemotaxis of invasive breast cancer**

Although normal mammary tissue cells are not known to be responsive to chemokines, breast cancer is characterized by distinct metastasis to lymph nodes and bone marrow. Malignant and invasive mammary epithelial cells have been shown to express CXCR4 and CCR7 chemokine receptors. Signalling through these receptors mediates actin polymerization and pseudopodia formation and induces invasive response [89]. *In vivo* studies showed that neutralizing CXCL12/CXCR4 interaction significantly impairs breast cancer metasta-

sis [89, 87]. Therefore it would be further interesting to test and compare the chemotactic response of normal and cancerous mammary epithelial cells as a function of the extracellular environment.

Microfluidic platform developed by R. Jannat [88] in our lab allows to apply a chemotactic gradient of one or two chemoattractants in addition to conserving the polyacrylamide gel ECM mimetic capabilities. Building on our findings of maximum cell motility observed on stiff and low ligand density and soft and high ligand density substrates, it would be interesting to test if the motility of normal mammary epithelial MCF10A cells increases with chemokine stimulation. If a change in motility is observed that means mechanical and biochemical cues of the ECM elicit intracellular changes in receptor expression, which can further be tested with immunostaining studies. This would be a great and novel finding because it shows that the changes in extracellular matrix alone can promote a cancerous phenotype and metastatic receptor expression in normal cells.

The microfluidic gel experimental set up can further answer questions of chemotactic breast cancer cell motility and how the ECM mediates the invasive phenotype. Can the substrate compliance alone inhibit or promote the motile chemotactic response of tumorigenic mammary epithelial cells, like MCF7 or MDA-MB-231? How will the presence of the chemoattractant inhibit the role of the mechanical and biochemical ECM cues?

Furthermore, with the new developed photoinitiator protocol the gel surface can be patterned with multiple ECM ligands or other proteins and the pattern spacing and geometries can be varied to test questions of adhesion size, combinatorial ligand mixtures, surface bound growth factors or cadherin molecules and much more in cell motility and force generation. Overall the traction force microscopy is a great platform to answer the cell invasion and motility related questions, which is what we have done in this thesis, and there are many more still left unclear and not completely understood.

## 7.4 Bibliography

- [87] A. Z. Fernandis, A. Prasad, H. Band, R. Kloserl, and R. K. Ganju. Regulation of cxcr4-mediated chemotaxis and chemoinvasion of breast cancer cells. *Oncogene*, 23:157–67, 2004.
- [88] R. A. Jannat, G. P. Robbins, B. G. Ricart, M. Dembo, and D. A. Hammer. Neutrophil adhesion and chemotaxis depend on substrate mechanics. *Journal of Physics: Condensed Matter*, 22:194117–31, 2010.
- [89] A. Muller, B. Homey, S. Hortensia, G. Nianfeng, D. Catron, M. E. Buchanan, T. McClanahan, E. Murphy, W. Yuan, S. N. Wagner, J. L. Barrera, A. Mohar, E. Verastegui, and A. Zlotnik. Involvement of chemokine receptors in breast cancer metastasis. *Nature*, 410:50–6, 2001.
- [90] M. Kanada, A. Nagasaki, and T. Q. P. Uyeda. Adhesion-dependent and contractile ring-independent equatorial furrowing during cytokinesis in mammalian cells. *Molecular Biology of the Cell*, 16(8):3865–72, 2005.
- [91] B. M. Jockusch and M. Rudiger. Crosstalk between adhesion molecules: vinculin as a paradigm for regulation by conformation. *Trends in Cell Biology*, 6:311–5, 1996.
- [92] E. E. Weiss, M. Kroemker, A.-H. Rudiger, B. M. Jockusch, and M. Rudiger. Vinculin is part of the cadherin-catenin junctional complex: complex formation between alpha-catenin and vinculin. *Journal of Cell Biology*, 141(3):755–64, 1998.
- [93] A. M. Shewan, M. P. Maddugoda, A. Kraemer, S. J. Stehbens, S. Verma, Kovacs E. M., and A. S. Yap. Myosin ii is a key rho kinase target necessary for the local concentration of e-cadherin at cell-cell contacts. *Molecular Biology of the Cell*, 16(10):4531–42, 2005.

- [94] M. Lambert, O. Thoumine, J. Brevier, D. Choquet, D. Riveline, and R. M. Mege. Nucleation and growth of cadherin adhesions. *Experimental Cell Research*, 313(19):4025–40, 2007.
- [95] M. P. Maddugoda, M. S. Crampton, Shewan A. M., and Yap A. S. Myosin vi and vinculin cooperate during the morphogenesis of cadherin cell-cell contacts in mammalian epithelial cells. *Journal of Cell Biology*, 178(3):529–40, 2007.
- [96] J. Silvestre, P. J. A. Kenis, and D. E. Leckband. Cadherin and integrin regulation of epithelial cell migration. *Langmuir*, 25(17):10092–9, 2009.
- [97] A. Ganz, M. Lambert, A. Saez, P. Silberzan, A. Buguin, R. M. Mege, and B. Ladoux. Traction forces exerted through n-cadherin contacts. *Biologie Cellulaire*, 98(12):721–30, 2006.
- [98] N. Borghi, M. Lowndes, V. Maruthamuthu, M. L. Gardel, and W. J. Nelson. Regulation of cell motile behavior by crosstalk between cadherin- and integrin-mediated adhesions. *PNAS*, 107(30):13324–29, 2010.